DETECTION QUALITY MEASURE IN SURVEILLANCE WIRELESS SENSOR NETWORKS

by

Can Komar

B.S., Department of Computer Engineering, Boğaziçi University, 2000

M.S., Department of Computer Engineering, Boğaziçi University, 2003

Submitted to the Institute for Graduate Studies in
Science and Engineering in partial fulfillment of
the requirements for the degree of
Doctor of Philosophy

Graduate Program in Department of Computer Engineering
Boğaziçi University
2012

DETECTION QUALITY MEASURE IN
SURVEILLANCE WIRELESS SENSOR NETWORKS

APPROVED BY:

Prof. Cem Ersoy (Thesis Supervisor)	.....
Assoc. Prof. Fatih Alagöz	.....
Prof. Emin Anarım	.....
Prof. Sema Oktuğ	.....
Assoc. Prof. Tuna Tuğcu	.....

DATE OF APPROVAL: 03.07.2012

To my mother...

ACKNOWLEDGEMENTS

First and foremost, I offer my sincerest gratitude to my supervisor, Prof. Cem Ersoy, who has guided me during all of my academic life including previous BSc and MSc studies and current PhD thesis. His supervision, guidance, and knowledge has been the major element in my academic life. I attribute the level of my computer science degrees to his encouragement and effort he provided during all my undergraduate and graduate life and without him this thesis, too, would not have been completed or existed. One simply could not wish for a better advisor and guide.

I would like to express my deepest thanks to all my teachers in the thesis jury, Assoc. Prof. Fatih Alagöz, Prof. Emin Anarım, Prof. Sema Oktuğ and Assoc. Prof. Tuna Tuğcu for their invaluable suggestions and the time they spared. Their comments have improved the quality of this thesis significantly.

As a proud graduate of the Computer Engineering Department of Boğaziçi University, I would like to thank all of my instructors. Their competence and enthusiasm have always been a source of inspiration for me.

In the analytical part of this thesis, I worked closely with Yunus Dönmez. We constructed the mathematical models for analysis and simulations with the help of his strong background in the mathematics. He is not only a fine mathematician converted computer scientist but he has always been a trustworthy companion and a great friend and support in the hard times. He has provided me with his deep insights about the representation and solution of real life problems. This thesis would never reach its current level without him.

I have shared the room ETA 47 and TAM building with a friendly and cheerful group of fellow colleagues. Murat Cihan, with his 'cold' jokes, Şerif Bahtiyar with his alternative approaches to problems, Ali Haydar Özer the resolute and invisible component of our small community, Itır Karaç by her knowledge in the mathematics and sailing have been my closest supporters during my thesis studies. The ideas that Gaye Genç and Yunus Emre Kara have provided about image processing have been a great help. In addition to them, there are many other valuable people that I had the privilege of sharing a moment during my academic life.

Last but not the least, my deepest appreciation and gratitude is to my family, for their continuous support and their never ending belief in me even when I did not have it. My endless love to my long gone father and to my perfect mother who raised me against all odds and made me the human being today. I really appreciate and love her more and more after each day. My brothers and sister who never let me go and always provided their love and support. I am so blessed to be born into such a family.

This work is supported by the State Planning Organization of Turkey (DPT) under the TAM Project, number 2007K120610, by the Scientific and Technological Council of Turkey (TUBITAK) under the grant number 108E207, by Boğaziçi University Research Fund (BAP) under the grant number 09A101P and by European Community's Seventh Framework Programme (FP7-ENV-2009-1) under the grant agreement FP7-ENV-244088 FIRESENSE.

ABSTRACT

DETECTION QUALITY MEASURE IN SURVEILLANCE WIRELESS SENSOR NETWORKS

The performance of a surveillance wireless sensor network is generally measured with its detection capability which is affected by various parameters such as the sensor count, the sensor range, the area width and the target mobility model. We assume that intruders prefer some favorite paths because of their geographical advantages and pass through them instead of following a random mobility model. These paths are generally in close vicinity of each other and they can be bounded in a region. In this thesis, we inspect the travelers' favorite region notions and propose some image processing tools to detect their location within a border area. Following this, we present a closed form of the detection probability as the detection quality measure in the existence of travelers' favorite paths. The detection probability is reduced to the geometric line intersection problem using bijection and the boundary conditions of intruder trajectories for the border area and the favorite regions are determined. The line intersection problem is solved using tools from the integral geometry and geometric probability. The effect of the favorable region on the detection quality under different conditions is calculated using probabilistic models. The accuracy of the proposed quality measure is validated by both analytical methods and simulation results. Furthermore, the importance of the intrusion model on the network performance is presented using realistic scenarios. It is shown that the existence of favorite paths has significant impact on the detection quality of the network. We extend our work to border areas with multiple favorite path regions and present a closed form of detection probability for such generic cases. We also inspect the effects of various system parameters such as the sensing model and application scenarios on the detection quality measure using both analytical tools and simulations. The proposed detection quality measure provides analytical tools to forecast the expected detection performance and to optimize the network according to the intruder mobility model.

ÖZET

GÖZETİM AMAÇLI KABLOSUZ ALGILAYICI AĞLARDA TESPİT KALİTESİ ÖLÇÜTÜ

Bir gözetim kablosuz algılayıcı ağın başarımı genellikle, algılayıcı sayısı, algılayıcı menzili, alanın genişliği ve hedefin hareketlilik modeli gibi çeşitli verilerden etkilenen hedef tespit kapasitesi ile ölçülmektedir. Hedeflerin rastgele bir hareketlilik modelini takip etmek yerine, coğrafi avantajları sebebiyle bir takım patikaları tercih ettiğini ve buralardan geçtiğini varsaymaktayız. Bu patikalar ise genel olarak birbirinin yakınında bulunmakta ve belirli bir alan içinde sınırlandırılabilmektedir. Bu tezde, hedeflerin sık kullandıkları bölgeleri incelemekte ve bir sınır bölgesi içindeki yerlerini tespit etmek için bazı görüntü işleme araçlarını kullanmaktayız. Bunun ardından, hedeflerin sık kullandıkları patikalar olması durumunda, bir tespit kalite ölçütü olarak tespit olasılığını bir formül halinde sunmaktayız. Hedef tespit olasılığı eşleşme metodu ile geometrik çizgi kesişim problemine dönüştürülmekte ve sınır alanı ve sık kullanılan alanlar içerisinde bulunan ve hedeflerin takip ettiği yolların geometrik sınır koşulları tespit edilmektedir. Çizgi kesişim problemi integral geometri ve geometrik olasılık yöntemleri ile çözümlenmektedir. Sık kullanılan alanların farklı koşullar altında hedef tespit kalitesine etkileri olasılıksal modeller kullanılarak hesaplanmaktadır. Sunulan kalite ölçütünün doğruluğu analitik sonuçlar ve benzetim sonuçları ile gösterilmektedir. Ayrıca, gerçekçi senaryolar ile hedef hareketlilik modelinin ağ başarımı üzerindeki önemi gösterilmektedir. Sık kullanılan patikaların varlığının hedef tespit kalitesi üzerine büyük etkisi olduğu gösterilmektedir. Çalışmamızı çoklu sık kullanılan alanlardan oluşan sınır bölgeleri için genelleştirmekte ve bu genel durum için tespit kalitesi ölçütü kapalı matematiksel form halinde sunmaktayız. Ayrıca algılama modeli, uygulama senaryoları ve diğer sistem parametrelerinin tespit kalitesi üzerindeki etkileri de analitik araçlar ve benzetimler ile sunulmaktadır. Önerilen yöntem bir ağın beklenen tespit performansını öngörmek ve hedef hareketlilik modeline bağlı olarak ağın başarımını iyileştirmek amacıyla kullanılabilecek araçlar sunmaktadır.

TABLE OF CONTENTS

LIST OF FIGURES

LIST OF TABLES

LIST OF SYMBOLS

$A_{T(\Upsilon_\phi)}$	Area of S covered by lines in Υ with parameter ϕ.
C	A bounded set.
C_i	A bounded subset.
$E(A_T)$	Expected area of S covered by lines in Υ.
$E(A_{T_t})$	Expected area of TFP region covered by lines in Υ_t.
$E(T)$	Expected thickness of S wrt Υ.
$E(T_i)$	Expected thickness of set S_i wrt Υ.
$E(T_t)$	Expected thickness of TFP region wrt Υ_t.
G	Intruder path line.
h	The height of the rectangular border.
h'	Thickness of the lines with slope α in S.
h'_t	Thickness of the lines with slope α in TFP region.
$m(G)$	Measure of a set of lines $G(p, \phi)$.
N_{d,s_i}	Number of detections made by the sensor s_i.
N_s	Number of deployed sensors.
N_t	Number of TFP regions.
p	Distance of the intruder line to the origin.
P	Intruder entry point into the deployment area.
P_D	Probability that the network detects an intruder.
$P_{D\|t}$	Probability of detection in a TFP path.
$P_{D\|\overline{t}}$	Probability of detection in a non-TFP path.
$P_{\overline{D}}$	Probability that the network misses an intruder.
P_{s_i}	Probability that a sensor s_i detects an intruder.
$P_{\overline{s}_i}$	Probability that a sensor s_i misses an intruder.
p_t	The total probability of selecting TFP region by an intruder.
p_{t_i}	The probability of selecting TFP region t_i by an intruder.
$p_{\overline{t}}$	The probability of selecting non-TFP region by an intruder.
r	Radius of sensing coverage of a sensor.
P	Intruder exit point from the deployment area.

S	Convex deployment area.
SSA	Sum of squares of factor A.
SSB	Sum of squares of factor B.
SSC	Sum of squares of factor C.
$SSAB$	Sum of squares of interaction between factors A and B.
$SSAC$	Sum of squares of interaction between factors A and C.
$SSBC$	Sum of squares of interaction between factors B and C.
$SSABC$	Sum of squares of interaction between factors A, B, and C.
SST	Sum of squares total.
s_y^2	The sample variance of y.
s_i	Index of a sensor.
S_i	Sensing coverage area of a sensor s_i.
t	TFP region.
t_i	TFP region i.
w	The width of the rectangular border.
w_t	The total width of the TFP region.
w_{t_i}	The width of the TFP region t_i.
X	The intruder.
y	Measure of performance in detection probability.
$\bar{y}$	The mean of results from all observations.
α_1	Minimum value for the parameter ϕ of lines in Υ.
α_2	Maximum value for the parameter ϕ of lines in Υ.
β	Elfes detection model parameter.
Γ	Gamma function.
γ	Angle limit of a line in a rectangular deployment site.
δ	The event that $C \cap \Upsilon_\phi \neq \emptyset$.
$\overline{\delta}$	The event that $C \cap \Upsilon_\phi = \emptyset$.
θ	Angle limit of a line in the TFP region.
λ	Elfes detection model parameter.
$T(\Upsilon_\phi)$	Thickness of line set crossing S with parameter ϕ.

Υ	Set of lines crossing S.
Υ_ϕ	Set of lines crossing S with parameter ϕ.
Υ_t	Set of lines in the TFP region.
$\Upsilon_{t,\phi}$	Set of lines in the TFP region with parameter ϕ.
$\Upsilon_{\overline{t}}$	Set of lines that are not in the TFP region. $\Upsilon_{\overline{t}} = \Upsilon \setminus \Upsilon_t$.
ϕ	Angle of line perpendicular to intruder line wrt. x axis.

LIST OF ACRONYMS/ABBREVIATIONS

DetQM	Detection Quality Measure
DQM	Deployment Quality Measure
PIR	Passive Infrared
ROI	Region of Interest
SWSN	Surveillance Wireless Sensor Network
TFP	Travelers' Favorite Path
UAV	Unmanned Aerial Vehicle
WSN	Wireless Sensor Network

1. INTRODUCTION

The wireless sensor networks (WSN) are generally composed of small and low-cost sensor nodes having limited computational and communication power. Although they have limited capabilities, they are designed to achieve certain tasks by collaboration in situations where alternative complex solutions are infeasible. Wireless sensor networks are generally deployed to inaccessible terrains by an airplane or the artillery. This situation requires a wireless sensor network to be self-organizing after deployment. Once the nodes are synchronized and the network is built, the sensor network starts collecting information about the environment such as temperature, motion, pressure, and magnetism. The sensor nodes forward the collected information to the sink node directly or with the help of intermediate nodes, but instead of sending the raw data, they generally perform simple calculations and filter out the unnecessary part of the data. The wide capability range of sensor nodes and their simplicity and low-cost in design allows them to be used in many application areas, such as agriculture [4–8], health care [9–11], environmental monitoring [12]. A general survey about wireless sensor networks can be found in [13–17].

In this thesis, we are focused on surveillance wireless sensor networks (SWSN). SWSNs are used to detect the movements within a monitored area. Some of the application examples of SWSNs are:

- Border surveillance against intruders
- Security sensitive area monitoring such as embassies, barracks
- Cultural heritage monitoring
- Wildlife monitoring

Like most of the other WSN types, also in SWSNs, after the deployment, the sensors wake up, organize themselves to construct a network and start the monitoring the area. When a sensor detects an event, it is reported to the sink node so that the necessary action can be taken by the network operators. The SWSNs are frequently used in security applications. The prerequisites and requirements for each application type may vary greatly.

The border surveillance is one of the popular SWSN applications, where the environmental conditions may impose different challenges. The border areas are generally in the shape of long, narrow bands that separate two countries. The mountains and valleys may cause significant altitude changes in the deployment zone. The length of the border zone which may be hundreds of kilometers in length may require the sensor network to be divided into smaller segments and be managed by different control centers. The segments of the network can be determined according to the terrain properties. The harsh climate conditions may require the sensor nodes to be modified accordingly.

Cultural heritage surveillance is another application area where the aim is to monitor the historical and archeological fields and items. The historical sites are generally public places vulnerable to dangers such as fire, theft and vandalism. Some parts of an historical site may be open to public during visiting hours whereas some parts of the site may be restricted to general access due to various reasons. Some parts of the old buildings and the castles under restoration are generally dangerous for a public visit. Most of the active archeological dig sites are generally under protection because of the sensitive conditions of the buried items which need special care during excavation.

There have been various surveillance wireless sensor network testbeds that are implemented using different sensor nodes for performance measurement under real life conditions. One of the early demonstrations is conducted in March 2001. Researchers from University of California at Berkeley deployed a sensor network onto a road from an unmanned aerial vehicle (UAV) [1, 18]. The deployed sensor nodes were equipped with magnetometers that have a typical range of 10 meters. The UAV with the sensor node to be deployed attached to the bottom of its wing can be seen in Figure 1.1. The network is used to detect and track vehicles passing through the area. This information was later collected from the sensor nodes using the UAV flying over the area.

The targets that are desired to be detected may have different properties. Their speed may vary greatly such as the case between a walking soldier and a moving vehicle. A walking soldier may carry high amount of metal in contrast to an unarmed man. The noise and vibration a vehicle produces is generally much more than a walking man. Such properties can be used to detect and classify targets [19]. In this study, the au-

Figure 1.1. The UAV with the sensor node under its wing to be deployed [1].

thors focused on the sensor nodes' physical properties and capabilities. The detection and classification capability of a sensor node is tested using different types of targets. Another type of sensor that can be used for detection is passive infrared (PIR) type sensors. The authors demonstrate a wireless network deployment for border surveillance using 10 PIR type sensor nodes [20]. The system consists of iSense nodes which contains an AMN14112 PIR sensor. Authors design and test protocols for trespasser and failure detection.

Although, there are various fields a WSN can be utilized in, WSN applications can be roughly divided into two main categories: monitoring and tracking [17]. The detection oriented applications are also classified in the monitoring category. Monitoring an area against movements is an important topic in surveillance systems. The capability of a surveillance wireless sensor network is generally inspected from two aspects: coverage and detection. In this section, we will provide some related work about coverage and detection from the literature.

Covering an area using various surveillance methods have been formulated in different domains in the past. One of the famous problems is the Art Gallery Problem in which the objective is to place guards in an art gallery such that every point of rooms is covered by at least one observer [21]. The coverage problem in the wireless sensor networks are differentiated according to the requirements and properties of the

network. In [22], the authors make a survey about the coverage problem in sensor networks and define three types of network coverage which are area coverage, point coverage and barrier coverage.

The area coverage which is also referred as full coverage or blanket coverage, is the most studied coverage type in the literature. In this type of coverage, the objective of the network is to monitor a given RoI with respect to different performance criteria such as coverage ratio, minimum number of sensors providing desired minimum coverage level during the maximum lifetime of the network. Generally, node sleep schedule algorithms are used for maximizing the network lifetime. Since the sleep scheduling problem is NP-hard, there is no certain optimal algorithm existing. For that purpose, several heuristics are proposed. More can be found in [22–24]. In another approach to network connectivity and coverage relationship, the authors propose an algorithm to maintain a desired coverage ratio while not crippling the network connectivity. The algorithm is run on the cluster heads in which each sensor node sends its position to the respective cluster head. The cluster head computes the mutually exclusive and disjoint set of common nodes. These sets are used to form the sleep schedule [25].

In point coverage, the object of the network is to monitor given targets during its lifetime. A target is considered covered if it is within the sensing range of an active sensor node. Most of the studies are focused on providing connected target coverage while optimizing other network parameters. In [26], the authors model the problem as a maximum cover tree problem and show that it is an NP-complete problem. They propose heuristic approximation algorithms to increase the lifetime of the network. In [27], the authors analyze the sparse surveillance networks against moving targets. For a moving target moving with a given speed a pill shaped region called target pill is formed which includes all possible locations of sensors that can detect the target. They formulate the region in terms of given parameters and propose a sensor placement framework. Due to the complexity of the optimization problem dimensions, two-stage optimization is used consisting of genetic search algorithm and nonlinear optimization program utilizing sequential quadratic programming algorithm. Deterministic deployment is another method in point coverage. In that case, the locations of the sensors are determined according to target positions and required coverage level. In [28], authors proposed

an approximation to the sensor deployment plan with constraints of minimum sensor cost and maximum target coverage which are spread across a geographical region. Their alpha-beta approximation is a combination of LP-rounding and greedy set-cover selection. They show using simulations that it outperforms previous approximations.

The barrier coverage aims forming a line made up from sensor coverage areas and tries to detect every object that breaches this line. One of the advantages of the barrier coverage over full coverage is its requirement for less number of sensors. In addition to this, they try to provide certain detection against breaches. One of the major limitations of the barrier coverage against the full coverage is that, it is not suitable for developing localized algorithms since the central nodes must be aware of other nodes' states to decide if the barrier is intact. Most of the algorithms used in the barrier sensor networks are centralized. In addition to this, the loss of a sensor node in a critical point can form a breach hole within the barrier. The barrier is as strong as the weakest node in the network. That makes the barrier networks vulnerable to jamming and physical attacks. Another weak point of the barrier coverage networks is their inability about determining the path of the intruders. The detection is performed within the coverage area of the barrier nodes which means that the observed section of the intrusion path is at most in the length of the coverage diameter. The path of the intruder before entering and after exiting the sensor coverage is not known. Most of the studies in the barrier coverage tries to improve the detection quality and lifetime of the barrier coverage using different sleep schedule and communication algorithms. In [29], to localize the barrier coverage problem, the authors divide a long border region into shorter rectangular segments. Within each segment, a horizontal barrier is constructed and along the connection strips of these segments, a vertical barrier is constructed. Compared to a centralized method, they use more sensor nodes but gain in terms of communication overhead and computation cost in the central node in addition to the reduced delay of forming a centralized barrier. In [30], the authors assume that most of the intrusions are performed within a narrow slice of the longer border region. They propose a localized sleep-wakeup protocol called Localized Barrier Coverage Protocol (LBCP) for maximizing the network lifetime. LBCP does not guarantee global barrier coverage like a centralized method does, but performs well under given assumptions. In [31],

the authors claim that sensor deployment may be linear instead of uniform random in some deployments such as dropped from an aircraft. They study the properties of barrier coverage of the network under such conditions.

In most of the coverage studies, it is assumed that the sensing range of the sensor nodes to be equal and homogeneous. The coverage of the network is calculated according to this assumption. This may not be true for all types of sensor networks. The network may be composed of different types of sensors with different sensing ranges, thus forming a heterogeneous network. Sensing areas of some sensor nodes may already be covered by other types of nodes with larger sensing area. These sensors are called unnecessary sensor nodes and they may be turned off without affecting the coverage of the network [32]. An algorithm can be used to determine these nodes and minimize the number of nodes to remain active.

The network may also be composed of the same type of sensors with dynamic sensing ranges. There are commercial sensor nodes whose sensing parameters can be adjusted accordingly [33,34]. When the targets are redundantly covered by the sensors, their sensing range can be adjusted and they can be grouped into sets to setup a sleeping schedule. This problem, which is called as Adjustable Range Set Covers by the authors is investigated in [35]. The problem is modeled mathematically and formulated using integer programming. A greedy heuristic algorithm based on integer programming is proposed as a solution. The proposed heuristic can be both applied in centralized and distributed cases. In their work, the researchers use the sensors with various sensing and transmission ranges instead of fixed ones [36]. It is stated that sensors with larger range consume more energy, thus have shorter lifetime. The problem is to select a subset of sensors with specified sensing and transmission radii such that they should cover all of the points within the region by their assigned sensing radii and they should be able to form a connected communication group by their assigned transmission radii. The goal is to minimize the sum of the sensing and communication energy cost of the sensors. A Voronoi-based algorithm is used to solve the k_1-connectivity and k_2-coverage problem where k_1 and k_2 are desired connectivity and coverage degrees.

Surveillance sensor networks are studied in terms of their detection capability, too. The detection of a target trespassing a monitored zone is essential to the functioning

of a surveillance wireless sensor network. Some of the work in this field investigate the sensor nodes in terms of their physical and sensing properties whereas some of the others combine different systems to improve the detection quality under different conditions.

In [37], the authors formally define the exposure and using it, they define the maximal breach and the minimum support paths. This information is used to estimate the reliability of the network against trespassing. In [38], authors calculate the quality of deployment and find breach paths in wireless networks in the existence of obstacles. They propose a method that converts the watershed segmentation of the field to a 2D auxiliary graph and calculate the weakest breach path. In [39], the detection problem is formulated to provide analytical results for target detection within a convex zone. The probability of target detection is calculated for both stochastic and deterministic deployments. Using the results of the analytical study, they propose a sensor placement heuristic to achieve better target detection. In [40], the authors calculate the detection quality of a sensor network in the existence of jammer attacks. They assume that the sensors that are within the range of jammer ceases functioning which results in a coverage hole within the monitored zone. They describe the system using the given parameters and formulate the detection quality measure in a closed form. They prove the correctness of the formulation both with analytical and simulation methods.

In a recent study, the authors built a wireless sensor network composed of PIR sensor nodes [41]. They propose an algorithm based on the Haar transform and support vector machine to be used in PIR sensor networks for detection. In another study, Li and Parker designed and implemented an intruder detection system that consists of a wireless sensor network and a mobile robot [42]. The sensor network utilizes neural network techniques to learn about the environment. When an intruder is detected by the network, a mobile robot is sent to the detection location. After deployment, using its light and sound sensors, the network constructs a base state of the environment. When there happens a change in the environment, the mobile node, which acts as a cluster head, is notified. The mobile robot calculates the path, reaches the detection site and starts tracking the intruder with its embedded camera system. In another study, the performance of particle filter to track targets by acoustic sensor nodes is

measured [43]. The authors analyze the theoretical bounds for tracking performance and compare it with the simulation results. Their testbed consists of Xbow MicaZ motes which are arranged such that they reach the data sink with single hop. They present the effects of various parameters in the target detection and recommend optimal values based on experiment results.

One of the common network type used in surveillance is barrier coverage type sensor networks which are generally employed in intrusion detection applications. In [30], authors are focused on the determination of the global barrier coverage of a network using local coverage information. They propose a localized barrier coverage protocol (LBCP) that is used to construct a sleep schedule and increase the network lifetime while providing required local coverage. It is expressed by the authors that most of the time local coverage provides global coverage due to nature of mobility. In [31], the authors claim that sensor deployment may be linear instead of uniform random in some deployments such as dropped from an aircraft. They study the properties of barrier coverage of the network under such conditions. To improve the reliability of barriers against failures and attacks, k-barrier coverage is proposed. An area is called k-barrier covered if an intruder traveling along any orthogonal crossing path can be detected by at least k sensors. The problem with the barrier coverage in a surveillance sensor network is its susceptibility to node failures and attacks. Most of the time, barrier coverage networks are deployed as a thin long line in order to maximize detection with minimum number of sensor nodes. This linear coverage is as strong as its weakest part, i.e. its thinnest part in terms of coverage. Any failure or coverage hole in that part will make the whole network obsolete. They are also considered more prone to jamming and physical attacks.

The detection capability of a sensor network is discussed in [44]. In this study, authors define the path exposure phenomenon to quantify the detection capability of a sensor network. They define the exposure of a target as the probability of detecting the target traversing along a minimum detection path. Their sensor model is based on the power of the signal emitted by the target at a distance. The detection probability is calculated according to the distance between the sensor node and the target. A sensor deployment strategy is proposed to reach the desired minimum exposure. In a similar

study, authors propose a formulation to determine the target detection probability using the minimum exposure path [45]. They investigate the effects of the shape of the field and the sensing range on the detection quality of the network. They assume that the target position is determined randomly and does not take the target mobility into account. In [46], authors analyze the k-sensed ratio of a path by a sensor network, which is the part of the path sensed by at least k sensors. Other performance metrics such as distance until first sensed, sensing holes, breach and support paths are also investigated using their model. They also provide a generalized version of their model using m-dimensional straight line paths sensed by an n-dimensional sensor network. In [39], authors formulate the target detection problem as a line-set intersection problem and use integral geometry to analyze it. They analytically evaluate the target detection probability and the mean free path until a target is detected, and show that detection probability is independent of the shape of the monitored zone. Their work assumes that the targets traverse all the monitored zone randomly and do not have a direction of travel over the zone. Similarly, most of the studies that investigate the sensor network detection ignore the behavior of the intruder when analyzing the detection probability or utilize mobility models inherited from previous wireless network and ad hoc network experiments. Most of these models employ random mobility either in single entity or a group of entities that are related to each other according to some properties [47]. More detailed surveys about mobility models can be found in [48–50]. Though these mobility models may be acceptable for representing the movement of an individual intruder, the intrusion preferences over the whole border region are generally not random. In a recent study, the authors propose an environment-aware mobility model to be used in wireless ad hoc networks [51]. They use obstacles and doorways to model different pathways. They present that the existence of regions of interest has significant impact on node mobility.

1.1. Motivation, Problems and Contributions

The surveillance wireless sensor networks are expected to have high detection probability while monitoring an area. The detection probability is affected by many parameters including the number of sensor nodes, the sensing range, the sensing model, the environmental conditions, the target mobility model, and the monitored zone di-

mensions.

In our study, we present that the properties of the application for which the SWSN will be used affect the mobility of the targets drastically. The movements of the targets are not random in the real life, but they have a purpose. In contrary to most of the models, we take the aim of the mobility into account. In general, the mobility of an intruder is shaped for achieving a goal. This goal generally depends on the type of the application. In a border area surveillance application, the goal of intruders is to pass through the region without being detected. In a cultural site area monitoring application, the goal of the tourists is to visit the historical places and see the ancient items. In this thesis, while studying the mobility models, we focus on border surveillance applications and study their properties, but the mathematical models we use are represented in a generic form and can be easily applied to other kinds of applications merely by changing the parameters in the proposed model.

In a border surveillance scenario, there are many factors that affect the system. Some of these factors are the existing security measures such as watch towers, sentries, razor wires and fences. The disadvantages of such security measures are that they are generally static and can be easily overcome or tricked by the intruders. The effective observable area from a watch tower is generally limited by the terrain and a path not seen from it can be easily explored. The schedules and routes of patrolling sentries can be easily determined and necessary precautions to avoid them can be taken. The fences and razor wires need constant maintenance to be kept in shape and they can be easily broken or cut off. The trespassers try to avoid these and other similar measures by preferring some advantageous regions over others which are also geographically feasible [52]. An example of this behavior is shown in Figure 1.2. In this figure, the trails of the intruders are seen clearly on the US side of the border where the terrain is grassy.

The TFP phenomenon is also being utilized in the current border watch applications. An example can be given from video cameras installed to monitor the US-Mexico border. The locations of these cameras are being chosen according to the observed trespassing behavior in the past. In a recent project, the feeds of these video cameras are opened to the public access over Internet. The volunteers who sign up for this free ser-

Figure 1.2. Trails of intruders along the US-Mexico border [2].

vice can access and watch the live streams from different points of the border. If they detect an activity as described within the site, they notify the officials [3]. In other words, a volunteer based watch system is being used for border surveillance. Some samples of the feeds watched by the volunteers can be found in Figure 1.3. Compared to a wireless sensor network, such a watch system has clear disadvantages. First of all, it is based on volunteering system and may not be always available. The coverage of the area is based on a watch system with unreliable quality. In addition to this, the cameras are generally mounted on high poles, thus easy to spot. The whole system can be avoided by choosing paths that are not in the visual range of the cameras or it can easily be disabled by an attack to the cameras. Furthermore, the website is accessible to everyone over the web without any restriction, hence the whole system is open to Internet based attacks. Another disadvantage of an open-to-everyone web-based system is that the intruders can learn insider information easily by just signing up to the service. The camera locations and their coverage can be easily determined by watching the feeds. Once this information is obtained, safe paths that are not in the detection

range of the cameras can be easily planned and other kinds of measures can be taken to avoid detection.

(a) (b)

Figure 1.3. Camera feeds from the BlueServo surveillance system [3]. (a) An area frequently used by drug smugglers. (b) A path frequently used by the trespassers.

Wireless sensor networks are appropriate tools for surveillance applications. However, there are many issues that may arise during the design of a SWSN. The specific problems we address in this thesis and our contributions can be summarized as following:

- The mobility of the targets in a SWSN is generally not random. It is based on the application type and the environmental conditions. In this thesis, we define the travelers' favorite path (TFP) and TFP region notions. The region that most of the trespasses are made through is referred to as TFP region. The localization of TFP region or regions within the border area and determining the properties is an important problem due to the effects on the detection quality of the network. Statistical and image processing based algorithms can be applied for finding the TFP regions.
- The essential function of a SWSN is the detection of the targets within the monitored zone. Hence, we choose the detection probability of a target as the main problem addressed in this thesis. The detection probability of a target by a SWSN is reduced to line-set intersection problem by bijection. A general closed form representation of the detection probability that can be applied for any convex regions is presented along with its proof and simulations.
- The mobility pattern affects the location, the width and the preference probability of a TFP region existing in a border area. We explore the effect of some factors to

the performance of a SWSN deployed in a border area with a single TFP region by the analytical models and simulations. The analyzed factors are border area width, sensor count, TFP region width and preference probability.

- The border area with a single TFP region scenario is generalized to a generic SWSN scenario consisting of multiple regions and an analytical detection quality measure is developed to calculate the performance of the network. Moreover, the detection model used in the analytical metric is applied to different detection models and the effects of detection model parameters on the quality metric are examined.
- Different applications based on the generic SWSN scenario are devised and the detection quality of the network is investigated. The effects of various factors on a SWSN performance are inspected using an analysis of factors and their impact on the result are shown. Furthermore, an optimized distribution of the sensor nodes based on the analytical detection quality measure is developed and its performance increase in the detection quality is demonstrated by the analytical methods and simulations.

2. TRAVELERS' FAVORITE PATH PROBLEM

In this chapter, we describe the travelers' favorite path (TFP) problem. Using different image processing methods, we present how to determine TFP and TFP regions. The travelers' favorite paths are the most preferred passing channels in the monitored area. The preference criteria is generally based on the environmental conditions and specific to the wireless sensor network deployment scenario. In border surveillance scenarios, the favorite paths are selected based on the terrain conditions such as valleys, mountains, bridges and rivers, the locations of the security measures such as watch towers, barbed wires, and sentries [2, 3, 52].

In cultural heritage scenarios, the favorite paths are generally selected based on the location of the statues, pictures and other cultural items, the archeological work sites where access is restricted to regular visitors and predetermined tour paths of local guides. Although there are differences between various scenarios, they have some common properties. The favorite paths are generally located close to each other and can be bounded within a region. We call these regions as travelers' favorite path regions. It is assumed that these regions are not known by the network operators.

In this section, we present how the travelers' favorite path problem is formulated. The sensors are deployed to the area using random deployment. Assuming that the travelers' are not aware of the sensors, target mobility models are constructed based on the travelers' favorite path scenarios. Travelers whose mobility patterns are based on these models traverse the monitored area and the detection data are obtained at the end of the simulation runs. Using these detection data, we formulate and calculate the detection of travelers' favorite paths.

2.1. Network Model

The sensor nodes are deployed to the field in a random manner by an airplane or the artillery. The deployment area is modeled in a grid structure in which the points of the grid are connected to each other along x and y dimensions. A sample field model is given in Figure 2.1. The horizontal axis is divided into $(m-1)$ and the vertical axis is divided into $(n-1)$ equal parts, thus, there are $(m \cdot n)$ grid points. The distance between each grid point is equal in both axis and there is no elevation. The direction

of the intrusion is from the insecure side to the secure side of the region.

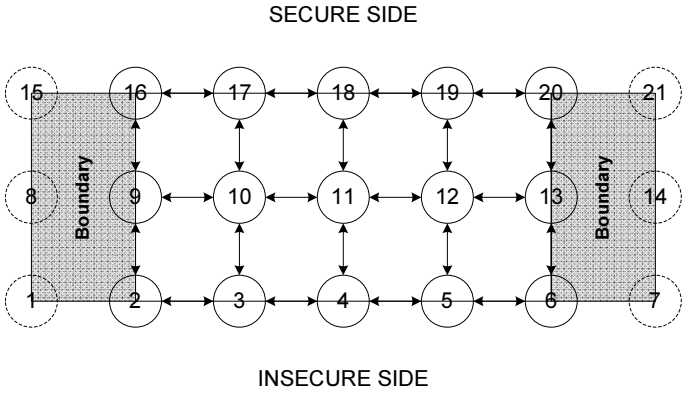

Figure 2.1. A sample field represented using grid structure.

The location of the sensor nodes are assumed to be known. The localization of wireless sensor nodes is a well studied topic and there are various solutions both in hardware and software to calculate the location of a sensor node. Placing a number of source signals, also with unknown locations, can be used to localize sensor nodes [53]. Each source in turn emits a calibration signal, and a subset of sensor nodes measures the time of arrival and direction of arrival of the signal emitted from that source. From these measurements, the locations and orientations of the nodes can be computed. Another method is to use a node with a known location as a reference point. A single mobile node that is aware of its own location, with the help of an integrated GPS device, can be used for localization [54, 55]. Sensor nodes receiving the beacon packets infer proximity constraints to the mobile beacon and use them to construct and maintain position estimates. The connectivity information of each sensor node, who is within communications range of whom, can also used for determining the locations of sensor nodes [56]. In addition to the connectivity information, additional information such as estimated distances between neighbors or known positions for anchor nodes can also be integrated to the localization process. A central method can be used to construct a global map whereas the distributed method constructs smaller local maps and these local maps can be patched to form a global map. Another method is to use the spatio-temporal properties of well controlled events to localize the sensor nodes [57]. Since the time and location of the controlled event is known, using the information of time the event is perceived by the sensor node the location can be calculated. The sensor nodes detect the events and report back to the base station. The base station computes the

locations of the nodes. More information on the localization of wireless sensor nodes can be found in [58–65].

There are N_t TFP regions within the border area whose locations are known by the intruders but not by the network operators. These regions are assumed to be rectangular and TFPs are bounded by these regions. The TFP regions lie across the border between insecure and secure sides. The width of each region may be different from each other and are generally narrow relative to the width of the whole field denoting narrow safe passages with respect to the intruders. If the width of the TFP region t_i is denoted with w_{t_i}, the ratio of TFP region to total width is

$$W_t = \frac{\sum_{i=1}^{N_t} w_{t_i}}{w} \tag{2.1}$$

where w is the border area width. The value of W_t is dependent on the scenario type and properties. It is generally low in the border surveillance scenarios. An intruder that will trespass through TFP selects one of the TFP regions, region t_i, with the probability p_{t_i}. The probability of selecting at least one of the TFP regions is

$$p_t = \sum_{i=1}^{N_t} p_{t_i} \tag{2.2}$$

where the value of p_t is also dependent on the scenario type and properties. It is generally high in the border surveillance scenarios because of travelers' bias towards these regions. A sample border area with two preferred regions is shown in Figure 2.2.

In the simulations, we assume that sensors operate according to the binary detection model, but the statistical tools that are presented can be easily applied to other sensing models, too. The binary detection model is a good approximation for the type of sensors which have sharp sensing ranges such as PIR sensors [66]. Many studies use the binary sensing model due to its simplicity. In this model, there is a range which determines the sensing probability in a certain manner. The detection probability of

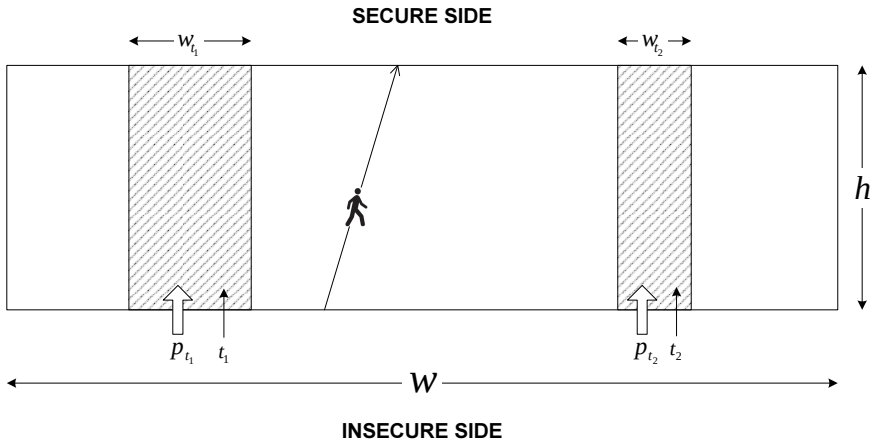

Figure 2.2. A sample field with two preferred regions.

the binary sensing is

$$P_D = \begin{cases} 1 & \text{if } d \leq r \\ 0 & \text{otherwise} \end{cases} \tag{2.3}$$

where r is the sensing range of the sensor and d is the distance between the target and the sensor.

2.2. Region Identification Problem

The travelers' favorite problem can be defined as dividing the border area into disjoint regions according to the preference probability by the travelers. The monitored zone is modeled as a grid and we know the positions of all sensors. The detection count of each sensor will be used for statistical analysis. We propose some methods that can be used in the identification of these regions and calculating the preferences of each region.

We assume that the sensors are distributed uniformly over the monitored zone. The number of detections made by a sensor that is located in region i is proportional to the preference rate of the region. If a target is detected at a point, this data can be stored and used for preference probability analysis. In that case, the region

identification problem can be stated as

$$\begin{aligned} &\text{Find } S = t_1 \bigcup t_2 \bigcup \ldots \bigcup t_i \\ &\text{s.t. } t_i \bigcap t_j = \emptyset, i \neq j \\ &\qquad N_{d,p_m} \sim N_{d,p_n}, m \neq n, p_m \in t_i, p_n \in t_i \end{aligned} \tag{2.4}$$

where $t_1, t_2, \ldots, t_i$ are the regions within the monitored zone, p_m and p_n are grid points and N_{d,p_m} and N_{d,p_n} are the number of detections belonging to these points, respectively. There are some issues in this approach. First of all, the storage of all detection statistics with location information in the sensor node requires a large amount of memory, which is a scarce resource. The transmission of this data to a central station for storage and processing requires large bandwidth and causes the sensor node to consume much of its limited and precious power supply. Even if the nodes have large amount of memory and an unlimited power supply such as a solar cell, the sensor network should have a complete coverage over the area to obtain reliable information about all points within the border area. For a wireless network to provide complete coverage, it should be densely deployed and all sensor nodes should be functioning without failure. This is generally far from the real life conditions. Another weak point of this problem is that, the detected locations of targets may not be accurate or the location of the target may not be calculated due to the capability restrictions of the sensor node. For the sake of applicability in real life conditions, we assume that we only have the detection count of each sensor and nothing else available. The detection count is an easy to collect and store statistics. It requires only a few bytes in the sensor node's memory storage and it is easy to transmit to the base station. Applying these restrictions, our original problem is transformed into

$$\begin{aligned} &\text{Find } S = t_1 \bigcup t_2 \bigcup \ldots \bigcup t_i \\ &\text{s.t. } t_i \bigcap t_j = \emptyset, i \neq j \\ &\qquad N_{d,s_m} \sim N_{d,s_n}, m \neq n, s_m \in t_i, s_n \in t_i \end{aligned} \tag{2.5}$$

where s_m and s_n are sensors that are located in the same region. Before further

inspecting this problem we will look at the mobility of intruders and the effects of their paths on the general detection distribution.

2.3. Effects of Mobility on the Detection Count

In our scenario, the intruders move from the insecure side to the secure side of the border area. A sample border surveillance scenario is shown in Figure 2.3. There is a watch tower and some part of the border area can be seen from the tower. Hence, most of the intrusions are being made through the region that is not observable from the watch tower. We assume that all intruders follow a straight path, which has more advantages compared to a segmented path for the benefit of the intruder. These advantages are explained and proved via simulations in the next chapter of the thesis.

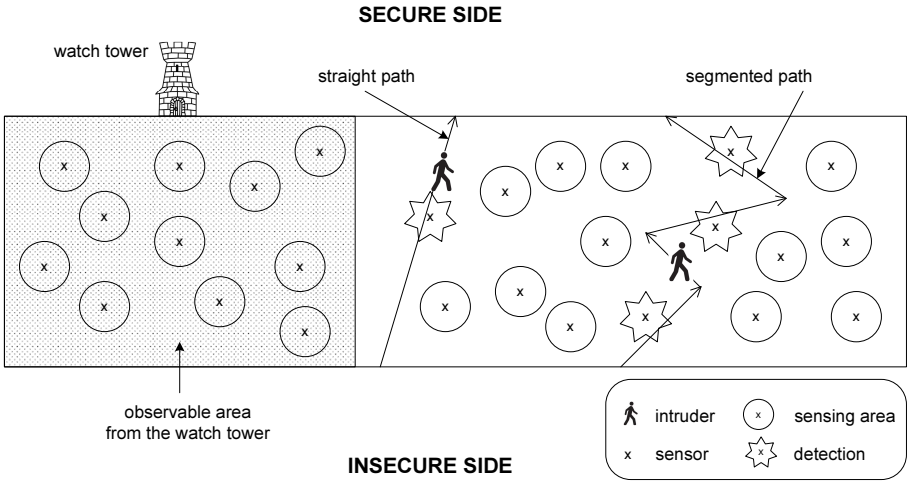

Figure 2.3. A border area with a watch tower.

This scenario can be represented as in Figure 2.4. The width of the observable area from the watch tower is denoted as w_1 and the width of the remaining area is $w_2 = w - w_1$. We draw some of the intruder paths represented with lines. We draw more lines in the region out of the visible range of the watch tower to represent its high preference ratio.

The direction and entry and exit point restrictions on the possible set of lines cause the intersection of the possible intruder paths to be denser in the center of the region. The probability of an intruder passing through a point in the center of the field is higher than passing through a point close to the side borders of the region. In order to show this effect more clearly, a heat map representing the density of lines passing through a region is prepared. For demonstrative purposes the dimensions of the heat

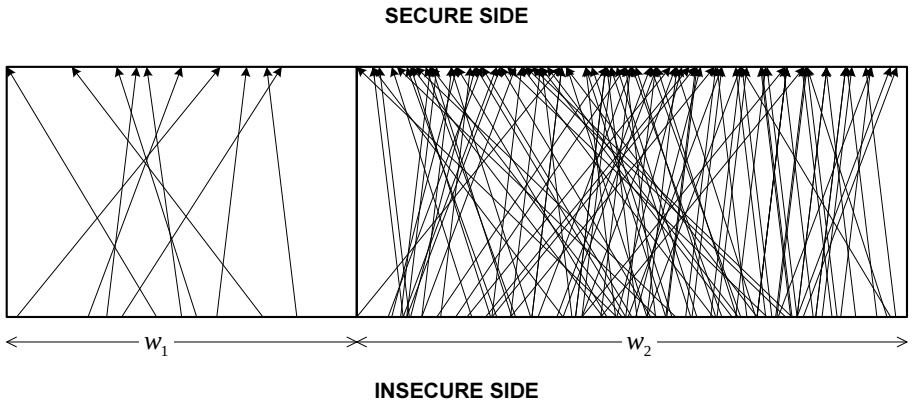

Figure 2.4. The graphical representation of intruder paths in a border area.

map region is selected to be $w = h = 100m$. The distance between each grid point is selected to be $1m$. The upper and lower sides of the heat map denotes the secure and insecure regions, respectively. All possible set of lines are drawn and the density corresponding to each grid point is calculated. The resulting heat map is shown in Figure 2.5. The heat map will help in understanding the shape of the statistical results to detect the region boundaries.

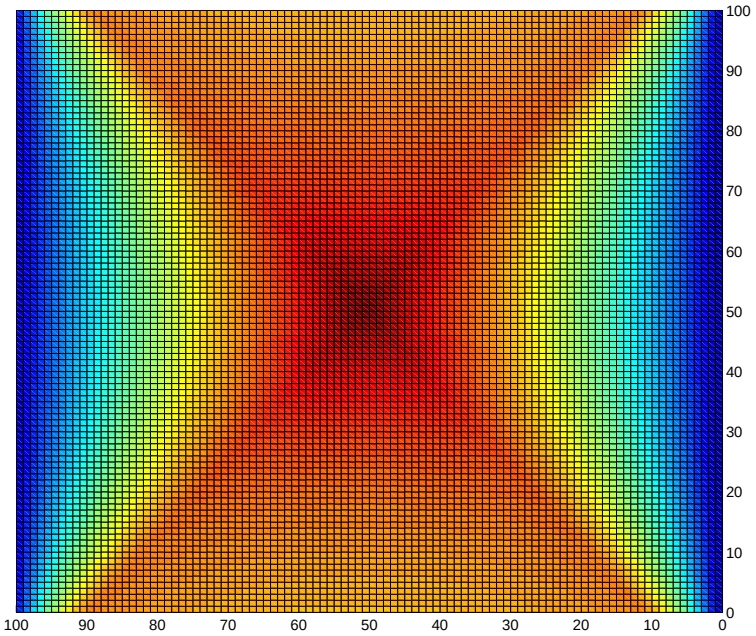

Figure 2.5. The heat map of possible intruder paths in a region.

2.4. Detection of the Region Boundaries

The heat map clearly shows that the expected number of detections will be most within the center of the region and will be less near the left and right side boundaries

of the region. The detection statistics of the sensor nodes is represented such that

$$N_{d,s} = \{N_{d,s_1}, N_{d,s_2}, \ldots, N_{d,s_i}\} \tag{2.6}$$

where N_{d,s_i} is the number of detections made by the sensor node s_i located at $s_i(x_i, y_i)$. The size of the statistics set $N_{d,s}$ is equal to the total number of sensors deployed which is N_s. The border area is divided into regions orthogonal to the x-axis and each region may have different preference probabilities as mentioned before in this chapter. It is important to estimate the boundaries of these regions and corresponding preference probabilities with minimum error in order to analyze the detection quality of the network correctly. In this section, we will provide two different methods that can be used for detection of the region boundaries.

For the simulation purposes, we investigated a border area consisting of two regions, each with equal length of $w_{t_1} = w_{t_2} = 500\ m$ and $h = 500\ m$. The simulation consists of 100 intruder passes. The preference of the first region is $p_{t_1} = 0.9$ and the second one is $p_{t_2} = 0.1$, 90 of the 100 intrusions are made through the first region and the remaining 10 are made through the second region. The number of sensors is 500 with binary sensing range, $r = 20\ m$, which are deployed to the border area in uniform random distribution.

2.4.1. Regional Maxima Method

In a typical border area, there are regions with different preference probabilities. The sensors in the highly preferred region will have high detection count and other sensors will have low detection count or no detection. To reveal the sensors that are in the highly preferred region, the initial step of the regional maxima method is to discard the sensors that have low detection count. For this purpose, we apply the filter

$$N_{d,s_i} = \begin{cases} N_{d,s_i} & \text{if } N_{d,s_i} \geq \mu, \\ 0 & \text{otherwise} \end{cases} \tag{2.7}$$

where μ is the mean of the detection data. This filter isolates the sensor nodes that have a detection count above the average. The elimination of these less critical sensors enable us to focus on more important sensor locations. Following the initial filtering

step, to find out the local maxima points, the regional maxima filter is applied. A regional maximum is a flat zone not adjacent to a flat zone with higher gray value [67]. The result is shown in Figure 2.6. The resulting figure shows only the points that have significant weight in the detection statistics and eliminates the rest. In our scenario, this corresponds to the region with the preference ratio of 0.9. The boundaries of this region can be easily found by fitting the convex region that contains all regional maxima points.

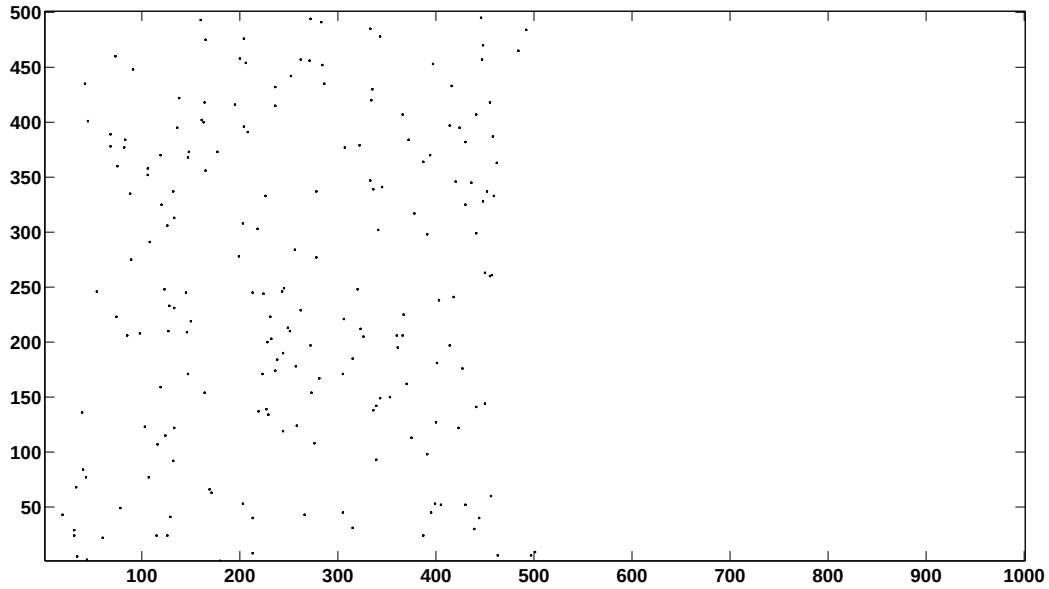

Figure 2.6. Detection data after local maxima filter is applied.

2.4.2. Contour Map Method

If the sensor points are represented with heights proportional to their detection count, we obtain a contour map. But, since the detection data is not based on the target detection location but the sensor location, the contour map will show only points corresponding to the locations of sensor nodes similar to the one shown in Figure 2.6. The detection data is averaged on the sensor coverage area of the sensor node by applying disk filter, so, the point based detection data is converted to coverage based 2-D detection data. The disk filter returns a circular averaging filter (pillbox) within the square matrix of side $2 * radius + 1$ [68]. When the disk filter is applied, a graphical representation of sensors with their relative detection count is obtained. A sample simulation result is shown in Figure 2.7 when $radius = r = 20$ where r is the sensing radius of sensors used in the simulation. This figure represents the sensor coverage

areas with an averaged detection value. The detection difference between sensor nodes are shown by the heat map and it is clear that some of the sensors are hotter than the others.

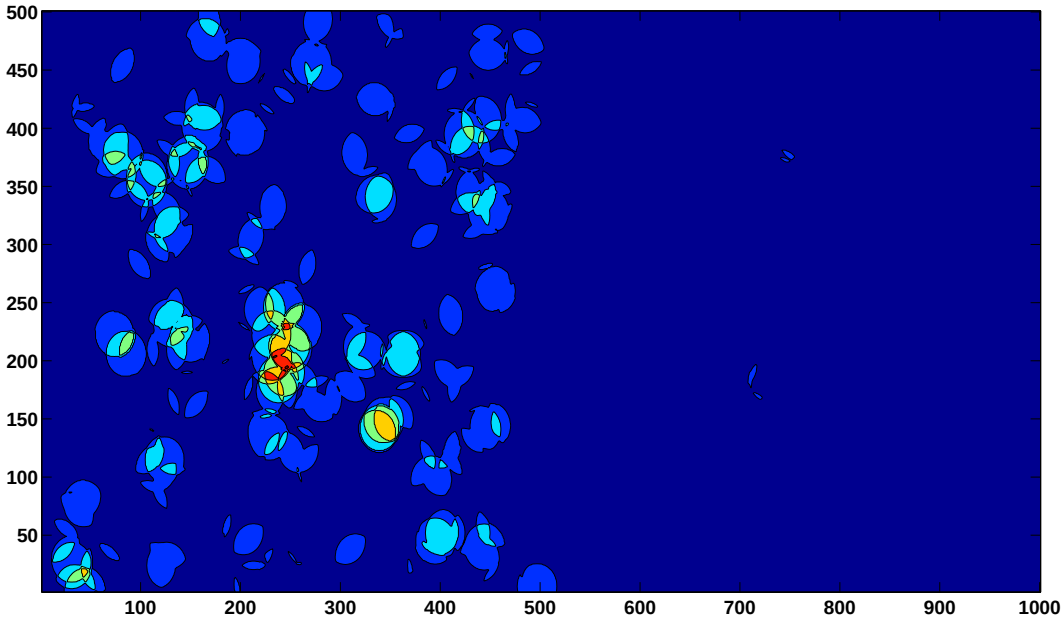

Figure 2.7. The contour map with disk filter $radius = 20$.

In order to reduce the effect of the physical coverage gaps between the sensors in the contour map, we need to apply a disk filter with a large enough radius that will provide an expected coverage ratio. The expected area that randomly placed circles may cover in a plane has been analyzed before by Hall [69]. He solved the problem of border effects in such a plane by using torus convention. Torus convention models the network topology in a way that nodes nearby the border are considered as being close to nodes at the opposite border. By modeling the deployment region as a torus a sensor's sensory region is considered completely within the deployment area. Let denote the area of the deployment region S with $A = w \cdot h$. Hall proves that when $N_s/A \rightarrow \kappa$ where $0 < \kappa < \infty$, the ratio of uncovered area in the deployment region approaches $e^{-\kappa\pi r^2}$ as r increases [69]. Using Hall's estimation we can obtain the radius of the disk filter that will provide a certain coverage degree ς such that

$$r = \sqrt{-\frac{ln(1-\varsigma)}{\kappa\pi}} \tag{2.8}$$

where $ln(x)$ is the natural logarithm of x. We choose the coverage degree as $\varsigma = 0.99$

and calculate the corresponding disk radius accordingly. The disk filter is applied to the detection data using the new radius and the improved contour map of the deployment area by the disk filter with the modified radius is shown in Figure 2.8. The extended coverage map also shows similarity with the heat map shown in Figure 2.5, where the intensity of detection counts are intense on the center of the region. The outer rim of the contour map is selected as the region boundary.

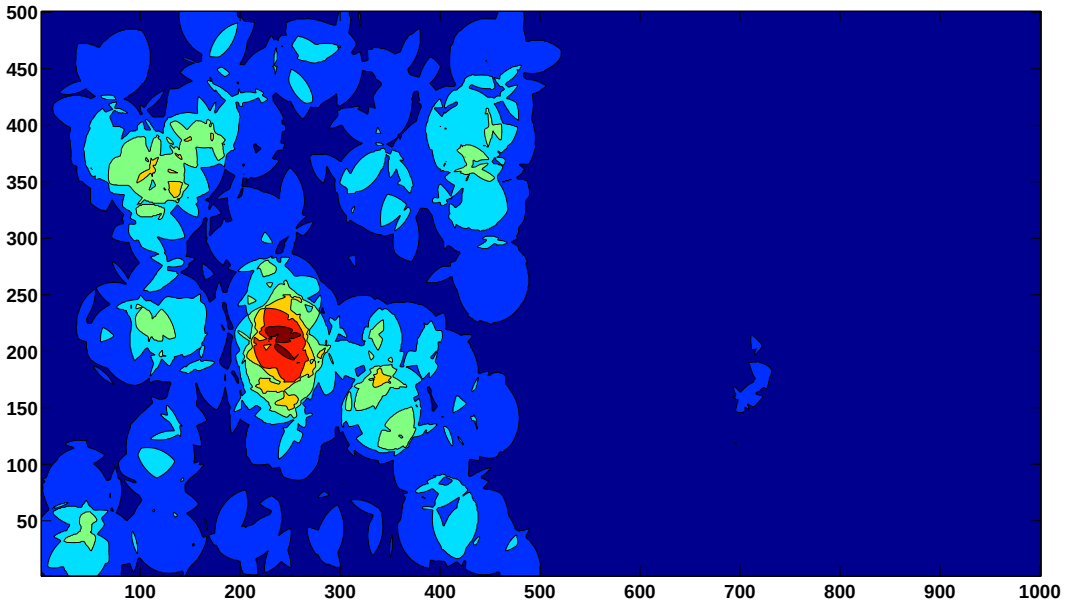

Figure 2.8. The contour map with modified disk filter.

In this section, we presented two different methods to calculate the boundaries of regions. The regional maxima method is effective in the scenarios where there is a large difference between the preference probabilities of regions. When the difference gets smaller, there appears some points that are not eliminated by the first filter. In that case, the final regional maxima figure contains some points that belong to different regions and an ambiguity between regions can occur. In order to eliminate these points the cut-off level of the elimination filter can be modified. The contour map method is a useful tool for representing the distribution of heat points and region centers among a border area. Using the contour map, a rough idea about the locations of and density of the regions can be obtained and by using this information, the performance of the regional maxima method can be improved.

2.5. Calculation of Preference Probabilities

After detecting the region borders, the preference probability is simply calculated according to the ratios of detection count of each region to the total detection count. The preference probability of region t_i is:

$$p_{t_i} = \frac{\sum\limits_{s_i \in t_i} N_{d,s_i}}{\sum\limits_{j=1}^{N_s} N_{d,s_j}} \tag{2.9}$$

where N_s is the total number of the sensors. The calculated preference probabilities of regions according to the simulation results are given in Table 2.1. As seen from the table, the calculated probabilities are very close to the actual values.

Table 2.1. Preference probability according to detection count.

	Region 1	**Region 2**	**Total**
Detection Count	1899	207	2106
Ratio	0.902	0.098	

In this chapter, we defined the travelers' favorite path problem and presented some methods to solve it. The presented methods that utilize some image processing and the statistical analysis tools can be used in the identification of the regions in a border area. In addition to the presented methods, alternative methods may be devised that can be used in the region identification process and improve its performance. In addition to this, there are various means to improve the accuracy of the given region localization method. If the number of sensors in the border area is increased, the accuracy of the statistics will increase and the segmentation process will be finer. In addition to this, the size of the collected data and more detailed information such as the precise coordinates of the detected target within the sensing range may also improve the quality of the region identification process.

3. DETECTION QUALITY MEASURE PROBLEM

In this chapter, we describe the detection quality measure problem. Using tools from the geometric probability, we present how to calculate the detection quality measure for a given surveillance wireless network.

3.1. Detection Quality Measure Problem in a Field with Single Region

The performance of a SWSN can be measured with its target detection probability, which is defined as the detection of the target moving inside the monitored zone by at least one sensor node. We define the detection quality measure problem as calculating the detection probability of the target moving in the monitored zone from one side to another.

3.1.1. Network Model

In the detection probability analysis, we assume a convex 2-D border area, S, which is further simplified to a rectangle that has a width of w and a height of h for demonstrative purposes. There are N_s sensors deployed randomly within the area. Each sensor s_i is assumed to have convex sensing coverage of S_i with radius r_i, uniformly and independently distributed within S. The border area separates the secure side from the insecure side. The direction of the trespassing is from insecure side to the secure side, thus along the y-axis of the region. There is one TFP region in which the TFPs reside. The location of the TFP region is not known by the network operators but known by the trespassers. The probability of selecting the TFP region for trespassing by an intruder is p_t. The width of the TFP region is w_t.

We assume that, the intruders have limited or no knowledge about the deployment of the sensor network similar to the assumptions in [70]. On the other hand, the intruders have knowledge about other security measures such as the locations of watch towers, mine fields and highly patrolled areas. They try to avoid these non-sensor detection measures by selecting preferable paths which they possibly have learnt from previous experiences. Thus, we can say that the location of the TFP paths are indirectly determined by the conventional intrusion surveillance methods. The coordinates of the TFP region that consists of the TFP paths is not known by the network operators.

The sensor deployment is done with an airplane or artillery because of the acces-

sibility difficulties to the border region. The sensor nodes are distributed in a random manner over the area. The intruder has no knowledge about the coordinates of the sensor nodes in the monitored zone. If the intruder had the deployment map of the sensor network, he could avoid detection by following longer but safer paths around the sensor nodes. However, the lack of such information prevents the intruder to take such evasive actions and enforces him to choose the path which will reduce his exposure probability. The path which minimizes the detection probability under these conditions is the shortest path from the entry point to the exit point. Such linear paths are the least detection paths with respect to the intruder. Although this situation limits the path diversity and excludes the curved and segmented paths, it is a preferred choice for the benefit of the intruder. One advantage of using a linear trajectory is that, the worst detection performance of the sensor network can be calculated which is an important threshold for the network quality. As seen in Figure 3.1, segmented paths are generally longer than the straight path, and the detection probability of the intruder following a segmented or curved path increases significantly. In Section 3.1.4, we show the validity of this statement by the simulations. Other advantage of the straight line path is the parametrization of linear trajectories which can be easily applied both in the analytical studies and physical representation of the network model.

The sensors operate using a binary detection model. In this model, if the target is within the sensing range of the sensor node, it is certainly detected. If the target is out of the sensing range, it avoids detection. Though it is a simple model, it can be safely used for micropower impulse radar (MIR) sensors. The MIR sensors are radar-based low-power sensors that use ultra-wideband (UWB) pulses [71, 72]. Their range are relatively larger compared to other types of sensors which make them more preferable in border surveillance sensor networks. There are commercially available MIR sensors such as SEGA-Node TIMS Radar [33]. In the MIR sensors, a transmitting antenna radiates a pulse. Reflections from the target are listened by a receiving antenna, and using the time difference, the distance of the target is calculated [73].

3.1.2. Problem Definition

In this section, we will provide a formal definition of the border SWSN intruder detection problem with a TFP region. Moreover, we will provide two additional prob-

lems which will be mapped to each other to derive a solution for the geometric domain utilizing metrics and tools from Integral Geometry and Geometric Probability.

Problem 3.1. ***Border surveillance intruder detection with TFP region problem:*** *We have a convex deployment area, S, sensed by N_s sensors where each sensor s_i has a sensing coverage S_i with a radius of r_i, uniformly and independently distributed within S. The deployment area separates the insecure region from the secure one. The trespassers enter into the deployment area from the insecure side and exit from the secure side, following a linear trajectory. The trespassers prefer the TFP region with probability p_t and make their passage through this region. They choose any other path within the border area with probability of $p_{\overline{t}}$. What is the probability P_D that an intruder X randomly crossing S is detected by at least one sensor?*

A graphical representation of Problem 3.1 is given in Figure 3.1. The probability P_D is defined as the detection quality measure (DetQM) of such a sensor network.

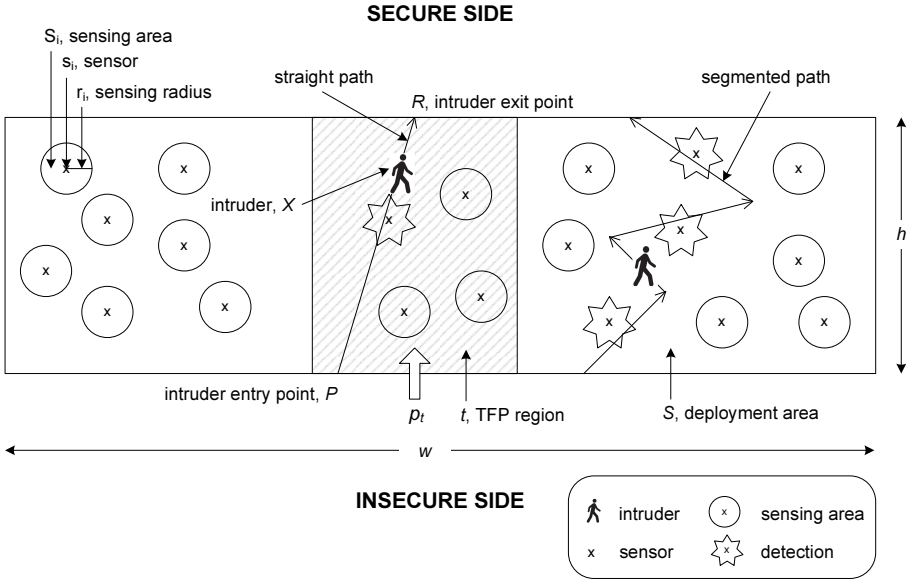

Figure 3.1. Border surveillance intruder detection with TFP region problem.

The solution of this problem requires the calculation of the probability of detection for a set of sensors in the network. In order to provide a solution for this problem, we introduce two additional problems. The first one, Problem 3.2, is the simplified version of Problem 3.1 which does not consider any TFP regions. The second one, Problem 3.3, corresponds to the geometric interpretation of such a sensor network. We

will provide a mapping between these two problems to show that they are equivalent, so, both can be reduced to each other.

Problem 3.2. ***Border surveillance intruder detection problem:*** *We have a convex deployment area, S, sensed by N_s sensors where each sensor s_i has a sensing coverage S_i with a radius of r_i, uniformly and independently distributed deployed within S. The deployment area separates the insecure side from the secure one. The trespassers enter into the deployment area from the insecure side and exit from the secure side, following a linear trajectory. What is the probability P_D that an intruder X randomly crossing S is detected by at least one sensor?*

Problem 3.3. ***Constrained Line-Set intersection problem:*** *We have a bounded convex set C of identical shape with S and N_s sets C_i of identical shape with S_i in Problem 3.2, uniformly and independently distributed inside C. What is the probability P_D that a random line G intersecting C with the same constraints as in Problem 3.2, also intersects at least one of the sets C_i, $i = 1 \ldots N_s$?*

Our analytical study relies on the fact that these two problems can be reduced to each other with a bijection between physical and geometric domains. The following lemma presents this bijection.

Lemma 3.4. *Border surveillance intruder detection problem and the constrained line-set intersection problem are equivalent, so, they can be reduced to each other with a bijective mapping.*

Proof. We provide our proof extending the method used in [39]. The deployment area S is represented in the map domain as a collection of points, C, each representing a coordinate in S. Clearly, the 2-D geometric representation, C, is of identical shape with S. Hence we map the the deployment area, S, to the bounded and convex set C. By the same rationale, the sensing area, S_i of sensor s_i is mapped to the bounded set C_i of identical shape with S_i, uniformly and independently distributed in C. The geometric representation of a linear trajectory of an intruder X is a straight line $G(p, \phi)$ in the plane, defined by p as the shortest distance of G to the origin O of a coordinate system, and ϕ as the angle of the line perpendicular to G with respect to the x axis. Clearly, the intersection constraints of the line G with set C and C_i are the same as the

trespassing constraints in the geographic domain. This provides a mapping between the mobile target detection problem for a stochastic sensor network and the line-set intersection problem. Hence, we conclude that both problems are equivalent. □

The mapping stated in Lemma 3.4 between Problem 3.2 and Problem 3.3, provides a bijection between the physical sensor network domain and the geometric domain. In the next section, we will provide a solution for the probability of detection of a target by a single sensor in the geometric domain since we have shown that Problem 3.2 and Problem 3.3 can be reduced to each other. The provided solution will be extended to derive the detection for a given set of sensors. Next, we will integrate the effect of the TFP region and TFP probability, in this formulation. Finally, we will provide a closed-form solution for the probability of detection in Problem 3.1.

3.1.3. Detection Quality Measure

In this section, we will find an analytical representation of the DetQM metric for a border SWSN with TFP region. Since we have shown that the probability of target detection P_D is equivalent to the probability of lines to intersect geometric shapes, the problem can be simplified as a frequency count of lines intersecting geometric shapes. In our problem, we consider only the set Υ of all possible linear trajectories crossing the deployment area from the insecure side to secure side with some constraint. Therefore, P_D is equal to the quotient of the number of lines that intersect any of the sensing areas, over the number of lines that intersect the deployment area given that these lines are in Υ. However, the set of lines in Υ intersecting a given convex set is uncountable.

Hence we will introduce the line measure tool from the integral geometry to derive an analytical solution to the Line-Set intersection problem. For any straight line $G(p, \phi)$, the density of the line is formulated as

$$dG = dp \wedge d\phi \tag{3.1}$$

The measure $m(G)$ of a set of lines $G(p, \phi)$ is the integral of the density of the line, which is in the differential form, over the set [74]. Hence,

$$m(G) = \int dp \wedge d\phi \tag{3.2}$$

Our problem requires these lines to cross insecure and secure sides of the deployment area with possibly more constraints. Such lines constitute the subset Υ of the lines measured in Equation 3.2. Hence we need a geometric interpretation of the measure of a given set of lines. For this purpose, we introduce the notion of the thickness of a bounded set for lines determined by angle ϕ in set Υ, $T(\Upsilon_\phi)$, where $\Upsilon_\phi = \{G(p,\phi) : G \in \Upsilon\}$.

Let U be the intersection of set C with Υ_ϕ, the area of the region traversed by the lines determined by angle ϕ in the line set Υ. $T(\Upsilon_\phi)$ is defined as the length of the projection of U to a line with direction parameter ϕ [74]. The measure of a set of lines intersecting with C at a fixed direction ϕ and in line set Υ is equal to the thickness $T(\Upsilon_\phi)$ of the set in that direction. Let δ be the event $C \cap \Upsilon_\phi \neq \emptyset$ and $\overline{\delta}$ be the complement of δ, i.e. $C \cap \Upsilon_\phi = \emptyset$. Given that the trajectories are constrained to be in the set, Υ, the measure of the set of lines in Υ that pass over a bounded convex set, C, defined by the support function $p = p(\phi)$ of the convex set, is given as:

$$\begin{aligned} m(G : G \cap C \neq \emptyset | G \in \Upsilon, \delta) &= \int_{G \cap C \neq \emptyset | G \in \Upsilon, \delta} dp \wedge d\phi \\ &= \int_{\alpha_1}^{\alpha_2} T(\Upsilon_\phi) d\phi \\ &= (\alpha_2 - \alpha_1)\, E(T) \end{aligned} \tag{3.3}$$

where α_1 and α_2 are the minimum and maximum values respectively for parameter ϕ of lines in Υ and $E(T) = \int_{\alpha_1}^{\alpha_2} \frac{1}{\alpha_2 - \alpha_1} T(\Upsilon_\phi) d\phi$. Since the border area is convex and the trespasser trajectories are linear from the insecure to the secure side, the target trajectories in Υ are allowed to have parameters in range $[\alpha_1, \alpha_2]$. By Equation 3.3, the average thickness of the set of lines for a given constraint on line-set intersection, Υ can be used to calculate the intersection of a random line with a convex set C_i within C, which will be used for the proof of the following lemma.

Lemma 3.5. *Let S be the deployment area of a sensor network and let s_i be any of the sensors deployed in the area. The probability that an intruder randomly passing through S with a trajectory from the line set, Υ, is detected by the single sensor, s_i is*

equal to

$$P_{s_i} = \frac{E(T_i)}{E(T)} \frac{E(A_T)}{A}, \tag{3.4}$$

where $E(T_i)$ is the average thickness of the sensor coverage area, $E(T)$ is the average thickness of the deployment area for the given line-set intersection constraint which determines Υ, $E(A_T)$ is the average area of the deployment site covered by lines in Υ and A denotes the area of the deployment site.

Proof. The probability that an intruder randomly passing through S with a trajectory in Υ is detected by a single sensor, s_i, is derived as follows. By the mapping of the intruder detection problem to line-set intersection problem provided in Lemma 3.4, this probability is equivalent to the probability that a line G intersecting C in line set Υ, also intersects C_i. In terms of the measures, this probability is equal to the ratio of the measure of the set of lines in Υ that intersect both C and C_i to the measure of the set of lines that intersect C.

$$\begin{aligned}
P_{s_i} &= Pr\left[G \cap C_i \cap C \neq \emptyset | G \cap C \neq \emptyset, G \in \Upsilon\right] \\
&= Pr\left[G \cap C_i \cap C \neq \emptyset | G \cap C \neq \emptyset, G \in \Upsilon, \delta\right] Pr\left[\delta\right] \\
&+ Pr\left[G \cap C_i \cap C \neq \emptyset | G \cap C \neq \emptyset, G \in \Upsilon, \overline{\delta}\right] Pr\left[\overline{\delta}\right] \\
&= \frac{m(G : G \cap C_i \cap C \neq \emptyset | G \in \Upsilon, \delta)}{m(G : G \cap C \neq \emptyset | G \in \Upsilon, \delta)} Pr\left[\delta\right] \\
&+ \frac{m(G : G \cap C_i \cap C \neq \emptyset | G \in \Upsilon, \overline{\delta})}{m(G : G \cap C \neq \emptyset | G \in \Upsilon, \overline{\delta})} Pr\left[\overline{\delta}\right]
\end{aligned} \tag{3.5}$$

The measure of the set of lines is 0 if the convex set does not intersect with the area $A_{T(\Upsilon_\phi)}$ of the region traversed by the lines determined by angle ϕ in the line set Υ. In addition, C_i is known to be inside the convex set C. Hence, Equation 3.5 can be reduced to

$$P_{s_i} = \frac{m(G : G \cap C_i \neq \emptyset | G \in \Upsilon, \delta)}{m(G : G \cap C \neq \emptyset | G \in \Upsilon, \delta)} Pr\left[\delta\right] \tag{3.6}$$

The expected area of the regions determined by ϕ measured in Υ is given as:

$$E(A_T) = \int_{\alpha_1}^{\alpha_2} \frac{1}{\alpha_2 - \alpha_1} A_{T(\Upsilon_\phi)} d\phi \tag{3.7}$$

The probability that a sensor s_i to reside in this expected area determined by Υ is found as:

$$Pr\left[\delta\right] = \frac{E(A_T)}{A} \tag{3.8}$$

Using Equation 3.3 and Equation 3.8, Equation 3.6 becomes

$$P_{s_i} = \frac{(\alpha_2 - \alpha_1)\, E(T_i)}{(\alpha_2 - \alpha_1)\, E(T)} \frac{E(A_T)}{A} = \frac{E(T_i)}{E(T)} \frac{E(A_T)}{A} \tag{3.9}$$

□

Thus, using the mapping provided in Lemma 3.4, the probability that an intruder randomly passing through S is detected by a single sensor, s_i, is found in terms of $E(T)$, the expected thickness of deployment area, and $E(T_i)$, the expected thickness of the sensing coverage of a sensor. Now, we need to derive the detection quality of a sensor network with a trespasser trajectory in line set Υ with no favorite paths, i.e. the selection of all trajectories are equally likely.

Theorem 3.6. *The DetQM of any sensor network with N_s sensors deployed in the area with a trespasser trajectory pattern determined by the line set Υ with no favorite paths is*

$$P_D = 1 - \prod_{i=1}^{N_s} \left(1 - \frac{E\left(T_i\right)}{E(T)} \frac{E\left(A_T\right)}{A}\right) \tag{3.10}$$

where $E(T_i)$ is the average thickness of the sensor coverage area, $E(T)$ is the average thickness of the deployment area for the given line-set intersection constraint which determines Υ, $E(A_T)$ is the average area of the deployment site covered by lines in Υ and A denotes the area of the deployment site.

Proof. By Lemma 3.5, the probability of all sensors to miss the target, $P_{\overline{D}}$ and the overall target detection probability, P_D are calculated as:

$$\begin{aligned} P_{\overline{D}} &= \prod_{i=1}^{N_s} (1 - P_{s_i}) \\ &= \prod_{i=1}^{N_s} \left(1 - \frac{E(T_i)}{E(T)} \frac{E(A_T)}{A}\right) \end{aligned} \tag{3.11}$$

$$\begin{aligned} P_D &= 1 - P_{\overline{D}} \\ &= 1 - \prod_{i=1}^{N_s} \left(1 - \frac{E(T_i)}{E(T)} \frac{E(A_T)}{A}\right) \end{aligned} \tag{3.12}$$

□

Next, we will generalize Theorem 3.6 for the cases where trespassers follow favorite paths in the deployment site.

Theorem 3.7. *The DetQM of any sensor network with N_s sensors deployed in the area with a trespasser trajectory pattern determined by the line set Υ with favorite paths in the TFP region is*

$$\begin{aligned} P_D = 1 &- p_t \cdot \prod_{i=1}^{N_s} \left(1 - \frac{E(T_i)}{E(T_t)} \frac{E(A_{T_t})}{A}\right) \\ &- (1 - p_t) \cdot \prod_{i=1}^{N_s} \left(1 - \frac{E(T_i)}{E(T - T_t)} \frac{E(A_T - A_{T_t})}{A}\right) \end{aligned} \tag{3.13}$$

where p_t is the probability of the trespassers to follow favorite paths, $E(T_t)$ and $E(T-T_t)$ are the average thickness of TFP and non-TFP regions respectively, whereas $E(A_{T_t})$ and $E(A_T - A_{T_t})$ are the average area of the TFP and non-TFP regions respectively covered by lines in Υ which satisfies the region crossing constraints.

Proof. Since, TFP region is a subset of the deployment area, the target detection probability in the TFP region is calculated using the subset of lines satisfying the region crossing constraints, Υ_t:

$$P_{D|t} = 1 - \prod_{i=1}^{N_s} \left(1 - \frac{E\left(T_i\right)}{E(T_t)} \frac{E\left(A_{T_t}\right)}{A}\right) \tag{3.14}$$

Similarly, for the non-TFP region which is the complement of the TFP region, we calculate the target detection probabilities using the measure of the set $\Upsilon_{\overline{t}} = \Upsilon \setminus \Upsilon_t$:

$$P_{D|\overline{t}} = 1 - \prod_{i=1}^{N_s} \left(1 - \frac{E\left(T_i\right)}{E(T_{\overline{t}})} \frac{E\left(A_{T_{\overline{t}}}\right)}{A}\right) \tag{3.15}$$

Since $\Upsilon_{\overline{t}}$ and Υ_t are disjoint, by the definitions of $E(T_{\overline{t}})$ and $E\left(A_{T_{\overline{t}}}\right)$,

$$\begin{aligned} E(T_{\overline{t}}) &= \int_{\alpha_1}^{\alpha_2} \frac{1}{\alpha_2 - \alpha_1} T(\Upsilon_{\overline{t},\phi}) d\phi \\ &= \int_{\alpha_1}^{\alpha_2} \frac{1}{\alpha_2 - \alpha_1} \left(T(\Upsilon_\phi) - T(\Upsilon_{t,\phi})\right) d\phi \\ &= E(T - T_t) \end{aligned} \tag{3.16}$$

$$\begin{aligned} E\left(A_{T_{\overline{t}}}\right) &= \int_{\alpha_1}^{\alpha_2} \frac{1}{\alpha_2 - \alpha_1} A_{T(\Upsilon_{\overline{t},\phi})} d\phi \\ &= \int_{\alpha_1}^{\alpha_2} \frac{1}{\alpha_2 - \alpha_1} \left(A_{T(\Upsilon_\phi)} - A_{T(\Upsilon_{t,\phi})}\right) d\phi \\ &= E\left(A_T - A_{T_t}\right) \end{aligned} \tag{3.17}$$

By the definition of the conditional probability, the detection probability of the trespasser is found as:

$$P_D = P_{D|t} \cdot p_t + P_{D|\overline{t}} \cdot p_{\overline{t}} \tag{3.18}$$

which yields Equation 3.13. □

In our derivations, we only require all sets to be convex and bounded. However for simplicity, we assume circular sensing coverage, and rectangular deployment area. The following corollary is a demonstrative example for our analysis. Simulations are based on this corollary.

Corollary 3.8. *If the sensors have identical circular sensing coverage, then the DetQM of a sensor network with a rectangular deployment area is equal to:*

$$P_D = 1 - p_t \cdot \left(1 - \frac{2r}{E\left(T_t\right)} \cdot \frac{E\left(A_{T_t}\right)}{h \cdot w}\right)^{N_s} - \left(1 - p_t\right) \cdot \left(1 - \frac{2r}{E\left(T_{\bar{t}}\right)} \cdot \frac{E\left(A_{T_{\bar{t}}}\right)}{h \cdot w}\right)^{N_s} \tag{3.19}$$

and

$$\begin{aligned}
&\theta = \arctan(h/w_t) \\
&\gamma = \arctan(h/w) \\
&T(\Upsilon_{\frac{\pi}{2}+\alpha}) = w\sin(\alpha) - h\cos(\alpha) \\
&T(\Upsilon_{t,\frac{\pi}{2}+\alpha}) = w_t\sin(\alpha) - h\cos(\alpha) \\
&E\left(T_t\right) = \int_{\theta}^{\pi-\theta} \frac{T(\Upsilon_{t,\frac{\pi}{2}+\alpha})}{\pi - 2\theta} d\alpha \\
&E\left(T_{\bar{t}}\right) = \int_{\gamma}^{\pi-\gamma} \frac{T(\Upsilon_{\frac{\pi}{2}+\alpha}) - T(\Upsilon_{t,\frac{\pi}{2}+\alpha})}{\pi - 2\gamma} d\alpha \\
&E\left(A_{T_t}\right) = \int_{\theta}^{\pi-\theta} \frac{T(\Upsilon_{t,\frac{\pi}{2}+\alpha})\frac{h}{\sin(\alpha)}}{\pi - 2\theta} d\alpha \\
&E\left(A_{T_{\bar{t}}}\right) = \int_{\gamma}^{\pi-\gamma} \frac{\left(T(\Upsilon_{\frac{\pi}{2}+\alpha}) - T(\Upsilon_{t,\frac{\pi}{2}+\alpha})\right)\frac{h}{\sin(\alpha)}}{\pi - 2\gamma} d\alpha
\end{aligned} \tag{3.20}$$

where r is the radius of the sensing coverage of a sensor, w_t is the width of the TFP region, w is the width of the deployment are and h is the height of the deployment area.

Proof. A sample rectangular deployment site is illustrated in Figure 3.2 to be used throughout this proof. The whole border region is represented with the rectangle $ABCD$. The width of the border region is w and the height of the border region is h. The shaded region within the rectangle $KLMN$ shows the TFP region which includes the TFPs in the border. The width of the TFP region is w_t whereas the height is equal to h. The sensors deployed within the border area have circular sensing with a radius of r. On the figure, only one of the deployed sensors is shown as a sample. The rest of the figure is explained within the analysis.

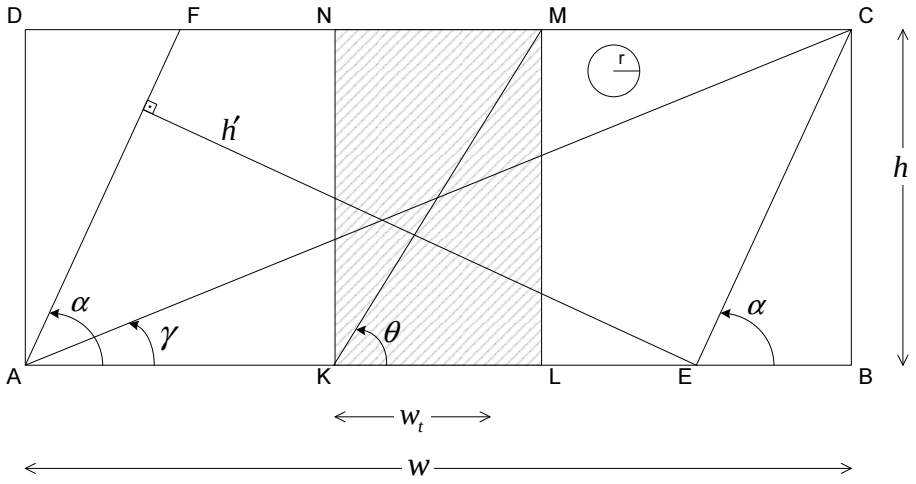

Figure 3.2. The representation of a rectangular deployment site.

By the assumption of identical circular sensing coverage for the sensors, the average thickness of each sensor is equal to the diameter of the circle which is $2r$.

The trajectories in Υ are restricted to pass through the deployment site from the insecure side (bottom side) to the secure side (top side). Hence, the lower bound of these linear trajectories is the angle γ, which is the angle between the diagonal of the rectangle and the x axis. Similarly, the upper bound is the angle of the opposite diagonal which is $\pi - \gamma$. In addition, since the height of the site is h and the width of the site is w, we have:

$$\gamma = \arctan(h/w) \tag{3.21}$$

In the same way, trajectories in the subset Υ_t pass through the TFP region of width w_t and are bounded by the angles, θ and $\pi - \theta$, where

$$\theta = \arctan(h/w_t) \tag{3.22}$$

The thickness of the lines with slope α is determined by measuring the set of lines in Υ_ϕ and $\Upsilon_{t,\phi}$ where $\phi = \frac{\pi}{2} + \alpha$ since these lines are parameterized by the slope of the perpendicular line passing from the origin. The thickness of Υ_ϕ and $\Upsilon_{t,\phi}$ are equal to the height h' and h'_t of the parallelograms respectively formed by the lines with slope

α. Clearly

$$h' = T(\Upsilon_{\frac{\pi}{2}+\alpha}) = w\sin(\alpha) - h\cos(\alpha)$$
$$h'_t = T(\Upsilon_{t,\frac{\pi}{2}+\alpha}) = w_t\sin(\alpha) - h\cos(\alpha) \tag{3.23}$$

The average thickness of the TFP region is equal to the average of the thicknesses, h'_t, of the parallelograms formed by lines in all directions between θ and $\pi - \theta$.

$$E\left(T_t\right) = \int_{\theta}^{\pi-\theta} \frac{T(\Upsilon_{t,\frac{\pi}{2}+\alpha})}{\pi - 2\theta} d\alpha \tag{3.24}$$

Since the TFP trajectories does not belong to $\Upsilon_{\bar{t},\phi}$, the thickness of the non-TFP region can be found by subtracting the measure of lines in $\Upsilon_{t,\phi}$ from the measure of Υ_{ϕ}. This is equivalent to subtracting the thickness h'_t from thickness of the deployment area, h'. Hence, the average thickness of the non-TFP region is equal to the average of the thicknesses, $h' - h'_t$, of the parallelograms formed by lines in all directions between γ and $\pi - \gamma$. Note that, $h'_t = 0$ if $\alpha \notin [\theta, \pi - \theta]$, since $\Upsilon_{t,\frac{\pi}{2}+\alpha} = \emptyset$.

$$E\left(T_{\bar{t}}\right) = \int_{\gamma}^{\pi-\gamma} \frac{T(\Upsilon_{\frac{\pi}{2}+\alpha}) - T(\Upsilon_{t,\frac{\pi}{2}+\alpha})}{\pi - 2\gamma} d\alpha \tag{3.25}$$

The average area of the TFP region covered by Υ_t is equal to the average of the areas, $A_{T(\Upsilon_{t,\phi})}$, of the parallelograms formed by lines in all directions between θ and $\pi - \theta$. The thickness h'_t of the region formed by trajectories with slope α is the height of the parallelogram. The length of these trajectories in TFP region is equal to $\frac{h}{\sin(\alpha)}$. Hence the average area $E\left(A_{T_t}\right)$ is equal to:

$$\begin{aligned} E\left(A_{T_t}\right) &= \int_{\theta}^{\pi-\theta} \frac{h' \cdot \frac{h}{\sin(\alpha)}}{\pi - 2\theta} d\alpha \\ &= \int_{\theta}^{\pi-\theta} \frac{T(\Upsilon_{t,\frac{\pi}{2}+\alpha}) \cdot \frac{h}{\sin(\alpha)}}{\pi - 2\theta} d\alpha \end{aligned} \tag{3.26}$$

Similar to the derivation of $E\left(T_{\bar{t}}\right)$, the area of the non-TFP region covered by $\Upsilon_{\bar{t},\phi}$ is derived by subtracting the area of the TFP region covered by $\Upsilon_{t,\phi}$ from the area of the deployment area covered by Υ_{ϕ}. Hence the average area $E\left(A_{T_{\bar{t}}}\right)$ is equal to:

$$\begin{aligned} E\left(A_{T_{\bar{t}}}\right) &= \int_{\theta}^{\pi-\theta} \frac{\left(A_{T(\Upsilon_{\frac{\pi}{2}+\alpha})} - A_{T(\Upsilon_{t,\frac{\pi}{2}+\alpha})}\right)}{\pi - 2\gamma} d\alpha \\ &= \int_{\theta}^{\pi-\theta} \frac{\left(h' \cdot \frac{h}{\sin(\alpha)} - h'_t \cdot \frac{h}{\sin(\alpha)}\right)}{\pi - 2\gamma} d\alpha \\ &= \int_{\theta}^{\pi-\theta} \frac{(h' - h'_t) \cdot \frac{h}{\sin(\alpha)}}{\pi - 2\gamma} d\alpha \\ &= \int_{\gamma}^{\pi-\gamma} \frac{\left(T(\Upsilon_{\frac{\pi}{2}+\alpha}) - T(\Upsilon_{t,\frac{\pi}{2}+\alpha})\right) \frac{h}{\sin(\alpha)}}{\pi - 2\gamma} d\alpha \end{aligned} \tag{3.27}$$

We provide the derivations for the list of equations in Equation 3.20. By substituting these equations in Equation 3.13, we provide Equation 3.19. □

In this section, we derived a formulation for the probability of intruder detection in a border surveillance sensor network using the line measure and thickness tools from the geometric probability. The initial formulation covers the heterogenous sensing coverage and convex bounded condition. The closed form formulation is further simplified by the assumption of homogenous and circular sensing coverage and a rectangular deployment site.

3.1.4. Straight Trajectory vs. Segmented Trajectory

We assume that the intruder follows a straight path within the monitored zone. This assumption is made to observe the worst case performance of the network. If the intruder follows a segmented path instead of a straight path, the detection probability increases and so the performance of the network. The performance difference between two cases are shown using simulations.

Straight and segmented trajectory simulations are run within a border area with uniform random deployment using the same dimension and deployment parameters. Two sample trajectories are depicted in Figure 3.1. In the straight trajectory case, the intruder X follows the straight path L between the entry point P and the exit point R. In the segmented trajectory case, the intruder follows a path L' with ψ waypoints

between the entry point P' and exit point R' such that:

$$L' = \{(P'(x_0, 0), \psi_1(x_1, y_1), ..., \psi_i(x_i, y_i), R'(x_{i+1}, h)\} \tag{3.28}$$

where

$1 \leq i \leq \psi_{max}$

$0 \leq y_1 \leq ... \leq y_i \leq h$

The simulations are run in a single region border scenario with height $h = 2000\ m$ and width w changing between 2000 m and 10000 m. There are 100 sensors deployed to the region. The maximum number of waypoints is $\psi_{max} = 5$. This means that an intruder moving along a segmented trajectory will change direction at most 5 times following a path consisting of maximum 6 segments until reaching the other side. The number of waypoints is selected to be uniform random between 1 and 5 for each trajectory. The direction change at each waypoint is limited to forward direction, there is no turning back in the followed path.

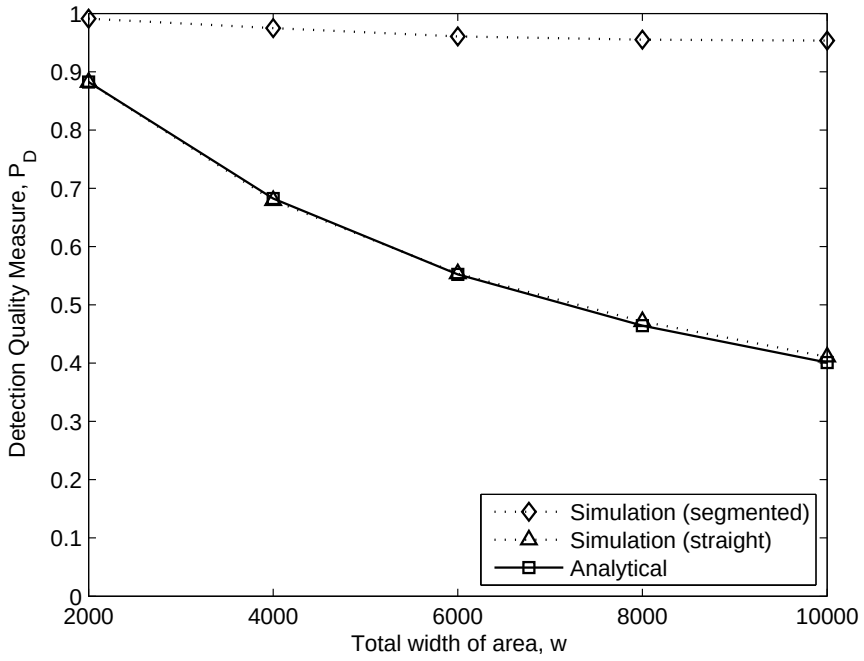

Figure 3.3. Detection probability using straight and segmented trajectories.

Another set of simulations are done in order to see the effect of the segment

count on the detection probability. In this scenario, the height and width of the region are kept constant, $h = 2000\ m$ and $w = 10000\ m$, respectively. There are 100 sensors deployed to the region. The number of segments within the segmented path is increased from 1 to 8, and kept constant at each simulation set. The detection probability is measured and plotted for different segment counts. The result is shown in Figure 3.4. The initial point of the figure in which there is only one segment within the trajectory also corresponds to the straight trajectory case. The detection probability increases with each segment count and reaches to the certain detection probability of $P_D = 1$ at 6 segments.

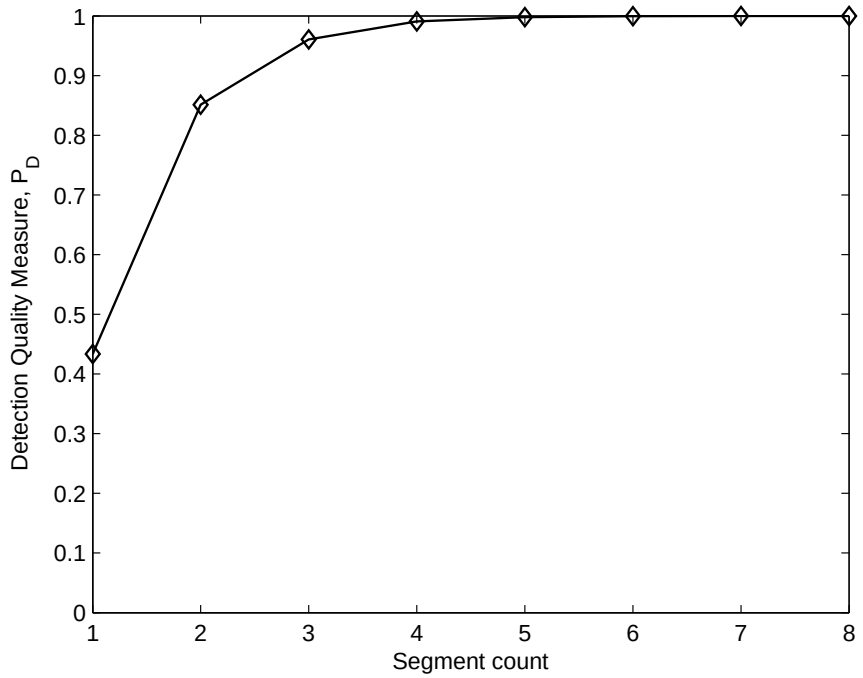

Figure 3.4. Detection probability at different number of segmented trajectory.

The comparison of trajectory simulations clearly shows that the detection probability in the segmented path scenario is always larger than the straight path scenario. It can be concluded that, in terms of detection performance, our straight path analysis gives the worst performance of the sensor network. For the network operators, estimating the worst case performance is generally more important than the average case, especially in SWSN applications.

3.1.5. Analytical and Simulation Results

We provide a comparison between the analytical and the simulation results to present the validity of our analytical estimation. In order to observe the effects of the

individual parameters in the model, the following assumptions are made to minimize the effects of external parameters on our results.

- A binary sensing model is assumed, where for a given sensor s located at z_s, probability of detection $P_D(s)$ of a point x is:

$$P_D(s) = \begin{cases} 1, & if\ d(x, z_s) < R_s \\ 0, & otherwise \end{cases} \tag{3.29}$$

- A circular sensing range is assumed, on a 2-D flat world deployment region.
- Intruders prefer the TFP region more than the other for trespassing.
- TFP region consists a small ratio of the deployment area.
- Intruders follow a straight line while they are trespassing the deployment area.
- Sensing equipments of sensors are awake and able to detect the intruders at all times.

For testing the validity of analytical results, simulations are run and tested against different parameter sets in the MATLAB platform. The simulations are repeated for different parameter sets. For each set, 1000 random sensor network deployments and TFP region placements are performed. For each random sensor network deployment, 10000 lines, each representing one trespassing, are generated. Thus, for each parameter, we have a result set in the size of 10^7 detection logs and the probability of detection is calculated using these logs. The results represented in the graphs are the mean values of these simulation runs.

In Table 3.1, the values indicated with * are used as the default values for the simulations. The region dimensions extend from 2000 m x 2000 m that represents a square border region to 2000 m x 20000 m that represents a long narrow border region. By executing simulations using different dimensions, various border region shapes are analyzed. For the sensor count, two different parameter sets (*low* and *high*) are defined to simulate low and high density sensor deployment networks. Since the aim of the study is to analyze the effect of the TFP region and its properties, sensing range is selected as constant and fixed at 25 m which is a plausible value for MIR type sensor networks.

Table 3.1. Tested parameters for different TFP scenarios.

Parameter	**Tested Values**
Border Width	2000, 4000, 6000, 8000, 10000, 12000, 14000, 16000, 18000, 20000* (m)
Border Height	2000 m
TFP Region Width	200*, 400, 600, 800, 1000, 1200, 1400, 1600, 1800, 2000 (m)
TFP Region Preference	0.0, 0.1, 0.2, 0.3, 0.4, 0.5, 0.6, 0.7, 0.8, 0.9*, 1.0
Sensor Count (*low*)	50, 100, 150, 200*, 250, 300, 350, 400, 450
Sensor Count (*high*)	500, 600, 700, 800*, 900, 1000
Sensing Range	25 m

We analyzed the effects of simulation parameters and compared the simulation results and analytical predictions to evaluate the accuracy of the analytical model.

The combined effect of sensor count and TFP probability on DetQM values : In these simulations, the sensor count deployed is increased step by step for different TFP preference probabilities to see its effect on the DetQM values. In all simulations, the width of the border region is 20000 m and the width of the TFP region is 200 m and the height of the border region is 2000 m. The negligible gap between the simulation results and analytical results show the accuracy of the theoretical model proposed in the previous section. The gap is at most 12.08 % for the low density deployment scenarios and 1.54 % for the high density deployment scenarios. As a general observation, it can be said that the differences between the simulation and analytical values get smaller with the increasing sensor count. Both the analysis and simulation results show that, when the TFP preference probability is increased, the detection ratio falls. This behavior is more clear in the low density deployment scenarios compared to high density deployment scenarios. For example, when 50 sensors are deployed to the border region, the detection ratio falls from $P_D = 0.158$ for the $p_t = 0$ to $P_D = 0.118$ for the $p_t = 1$. This represents a 25.3 % fall in the detection performance of the system. When the sensor count is increased to 450, the corresponding P_Ds are 0.787 and 0.676 for the respective TFP probabilities. This difference means 14 % decrease in the detection performance of the system. Hence, the rate of performance degradation due to increasing TFP preference decreases with the increase in the sensor

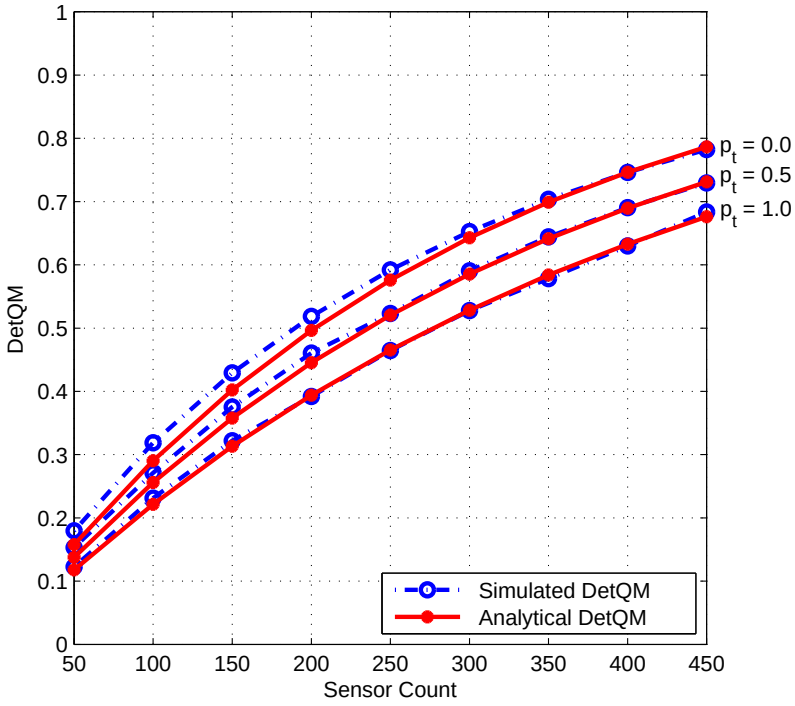

Figure 3.5. Effect of sensor count and TFP preference probability on analytical and simulated DetQM values. Low density sensor deployment (50 - 450).

count. The results are shown in Figure 3.5. The part (a) shows the DetQM values for the respective sensor counts and the part (b) shows the performance decrease in the DetQM.

The simulations are repeated for the high density sensor deployment scenarios. The border region and TFP region width parameters are kept constant, but the sensor count is increased from 500 to 1000 in steps of 100. For each step the DetQM for different TFP probabilities are measured and the decrease in the DetQM performance is noted as similar to the low density sensor deployment scenarios. The results are plotted in Figure 3.6. Only some of the simulation and analysis results are shown in the figures for the clarity of figures. All results can be found in Table A.2

The combined effect of border width and TFP probability on DetQM values with fixed TFP region ratio : In these simulations, the effect of the width of the border region and the TFP preference probability on the detection probability are measured. The ratio of the TFP region width to the whole border region width is kept constant at 0.01. The simulations are executed for two different sensor density scenarios. The

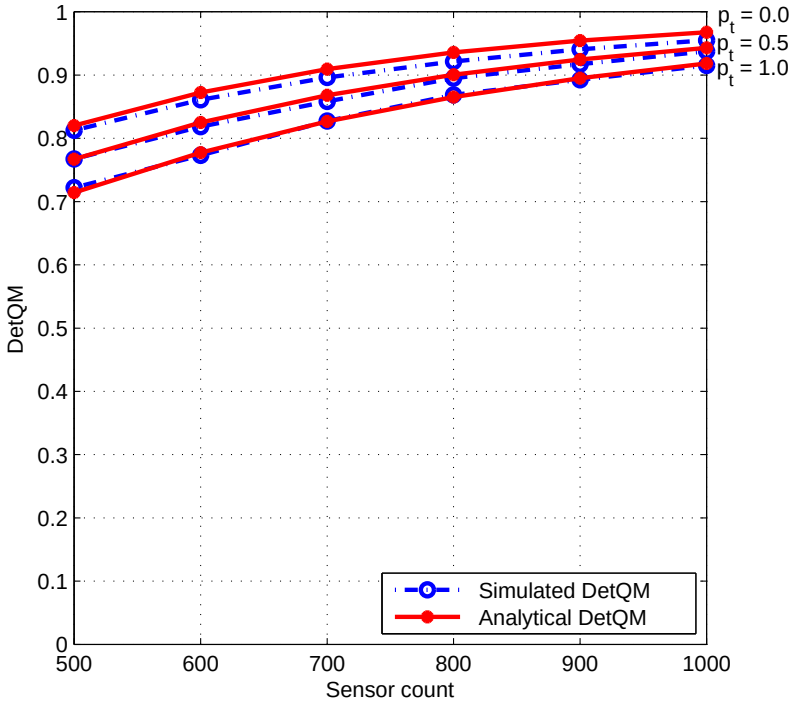

Figure 3.6. Effect of sensor count and TFP preference probability on analytical and simulated DetQM values. High density sensor deployment (500 - 1000).

part (a) of Figure 3.7 represents the sensor detection quality values for high density deployment whereas the part (b) represents the values for the low density deployment. As seen in the part (a), the width of the border region has a drastic effect on the detection probability in the low sensor deployment density. When the region width is 2000 m, the detection probability is $P_D = 0.9987$ and $P_D = 0.9982$ for $p_t = 0$ and $p_t = 1$, respectively. When we increase the region width to 20000 m, i.e. increase the deployment area 10 fold, hence decrease the sensor density, the detection probability decreases to $P_D = 0.563$ and $P_D = 0.485$ for $p_t = 0$ and $p_t = 1$, respectively. Although the gap is small, our analysis matches with the simulation results. It is also observed that, decreasing the sensor density increases the importance of TFP width on detection quality. DetQM metric falls 13.9 % when the trespassers prefer the TFP region instead of the non-TFP region.

The comments given are also valid with similar effects for the high sensor deployment (800 sensors) scenario. For the smallest area scenario where the border region width is 2000 m, there is no significant difference between the detection performance

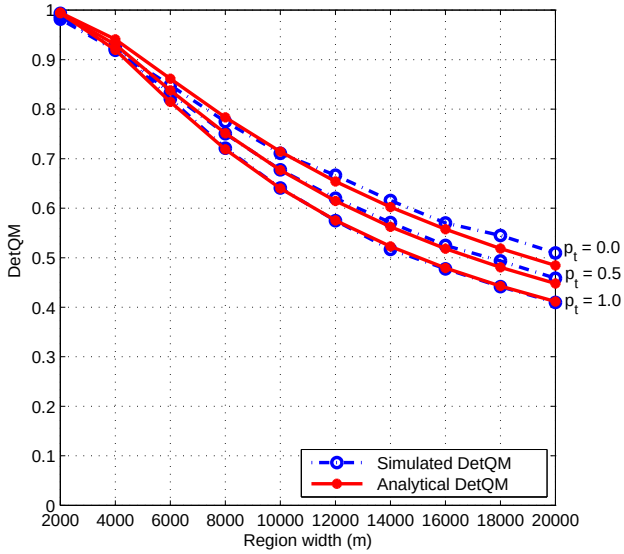

(a) Low density sensor deployment (200 sensors).

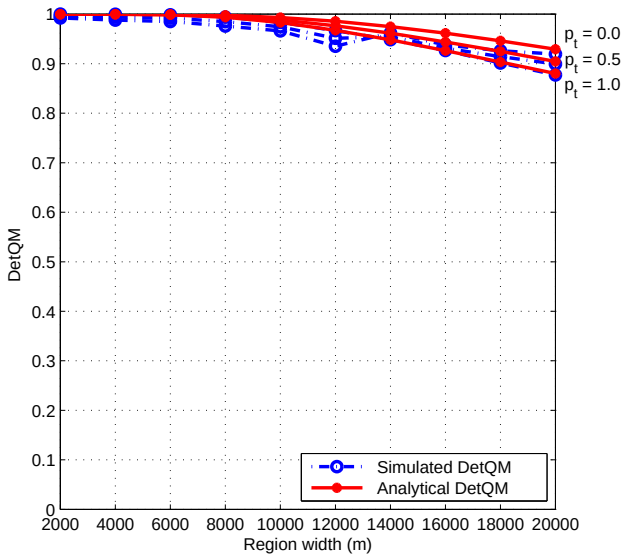

(b) High density sensor deployment (800 sensors).

Figure 3.7. Effect of border width with fixed TFP region ratio and TFP probability on DetQM values.

of opposite TFP preference scenarios. For both scenarios, the significant part of the detection probability metric converges to 1.00. If we increase the border region width to 20000 m, the detection probability values decrease to 0.917 and 0.863, respectively. In the small area scenario, there is no difference between the different TFP preference value simulations. In the large area scenario, the difference is 0.053, thus representing

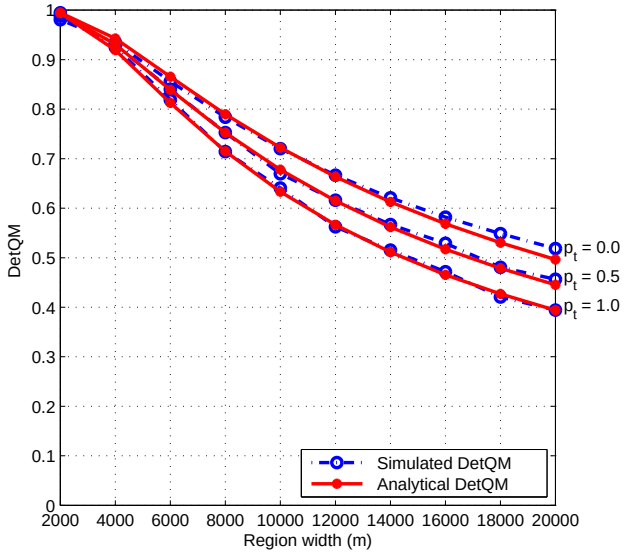

(a) Low density sensor deployment (200 sensors).

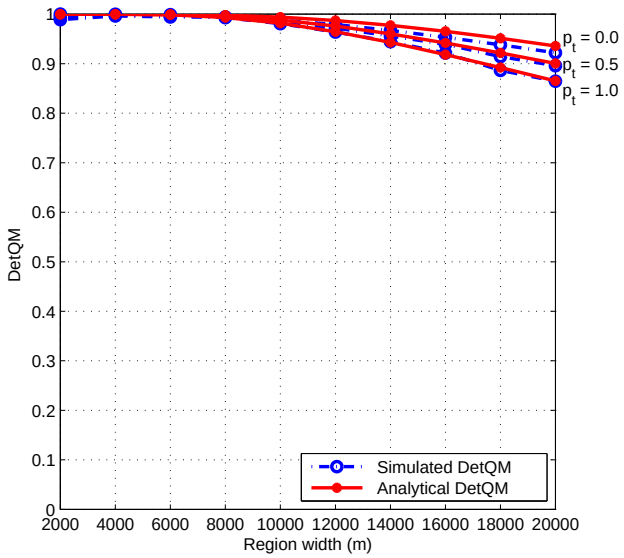

(b) High density sensor deployment (800 sensors).

Figure 3.8. Effect of border width with fixed TFP region width and TFP preference ratio on detection probability.

a 5.86 % fall in the detection probability performance.

The combined effect of border width and TFP preference on DetQM values with fixed TFP region width : In these simulations, the effect of the width of the border region and the TFP preference probability on the detection probability are measured. On the contrary of the simulations executed in the previous section, the ratio of the

TFP region width to the whole border region width is not constant, but the width of the TFP region is kept constant, 200 m. The simulations are executed for two different sensor density scenarios. The part (a) of the Figure 3.8 represents the sensor detection quality values for high density deployment whereas the part (b) represents the values for the low density deployment.

Similar to experiments performed with fixed TFP ratio, the border region width has a drastic effect on the detection probability performance. When the border region width is 2000 m and the TFP width is 200 m, the analytical detection probabilities are $P_D = 0.9987$ and $P_D = 0.9982$ for $p_t = 0$ and $p_t = 1$, respectively. When the border width is increased to 20000 m, the detection probability decreases to $P_D = 0.576$ and $P_D = 0.465$ for $p_t = 0$ and $p_t = 1$, respectively. These values are taken from the low sensor deployment scenario, 200 sensors. When the sensor count is increased to 800 sensors, as in the previous section, we observe the same behavior with less drastic effects on the detection probability, $P_D = 1.00$ for $p_t = 0$ and $p_t = 1$. The same probability values fall to 0.924 and 0.847 when the width of the border region is increased to 20000 m while the TFP region width is kept constant at 200 m. The DetQM fall ratios, in the low density sensor scenarios, are 42.34 % and 53.37 % for $p_t = 0$ and $p_t = 1$ whereas in the high density scenarios, they are 7.63 % and 15.28 % for $p_t = 0$ and $p_t = 1$, respectively.

DetQM vs TFP Preference : In order to perceive the effect of TFP preference on the detection performance, we measure the DetQM of the system with all parameters are fixed except the p_t. The border region width is 20000 m and the TFP width is 200 m. The p_t which denotes the TFP preference is increased from 0 to 1 with steps of 0.1. The result of the simulation is seen in Figure 3.9. The DetQM value for $p_t = 0$ is 0.497 and for $p_t = 1$, it is 0.394. This fall means about 20.7 % degradation in the DetQM performance between the values $p_t = 0$ and $p_t = 1$ which indicates the importance of the TFP preference on the detection quality. Although, no parameter is changed within the network including the deployed sensor count and sensor node configurations, the network performance deteriorates with increasing p_t. Another consequence of the TFP region is the inequality among the nodes in terms of duty and usefulness. Most of the detections are being achieved by a small subset of all sensors which cover TFP

paths. This means a heavy load on a small part of the network whereas the rest of the sensor network remains idle most of the time and rarely used. This setting results in early exhaustion of active sensors and potentially creating detection holes in those areas. Thus, it can be concluded that network operators should carefully inspect the network deployment area, uncover TFP paths within the border region and deploy sensors accordingly for an efficacious surveillance network.

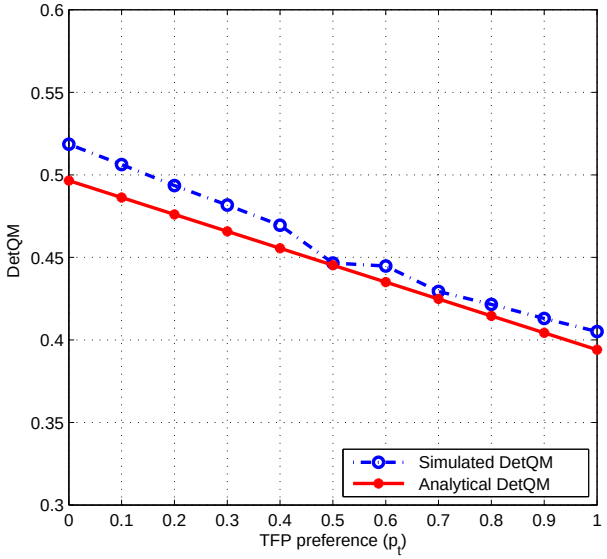

Figure 3.9. DetQM vs TFP preference (p_t).

3.2. Detection Quality Measure in a Field with Multiple Regions

In this section, the formal definition of the detection quality metric of an area with a heterogeneous intrusion pattern problem is stated and its analytical solution is given with the corresponding proof.

3.2.1. Network Model

In this subsection, we will present the network model briefly. We define a similar network model used in the previous section which discusses the detection quality metric problem with a single region. The differences between the models given in this subsection and the one given in Section 3.1.1 will also be mentioned.

We assume a convex 2-D border area, S, which is further simplified to a rectangle that has a width of w and a height of h for demonstrative purposes. There are N_s sensors deployed randomly within the area. Each sensor s_i is assumed to have convex sensing coverage of S_i with radius r_i, uniformly and independently distributed within

S. The border area separates the secure side from the insecure side. The direction of the trespassing is from insecure side to the secure side, thus along the y-axis of the region. There are N_t regions within the monitored zone. Each of the region has a width of w_{t_i} and intrusion probability of p_{t_i}. The intruders may prefer some of the regions due to security related issues, thus, the vales of the p_{t_i} may not be equal. The graphical representation of the network is shown in Figure 3.10. Sensors are not included in the figure for the sake of clarity.

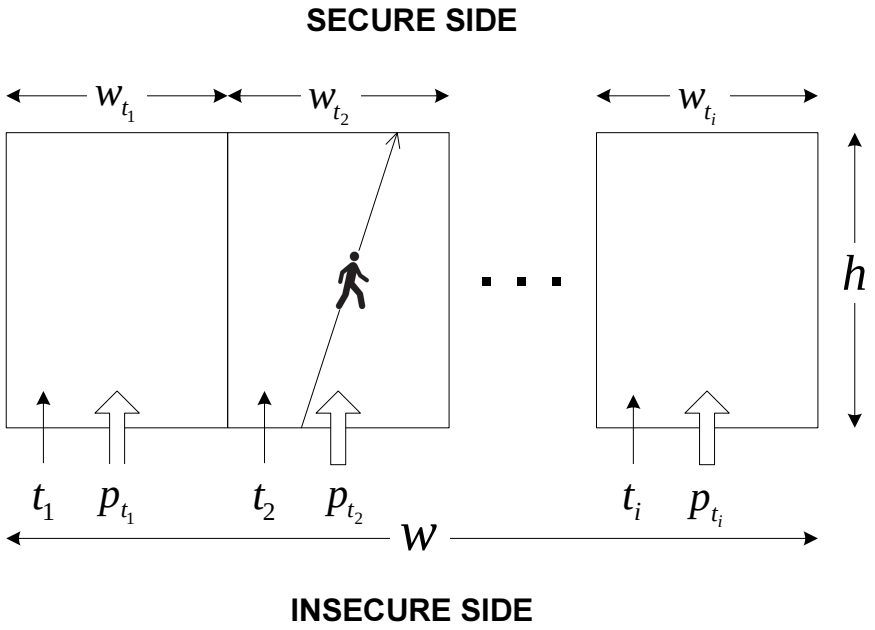

Figure 3.10. Graphical representation of the border SWSN model with multiple trespassing regions.

We employ the same assumptions about the knowledge of the intruder about the border area and the intrusion behavior given in the previous section. The deployment method and properties of the distribution are also same with the ones given in the previous section. The sensors operate according to binary detection model which is explained in detail in the previous section.

3.2.2. Problem Definition

In this section, we will provide a formal definition of the border SWSN intruder detection problem in a field with a multiple regions. Moreover, we will provide two additional problems which will be mapped to each other to derive a solution for the geometric domain utilizing metrics and tools from Integral Geometry and Geometric Probability.

Problem 3.9. ***Intruder with heterogeneous intrusion pattern detection problem :*** *We have a border area on which sensors are deployed. It is assumed that the border area, S, which is in convex form, have N_s sensors distributed uniformly and independently on it. Each sensor has a sensing radius of r_i and sensing coverage area of $S_i = \pi r^2$. The border area lies between the insecure side and the secure side and consists of regions with different intrusion patterns resulting in an heterogeneous intrusion pattern over the whole border area. The trespassers prefer one of the N_t regions with probability p_{t_i} and make their passage through this region. What is the probability P_D that an intruder X randomly crossing the border area S is detected by at least one sensor?*

3.2.3. Detection Quality Metric

In Section 3.1, we analyzed the detection probability in an area with single region and uniform intrusion probability. We also have provided Theorem 3.10.

Theorem 3.10. *The DetQM of any sensor network with N_s sensors deployed in the area with a trespasser trajectory pattern determined by the line set Υ with a single region is*

$$P_D = 1 - \prod_{i=1}^{N_s} \left(1 - \frac{E\left(T_i\right)}{E(T)} \frac{E\left(A_T\right)}{A}\right) \tag{3.30}$$

where $E(T_i)$ is the average thickness of the sensor coverage area, $E(T)$ is the average thickness of the deployment area for the given line-set intersection constraint which determines Υ, $E(A_T)$ is the average area of the deployment site covered by lines in Υ and A denotes the area of the deployment site.

In this section, we analyze the DetQM of a sensor network for the cases where there are more than one disjoint trespassing regions with a heterogeneous intrusion pattern in the border area. This is explained formally in Problem 3.9. In order to find a solution to this problem, we generalize Theorem 3.10 and provide Theorem 3.11 along with its proof.

Theorem 3.11. *The DetQM of any sensor network with N_s sensors deployed in the area, consisting of N_t disjoint regions that have p_t preference probabilities, with a tres-*

passer trajectory pattern determined by the line set Υ*, consisting of* Υ_{t_i} *subsets, is*

$$P_D = \sum_{j=1}^{N_t} p_{t_j} \left(1 - \prod_{i=1}^{N_{s,j}} \left(1 - \frac{E\left(T_i\right)}{E(T_{t_j})} \frac{E\left(A_{T,t_j}\right)}{A} \right) \right) \tag{3.31}$$

where $E(T_i)$ *is the average thickness of the sensor coverage area,* $E(T_{t_j})$ *is the average thickness of the trespassing region for the given line-set intersection constraint which determines* Υ_{t_j}*,* $E(A_{T,t_j})$ *is the average area of the region covered by lines in* Υ_{t_j}*,* A *is the area of the region and* p_{t_j} *denotes the preference probability of the region* t_j*.*

Proof. Since, each region is a subset of the deployment area, the target detection probability in one of the regions is calculated using the subset of lines satisfying the region crossing constraints, Υ_{t_i}:

$$P_{D|t_i} = 1 - \prod_{i=1}^{N_{s,t_i}} \left(1 - \frac{E\left(T_{t_i}\right)}{E(T_t)} \frac{E\left(A_{T,t_i}\right)}{A} \right) \tag{3.32}$$

Since the regions are disjoint, by the definition of conditional probability, the detection probability of the network is found as:

$$P_D = \sum_{i=1}^{N_{t_i}} P_{D|t_i} \cdot p_{t_i} \tag{3.33}$$

which yields Equation 3.31. □

In our derivations, we only require all sets to be convex and bounded. However, for the simplicity, we assume circular sensing coverage, and rectangular deployment area which are more applicable for a real life border region scenario. The following corollary is an applied example for our analysis and simulations are based on this corollary.

Corollary 3.12. *If the sensors have identical circular sensing coverage, then the DetQM of a sensor network with a rectangular deployment area is equal to:*

$$P_D = \sum_{i=1}^{N_t} p_{t_i} \cdot \left(1 - \left(1 - \frac{2r}{E\left(T_{t_i}\right)} \cdot \frac{E\left(A_{T,t_i}\right)}{h \cdot w_{t_i}}\right)^{N_{s,t_i}}\right) \tag{3.34}$$

and

$$\begin{aligned}
&\gamma_{t_i} = \arctan(h/w_{t_i}) \\
&T(\Upsilon_{t_i,\frac{\pi}{2}+\alpha}) = w_{t_i}\sin(\alpha) - h\cos(\alpha) \\
&E\left(T_{t_i}\right) = \int_{\gamma_{t_i}}^{\pi-\gamma_{t_i}} \frac{T(\Upsilon_{\frac{\pi}{2}+\alpha}) - T(\Upsilon_{t_i,\frac{\pi}{2}+\alpha})}{\pi - 2\gamma_{t_i}} d\alpha \\
&E\left(A_{T,t_i}\right) = \int_{\gamma_{t_i}}^{\pi-\gamma_{t_i}} \frac{\left(T(\Upsilon_{\frac{\pi}{2}+\alpha}) - T(\Upsilon_{t_i,\frac{\pi}{2}+\alpha})\right)\frac{h}{\sin(\alpha)}}{\pi - 2\gamma_{t_i}} d\alpha
\end{aligned} \tag{3.35}$$

where r is the radius of the sensing coverage of a sensor, w_{t_i} is the width of the region t_i and h is the height of the region.

Proof. A sample rectangular deployment site is illustrated in Figure 3.11 to be used throughout this proof. One of the trespassing regions, t_i, is represented with the rectangle $ABCD$. The width of the region is w_{t_i} and the height of the region is h. The sensors deployed within the region have circular sensing with a radius of r. On the figure, only one of the deployed sensors is shown as a sample. The rest of the figure is explained within the analysis.

By the assumption of identical circular sensing coverage for the sensors, the average thickness of each sensor's sensing area is equal to the diameter of the circle which is $2r$.

The trajectories in Υ_{t_i} are restricted to pass through the region from the insecure side (bottom side) to the secure side (top side). Hence the lower bound of these linear trajectories is the angle γ_{t_i}, which is the angle between the diagonal of the rectangle and the x axis. Similarly, the upper bound is the angle of the opposite diagonal which is $\pi - \gamma_{t_i}$. The thickness of the lines with slope α is determined by measuring the set of lines in $\Upsilon_{t_i,\phi}$ where $\phi = \frac{\pi}{2} + \alpha$ since these lines are parameterized by the slope of the perpendicular line passing from the origin. The thickness of $\Upsilon_{t_i,\phi}$ is equal to the

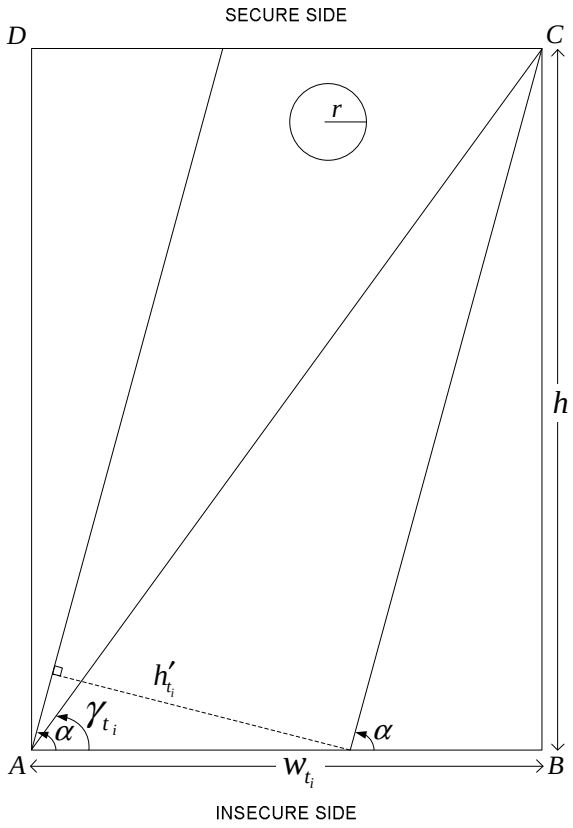

Figure 3.11. The representation of a region.

height h'_{t_i} of the parallelogram formed by the lines with slope α. Clearly

$$h'_{t_i} = T(\Upsilon_{t_i,\frac{\pi}{2}+\alpha}) = w_{t_i}\sin(\alpha) - h\cos(\alpha) \tag{3.36}$$

The average thickness of the region t_i is equal to the average of the thicknesses, h'_{t_i}, of the parallelograms formed by lines in all directions between γ_{t_i} and $\pi - \gamma_{t_i}$.

$$E\left(T_{t_i}\right) = \int_{\gamma_{t_i}}^{\pi-\gamma_{t_i}} \frac{T(\Upsilon_{t_i,\frac{\pi}{2}+\alpha})}{\pi - 2\gamma_{t_i}} d\alpha \tag{3.37}$$

The average area of the region t_i covered by Υ_{t_i} is equal to the average of the areas, $A_{T(\Upsilon_{t_i,\phi})}$, of the parallelograms formed by lines in all directions between γ_{t_i} and $\pi - \gamma_{t_i}$. The thickness h'_{t_i} of the region formed by trajectories with slope α is the height of the parallelogram. The length of these trajectories in the region is equal to $\frac{h}{\sin(\alpha)}$.

Hence, the average area $E\left(A_{T,t_i}\right)$ is equal to:

$$E\left(A_{T,t_i}\right) = \int_{\gamma_{t_i}}^{\pi-\gamma_{t_i}} \frac{h' \cdot \frac{h}{\sin(\alpha)}}{\pi - 2\gamma_{t_i}} d\alpha$$
$$= \int_{\gamma_{t_i}}^{\pi-\gamma_{t_i}} \frac{T(\Upsilon_{t,\frac{\pi}{2}+\alpha}) \cdot \frac{h}{\sin(\alpha)}}{\pi - 2\gamma_{t_i}} d\alpha \tag{3.38}$$

We provide the derivations for the list of equations in Equation 3.35. By substituting these equations in Equation 3.31, we provide Equation 3.34. □

In this section, we derived a formulation for the probability of intruder detection in a border surveillance sensor network using the line measure and thickness tools from the geometric probability. The initial formulation covers the heterogenous sensing coverage and convex bounded condition. The closed form formulation is further simplified by the assumption of homogenous and circular sensing coverage and a rectangular deployment site. In the next section, we will present our simulation scenarios and provide a comparison between the analytical and simulation results.

3.3. Analytical and Simulation Results

In this section, we present our analytical and simulation results. In order to minimize the effects of external parameters on the presented results, following simplifications are applied.

- A binary sensing model is assumed, where for a given sensor s located at z_s, probability of detection $P_D(s)$ of a point x is:

$$P_D(s) = \begin{cases} 1, & \textit{if } d(x, z_s) < R_s \\ 0, & \textit{otherwise} \end{cases} \tag{3.39}$$

- A circular sensing range is assumed, on a 2-D flat world deployment region.
- Intruders follow a straight line while they are trespassing the deployment area.
- Sensing equipments of sensors are awake and able to detect the intruders at all times.

For testing the validity of analytical results, we define different sensor network scenarios and run the simulations against different parameter sets in the MATLAB platform. The simulations are repeated for different parameter sets. For each set, 1000 random network deployment schemes are performed. For each random network deployment, 10000 travel trajectories are generated within the simulation area. Thus, for each parameter, we have a result set in the size of 10^7 detection logs and the network's detection performance is calculated with these logs. The results represented in the graphs are the mean values of these simulation sets.

3.3.1. Border Area with Multiple Regions

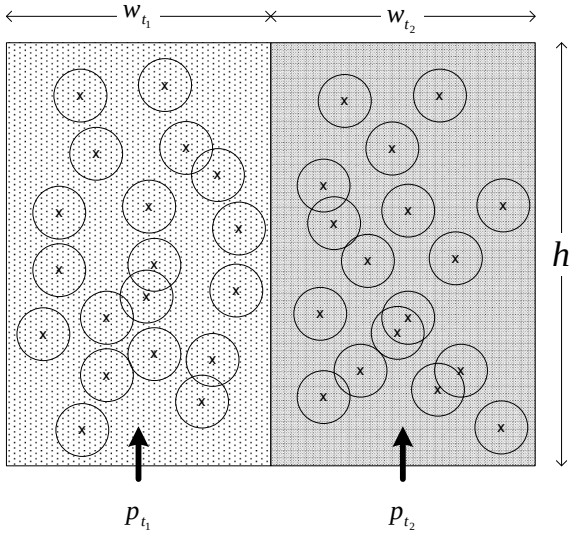

Figure 3.12. Graphical representation of the field used for comparative analysis.

The relative distribution of the sensors within a border zone can influence the detection quality drastically. The effect of the region preference can be measured best if other parameters are taken constant. For that purpose, a border zone with different trespassing preferences is simulated. The zone is made up of two equal width, $w_{t_1} = w_{t_2} = w_t$, and height, h, regions as shown in Figure 3.12. The probability that an intruder passes through each region is p_{t_1} and p_{t_2}, respectively. The detection probability of the network in this scenario is:

$$\begin{aligned} P_D = & p_{t_1} \cdot \left(1 - \left(1 - \frac{2r}{E\left(T_{t_1}\right)} \cdot \frac{E\left(A_{T,t_1}\right)}{h \cdot w_{t_1}}\right)^{N_{s,t_1}}\right) + \\ & p_{t_2} \cdot \left(1 - \left(1 - \frac{2r}{E\left(T_{t_2}\right)} \cdot \frac{E\left(A_{T,t_2}\right)}{h \cdot w_{t_2}}\right)^{N_{s,t_2}}\right) \end{aligned} \tag{3.40}$$

Table 3.2. Detection performance in different region preference probabilities.

	p_{t_1} = **0.1**		p_{t_1} = **0.5**		p_{t_1} = **0.9**	
N_{s,t_1}	**An.**	**Sim.**	**An.**	**Sim.**	**An.**	**Sim.**
0	0.8275	0.8151	0.4597	0.4481	0.0919	0.0927
10	0.829	0.8097	0.5595	0.5514	0.2901	0.2905
20	0.8196	0.8037	0.6313	0.6267	0.4429	0.4316
30	0.7987	0.8105	0.6794	0.6625	0.5602	0.5456
40	0.765	0.7447	0.7072	0.7211	0.6494	0.6551
50	0.7162	0.7034	0.7162	0.7066	0.7162	0.7271
60	0.6494	0.6316	0.7072	0.6965	0.765	0.7624
70	0.5602	0.5557	0.6794	0.6612	0.7987	0.7791
80	0.4429	0.4299	0.6313	0.6217	0.8196	0.8289
90	0.2901	0.2944	0.5595	0.5441	0.829	0.8182
100	0.0919	0.0901	0.4597	0.4576	0.8275	0.8149

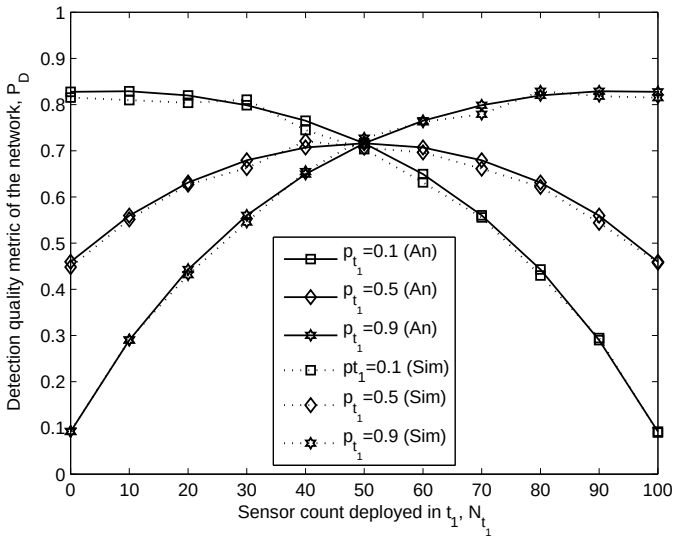

Figure 3.13. Detection performance in different region preference probabilities.

Since the regions are equal width and height regions, $E(T_{t_1}) = E(T_{t_2}) = E(T_t)$ and $E(A_{T,t_1}) = E(A_{T,t_2}) = E(A_{T,t})$ which clearly shows that the detection quality in this case depends on the region preference probability and the sensor count deployed in the region. Simulations are run compared with the analytical results. In these simulations, the sensor count deployed is kept constant at $N_s = 100$. The number of sensors deployed to the first region, t_1, is increased from 0 to 100 whereas the remaining ones are deployed to the second region, t_2. The simulations are run for different intruder

behavior scenarios. The numerical results of the analytical calculation and simulations are listed in Table 3.2. The results are plotted in Figure 3.13. It can be seen from the results that the analytical calculation matches with the simulation. In addition to this, it can be deduced that when the preferences are not equal, *i.e.* one region is preferred over another, the equal distribution of sensors perform poorly in terms of detection probability. Deploying more sensors into the more preferred region gives better detection results. Uniform random deployment gives the best performance if the intruders' behavior is uniform, too. Non uniform intruder behavior cases require different deployment schemes.

4. ANALYSIS OF DETECTION QUALITY MEASURE

In this chapter, we will analyze different properties of the DetQM and derive results based on this analysis. First of all, the closed form of the DetQM will be used to derive a method to find the optimal distribution of available sensors to a monitored zone. The performance of this optimized sensor distribution will be compared with the uniform random distribution of the sensors. In addition to this, the effects of different sensor detection models on the DetQM will be investigated with specific examples. The binary detection and Elfes detection models will be presented as specific cases. The parameters of each detection model will be listed and their effects on the general DetQM will be analyzed. Furthermore, different application scenarios from real life examples will be examined and scenario specific critical regions will be defined. The properties of the application scenarios and their effects on the DetQM will be measured. Moreover, we will inspect the parameters of different application scenarios and will perform a statistical factor analysis to find out their percentage of impact on the DetQM. Using the analysis results, we will summarize our findings about the effect of scenario parameters.

4.0.2. Optimization of Sensor Allocation

The allocation of the sensors among the regions affects the performance of the network drastically. Network operators should take the region properties into consideration while determining the number of sensors being deployed into a region. This problem can be expressed as the determination of the optimum number of sensors allocated per region. The definition of this optimization problem and the related criteria is

$$\begin{aligned} \text{Maximize} \quad & \sum_{i=1}^{N_{t_i}} P_{D|t_i} \cdot p_{t_i} && && (4.1) \\ \text{s.t.} \quad & \sum_{i=1}^{N_{t_i}} N_{s,t_i} = N_s, && i = 1, ..., N_{t_i} \\ & N_{s,t_i} \geq 0, && i = 1, ..., N_{t_i} \end{aligned}$$

This problem is an instance of the problem

$$\begin{aligned} \text{Minimize } & \sum_{i=1}^{n} f_i(x_i) \\ \text{s.t. } & \sum_{i=1}^{n} x_i = N \text{ and } x_i : \text{non-negative integers} \end{aligned} \tag{4.2}$$

which is called as a simple resource allocation problem and stated as NP-complete [75]. There are various algorithms proposed for the solution of such problems [76]. As an example, the border zone with a two-region scenario is simulated. The regions are defined to have intruder preference probabilities of $p_{t_1} = 0.1$ and $p_{t_2} = 0.9$, respectively. The width of each region is $w_t = 2000\ m$. The total number of sensors deployed to the whole area is chosen to be changing between 10 and 100 with steps of 10. At each step, the allocation of sensors between the regions that is maximizing the detection probability is found using an exhaustive search. This improved distribution is compared with the scenario in which available sensors are distributed among the whole zone using uniform distribution. The comparison of the performances corresponding to the optimized and uniform distribution is given in Figure 4.1 and the distribution of sensors for these cases are shown in Table 4.1. The DetQM values for different levels of p_{t_1} are listed in Table A.7 in the Appendix. In order to observe the effect of the region width to the detection performance, the same simulation is repeated with constant sensor count and variable region width. The sensor count is kept constant at 100, and the region width w_t is increased from 2000 m to 20000 m with steps of 2000 m. At each region width, the optimum number of sensors and the corresponding DetQM for the optimized distribution is calculated. In the uniform distribution, 50 sensors are deployed to each region, and the DetQM of the whole network is calculated. The comparison of the network performance between each scenario is given in Figure 4.2. Both of the figures clearly show the performance difference between two distributions. It is also important to note that when the sensor deployment is sparse, there is a significant performance difference in terms of detection capability. It can be safely concluded that the optimal allocation of sensors is critical especially for low budget deployments.

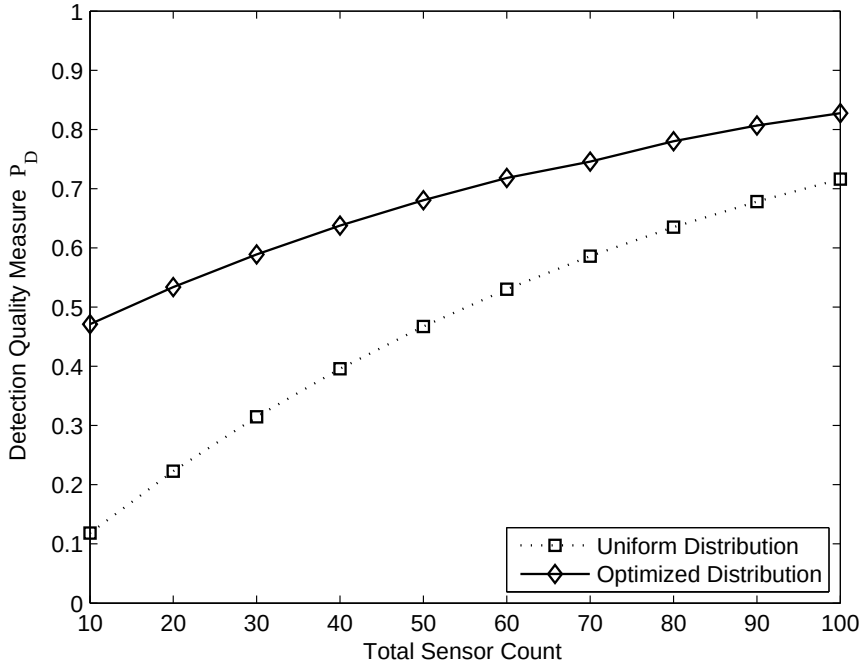

Figure 4.1. The detection performance comparison between uniform and optimized distributions.

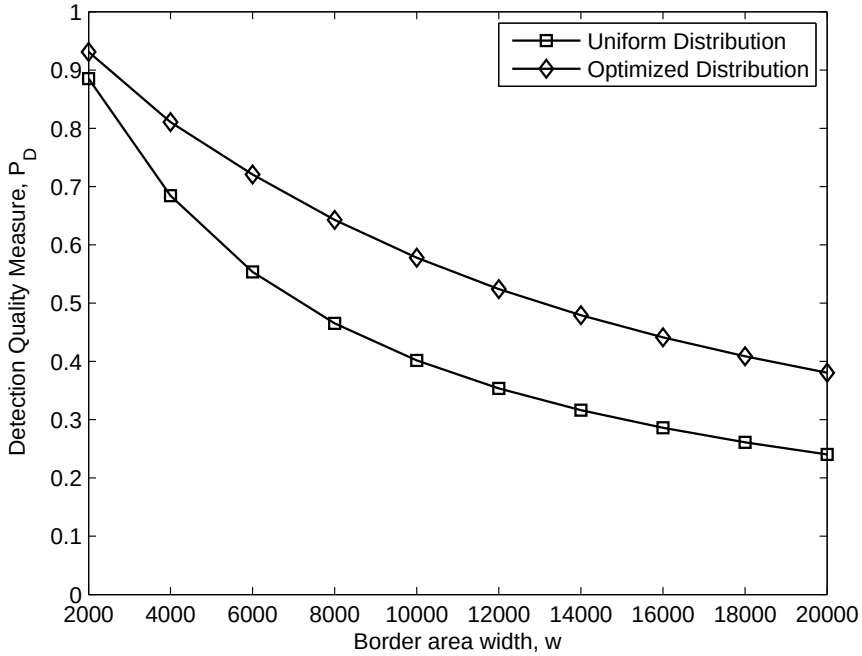

Figure 4.2. The detection performance comparison between uniform and optimized distributions.

4.1. Detection Quality Measure with Different Sensing Models

In this section, we investigate the effect of various wireless sensor network parameters on the detection quality measure of the network. The DetQM of any sensor

Table 4.1. Allocation of the sensors to regions using optimized allocation formulation.

Total	**Uniform**			**Optimized**		
N_t	N_{t_1}	N_{t_2}	P_D	N_{t_1}	N_{t_2}	P_D
10	5	5	0.195	0	10	0.316
20	10	10	0.351	0	20	0.521
30	15	15	0.478	0	30	0.654
40	20	20	0.579	0	40	0.741
50	25	25	0.661	0	50	0.797
60	30	30	0.727	5	55	0.836
70	35	35	0.780	10	60	0.868
80	40	40	0.823	15	65	0.894
90	45	45	0.857	20	70	0.914
100	50	50	0.885	25	75	0.931

network with N_s sensors deployed in the area, consisting of N_t disjoint regions that have p_t preference probabilities, with a trespasser trajectory pattern determined by the line set Υ, consisting of Υ_{t_i} subsets, is

$$P_D = \sum_{j=1}^{N_t} p_{t_j} \left(1 - \prod_{i=1}^{N_{s,j}} \left(1 - \frac{E\left(T_i\right)}{E(T_{t_j})} \frac{E\left(A_{T,t_j}\right)}{A} \right) \right) \tag{4.3}$$

where $E(T_i)$ is the average thickness of the sensor coverage area, $E(T_{t_j})$ is the average thickness of the trespassing region for the given line-set intersection constraint which determines Υ_{t_j}, $E(A_{T,t_j})$ is the average area of the region covered by lines in Υ_{t_j}, A is the area of the region and p_{t_j} denotes the preference probability of the region t_j.

In this study, the general form of the thickness of sensor coverage area are applied to different detection models and their difference in terms of the detection quality is investigated. If the probability distribution function of the detection model is denoted with $f(d)$ where d is the distance between the sensor and the target, the average thickness of the sensor coverage is the part of the cumulative distribution function of the sensor detection probability that is located within the trespassing area. The cumulative distribution function is equal to $\int f(d)$.

4.1.1. Binary Detection Model

The binary model is a good approximation for the type of sensors which have sharp sensing ranges such as PIR sensors [66]. Many studies use the binary sensing model due to its simplicity. In this model, there is a range which determines the sensing probability in a certain manner. The detection probability function of the binary sensing is:

$$P_D = \begin{cases} 1 & \text{if } d \leq r \\ 0 & \text{otherwise} \end{cases} \tag{4.4}$$

where r is the sensing range of the sensor and d is the distance between the target and the sensor. The detection probability function of the binary sensor with respect to the distance between the target and the sensor is plotted in Figure 4.3.

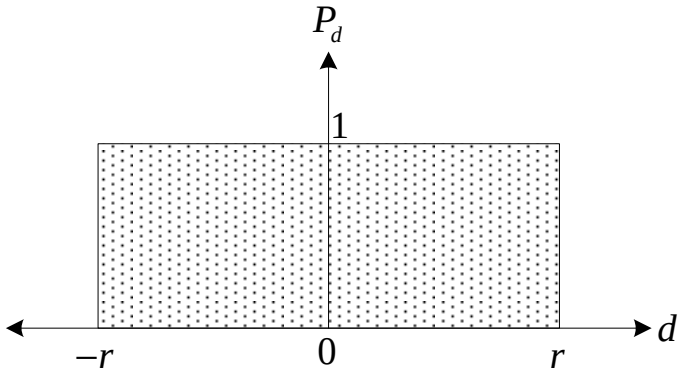

Figure 4.3. Detection probability function of the binary sensing.

The expected thickness of the sensor coverage area for the binary detection model, which corresponds to the shaded area in Figure 4.3 is:

$$\begin{aligned} E(T_i) &= \int_{-r}^{r} dx \\ &= 2r \end{aligned} \tag{4.5}$$

Substituting the $E(T)$ in Equation 4.3 gives us the DetQM of a sensor network

consisting of binary sensors:

$$P_D = \sum_{j=1}^{N_t} p_{t_j} \left(1 - \prod_{i=1}^{N_{s,j}} \left(1 - \frac{2r}{E(T_{t_j})} \frac{E\left(A_{T,t_j}\right)}{A} \right) \right) \tag{4.6}$$

4.1.2. Elfes Detection Model

Elfes detection model can be applied to a large variety of range of sensors, including infrared and laser scanners, sonar sensors, and stereo systems [77]. The detection probability of the Elfes sensing is:

$$P_D = \begin{cases} 1 & \text{if } d \leq r_e \\ e^{-\lambda(d-r_e)^\beta} & \text{if } r_e < d < r \\ 0 & \text{if } r \leq d \end{cases} \tag{4.7}$$

where the region between r_e and r denotes the uncertain detection range. The detection probability is determined by an exponential function within this range. λ and β are used to model sensor properties, d is the distance between the sensor and the target. The detection probability of Elfes sensing is plotted in Figure 4.4. The x-axis represents the distance between the target and the sensor and the y-axis represents the detection probability of the target.

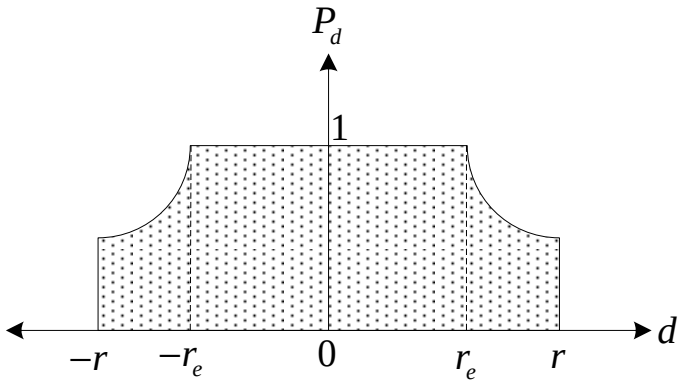

Figure 4.4. Detection probability of Elfes sensing.

The expected thickness of the sensor coverage area for the Elfes detection model, which corresponds to the integral of detection probability of Elfes detection, denoted

with the shaded area in Figure 4.4 is:

$$E(T_i) = \int_{-(r_e)}^{r_e} dx + \int_{r_e}^{r} e^{-\lambda(x-r_e)^\beta} dx + \int_{-r_e}^{-r} e^{-\lambda(x-r_e)^\beta} dx \tag{4.8}$$

The integration of the exponential function in Equation 4.8 can be expanded as:

$$\int_{r_e}^{r} e^{-\lambda(x-r_e)^\beta} dx = \frac{(r_e - x)(\lambda(x-r_e)^\beta)^{(-1/\beta)}\Gamma(\frac{1}{\beta}, \lambda(x-r_e)^\beta)}{\beta} + C \tag{4.9}$$

where $\Gamma(a, x)$ is the incomplete gamma function which is a generalized form of the gamma function [78]. In our simulations, we evaluate the integral numerically using the adaptive Simpson quadrature method provided in MATLAB [79].

4.1.3. Analytical and Simulation Results

In this section, we analyze the effects of some network parameters on the DetQM. The detection model is selected as the first parameter set. Two different detection models, binary detection and Elfes detection, are examined in terms of their impact on the DetQM. Following the detection model, two different surveillance scenarios are depicted and the critical regions are defined. Their differences in terms of intrusion patterns are also given. The significance of the different environmental conditions are investigated using these scenarios and they are compared to each other to find out a relation between the scenario properties and DetQM. In addition to this, the critical regions which are defined within the scenarios are also evaluated. The importance of their distribution within the whole border area is studied using different combinations and the results are presented in a comparative manner. In the last part of this section, the shape of the border area is inspected by defining different levels of height to width ratios. For each level, the DetQM of the network is calculated and the result is presented in a plot along with its interpretation.

4.1.3.1. Binary Detection. The binary detection probability is dependent only on the sensing range of the sensor which acts as a threshold between the detection and the non-detection areas. The effect of the sensing range on the detection probability is tested using a constant width single region border scenario. The dimensions of the

border area selected to be $w = 2000\ m$ and $h = 500\ m$. Three levels of the desired detection probability are defined and required number of sensors to achieve the desired level for different sensing ranges are calculated. The results are plotted in Figure 4.5.

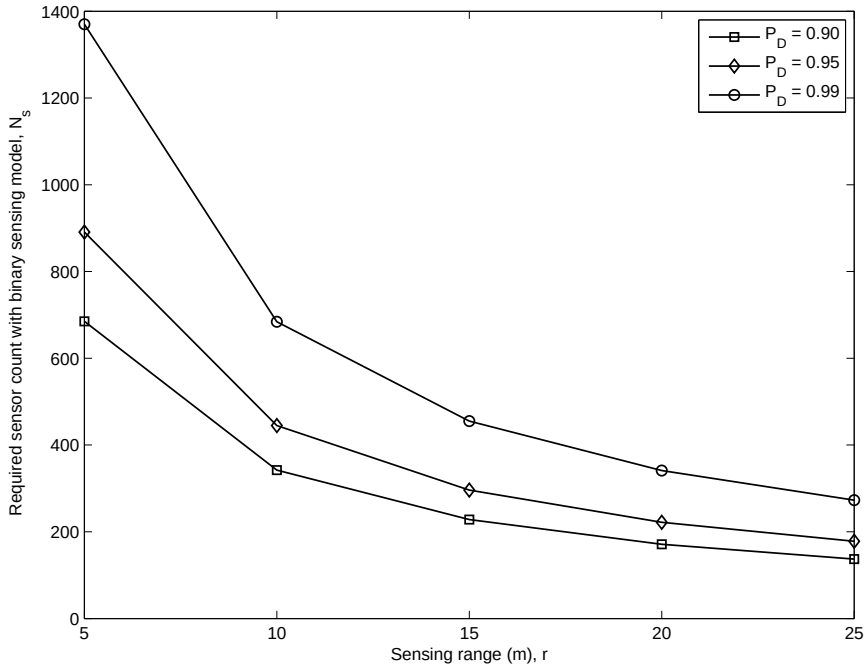

Figure 4.5. Effect of sensing range, r on the required sensor count.

The figure can be used for determining the required number of sensors to obtain a desired detection quality. If the sensors have variable sensing ranges, it may be useful in comparing the advantages and disadvantages of various sensing ranges [36, 80].

4.1.3.2. Elfes Detection. The Elfes sensor behaves as a binary sensor within its inner range. On the outer rim, the detection is expressed with an exponential probability. Within this region, the detection probability is dependent on the sensor specific parameters which are represented as the λ and β as shown in Equation 4.7. These parameters have different degrees of effects on the single node detection probability and the overall network detection probability. The single sensor node detection performance measurements are done with a sensor node that have an inner sensing radius of 10 meters and an outer sensing radius of 20 meters. The target is stationed at 18 meters. The detection probability is calculated for different combinations of λ and β values.

The effect of λ on the single sensor detection probability is given in Figure 4.6.

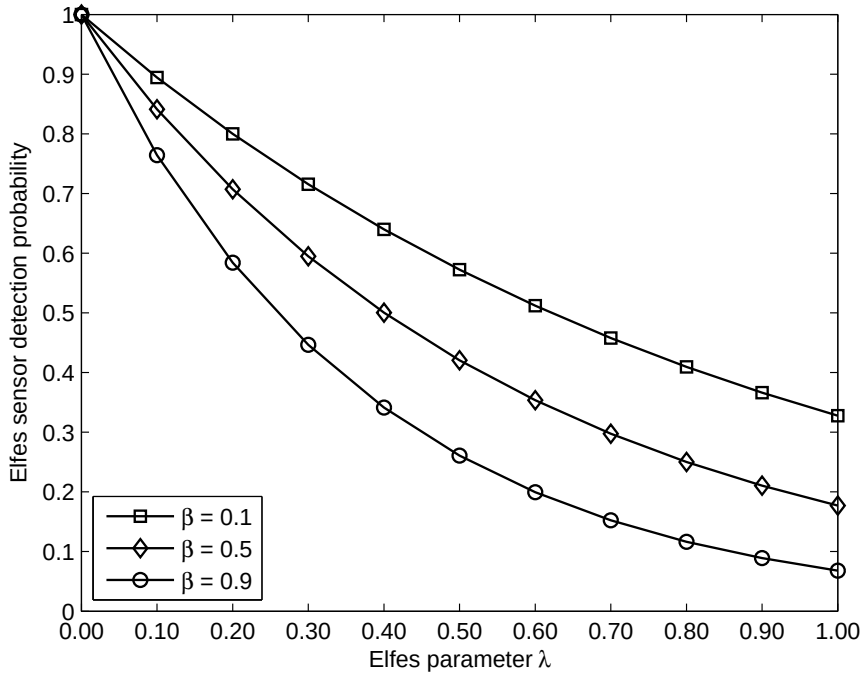

(a) Single sensor detection probability

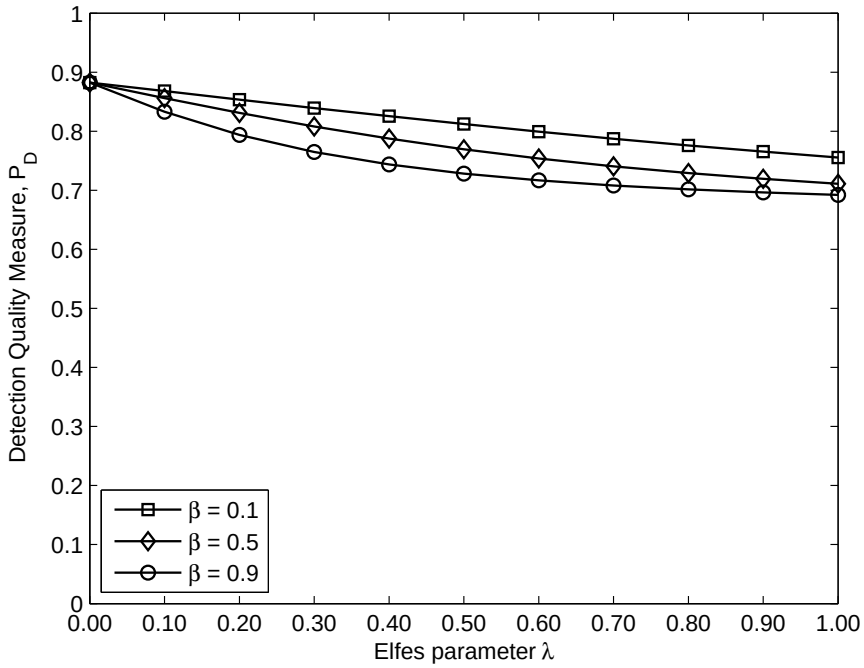

(b) Network DetQM

Figure 4.6. Effect of λ on the detection.

As can be seen from the figure, when λ is 0, the sensor behaves like a binary sensor and the target is certainly detected. The detection probability is monotonically decreasing with respect to λ. The detection probability of the system for three different β levels are given in the figure in order to see the relationship between λ and β. The same

simulation is repeated for the effect of β on the single sensor detection probability as given in Figure 4.7.

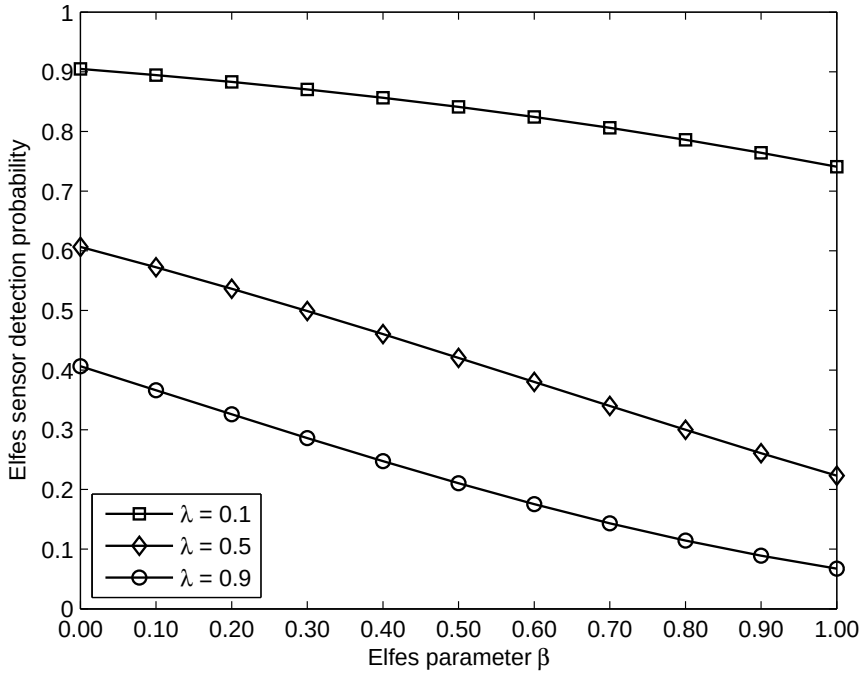

(a) Single sensor detection probability

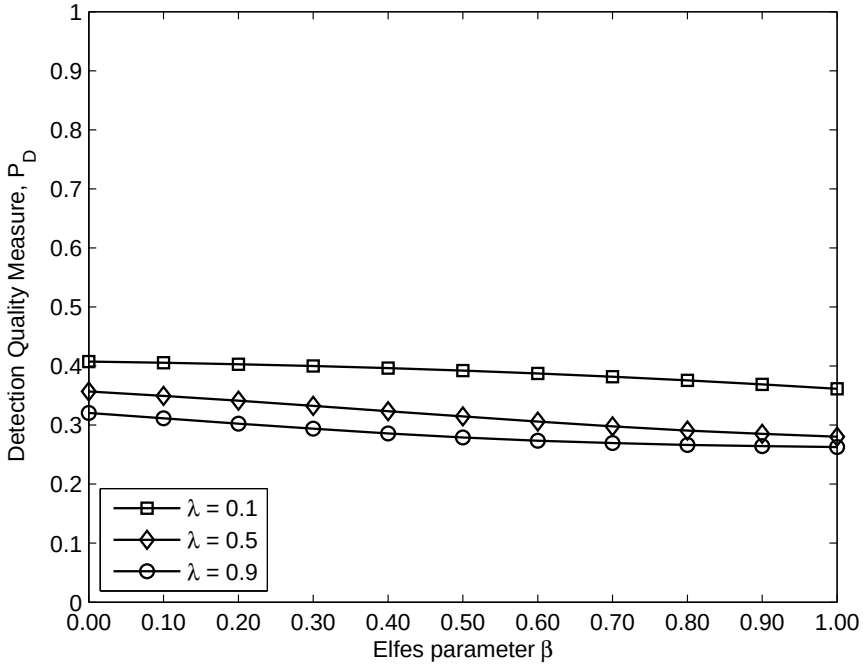

(b) Network DetQM

Figure 4.7. Effect of β on the detection.

One of the most important observations from the results is that, the parameters affect the detection quality of single sensor node significantly. On the other hand, this

situation is not valid for a network consisting of Elfes nodes. For the cases studied, the effect of Elfes parameters on a single sensor node is clearly diminished on a network wide scale. The DetQM differences between each level of the parameter value is not as significant as the single sensor node results.

4.2. Detection Quality Metric in Different Deployment Scenarios

The efficiency of the proposed closed form representation of the DetQM is examined using two different surveillance scenarios. In this part, we explain scenarios and define the critical and the non-critical regions according to environment properties.

Border Area Surveillance Scenario: In the border area surveillance (BAS) scenario, the sensor network is deployed to a border zone and it is used to monitor illegal intrusions through the border. The aim of the system is to detect and inform the network operators about these intrusions. The shape of the border zone is in the form of long rectangular area which separates two countries. The intruders trespass from one country to another. When doing so, they do not randomly select a path and follow it, but favor some regions over others due to environmental conditions such as security measures and terrain [3, 52]. The border area contains narrow regions through which most of the trespassers pass and wide regions which are not preferred very much. We mark these regions which are highly preferred by the intruders as the critical regions of the BAS scenario and the remaining regions as the non-critical ones.

Figure 4.8. An archeological site in the pyramids area.

Cultural Heritage Area Scenario: The monitoring of cultural heritage using wireless sensor networks is investigated in [81, 82]. In the cultural heritage area (CHA) scenario, monitoring a similar area is simulated. In this scenario, the sensor network

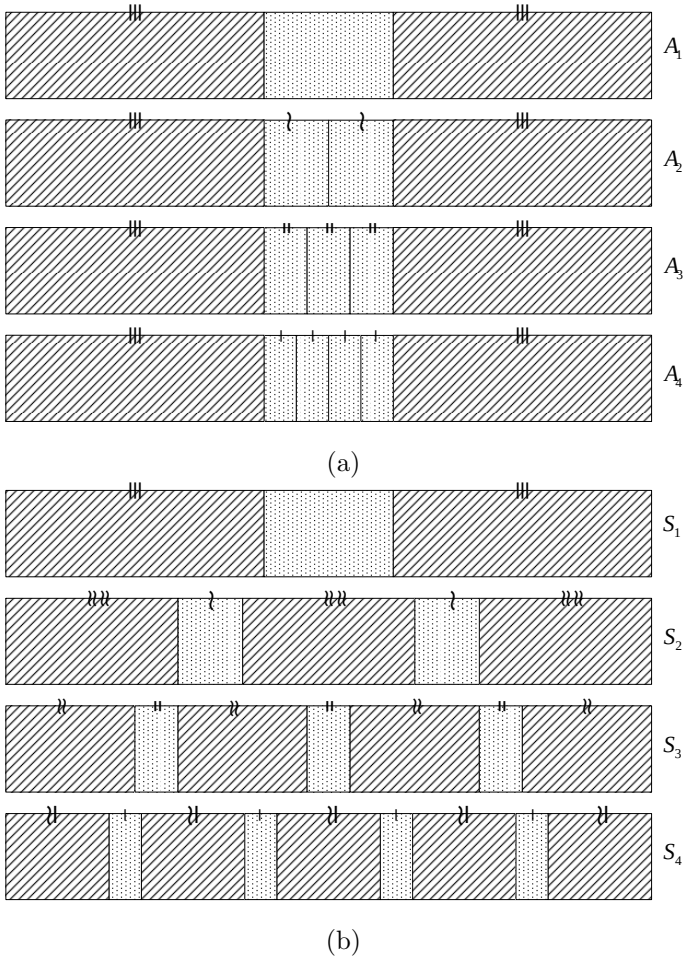

Figure 4.9. (a) Adjacent placements (A_1, A_2, A_3, A_4) of the critical regions. (b) Segregated placements (S_1, S_2, S_3, S_4) of the critical regions.

is deployed to a historical city site to monitor the visitors. The area contains wide regions which tourists pass through to visit ancient remains and narrow regions which are restricted to general access due to ongoing archeological work. In contrast to the BAS scenario, most of the traffic is distributed over the larger portion of the monitored zone, whereas a tiny fraction of the traffic is restricted to smaller portion of the monitored zone. For example, as seen in Figure 4.8, there is an ongoing work at the archeological site which is a restricted area, whereas the pyramids seen on the background of the picture are open to the visitor access [83]. We mark the regions where an active archeological work takes place as the critical regions of the CHA scenario and the remaining regions as the non-critical ones.

The dimensions of the simulation areas in both scenarios are chosen identical in order to simplify the comparison between them but they can be modified easily.

The distribution of the regions over the whole area is differentiated using two different distribution schemes, each of them with four different region counts. For the sake of simplicity, we define the favorite trespassing areas in BAS scenario and the excavation sites in CHA scenario as critical regions. In the layout graphics, these critical regions are denoted with dotted rectangles and non-critical regions are denoted with diagonal lined rectangles.

By the definition of the DetQM, the direction and angular mobility of the intruders are affected by the region count within the area. The rationale behind the disjoint regions is the existence of natural or artificial barriers between the regions which enforce the travelers to remain within the current region and the desire to pass the monitored zone using the shortest path available to reduce the detection probability. This is a frequently observed behavior in nature and also represented as ant paths or similar phenomena in the computer science. The relation between the number of regions and the detection probability of the network can give tools to network operator to improve the performance of the network by deploying the network according to geographical conditions or if possible by modifying the deployment area. By shaping the expected traffic pattern, the network detection performance can be increased without redeployments and additional sensor cost. The effect of the region shape is inspected using two different combinations of regions according to the placement of the critical regions.

Adjacent Placement: In this placement type, the critical region that is lying between two non-critical regions is divided into smaller equal width regions while keeping them physically together.

Segregated Placement: In this placement type, the critical region that is lying between two non-critical regions is divided into smaller equal width regions and each region is placed between non-critical regions such that they are separated from each other with equal width non-critical regions.

The resulting region placements are shown in Figure 4.9. The adjacent placements are named as A_i and the segregated placements are named as S_i where i is the number of critical regions. In the figures, the diagonal shaped blocks represent the non-critical regions and dotted blocks represent the critical regions. The same type regions have equal width in each placement. The intrusion probabilities are distributed to each part

equally according to its region type. For example, in the BAS scenario, the intrusion probability of the critical region is 0.8 and for the case in which the critical region is divided into two parts, i.e. in A_2 and S_2 placements, the intrusion probability of each part is set to 0.4. In a similar manner, the intrusion probability of the non-critical region is divided into equal parts.

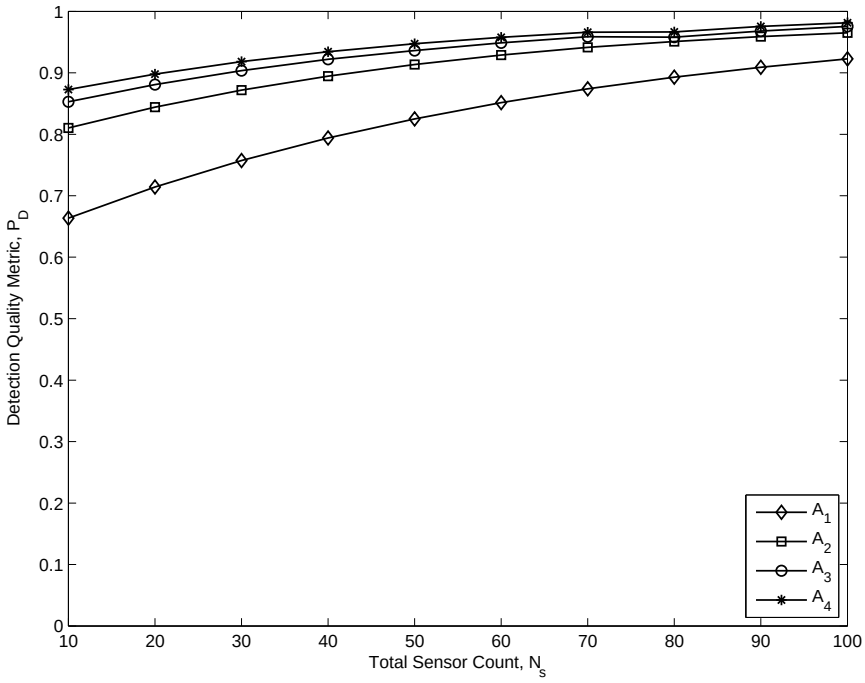

Figure 4.10. Network detection performance in BAS scenario adjacent critical regions.

4.2.1. Analysis of Factors

The numerical results of the experiments presented clearly show the relationship between different factors affecting the detection quality of the network. While keeping the sensor count constant, the effect of the region parameters on the network performance is examined using the factor analysis method. The 2^k factorial design is selected for the factor analysis which is explained in [84]. Here, we define the factors and present the method used for the analysis. In our case, we used three factors each defined at two levels. The factors and their corresponding levels are listed in Table 4.2. The detection probability for each level of each factor is given in Table 4.3.

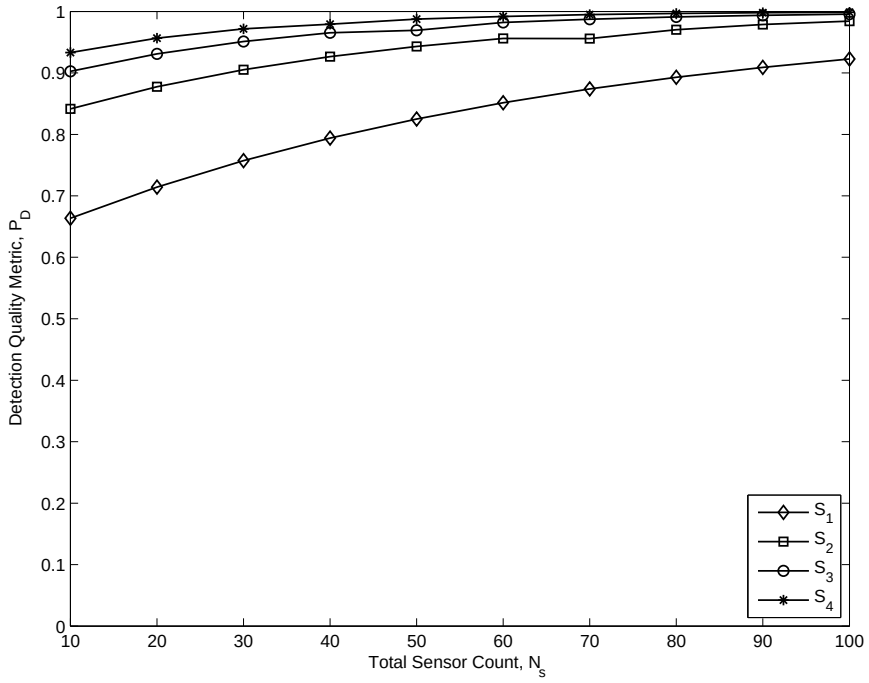

Figure 4.11. Network detection performance in BAS scenario segregated critical regions.

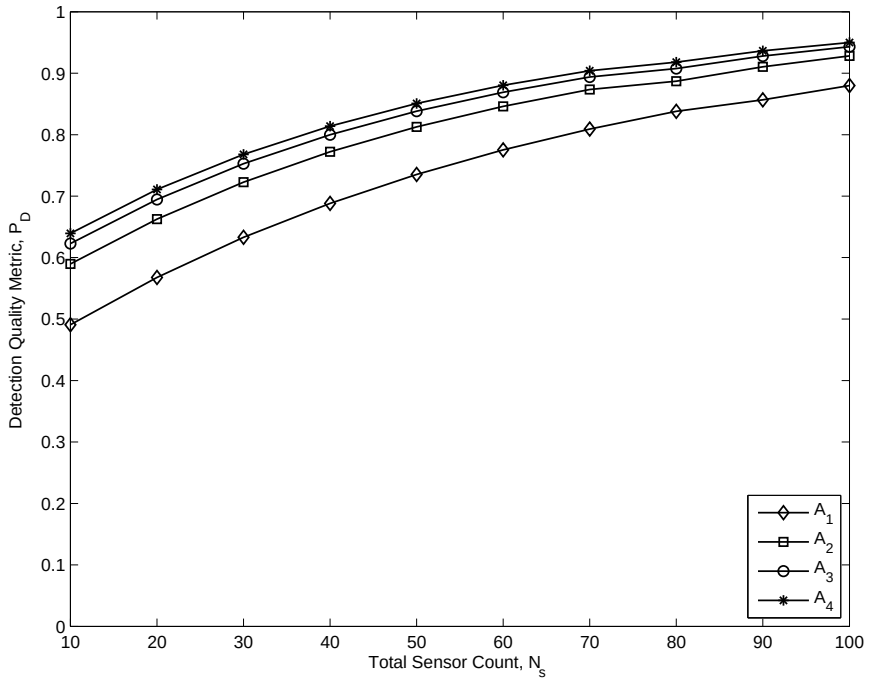

Figure 4.12. Network detection performance in CHA scenario adjacent critical regions.

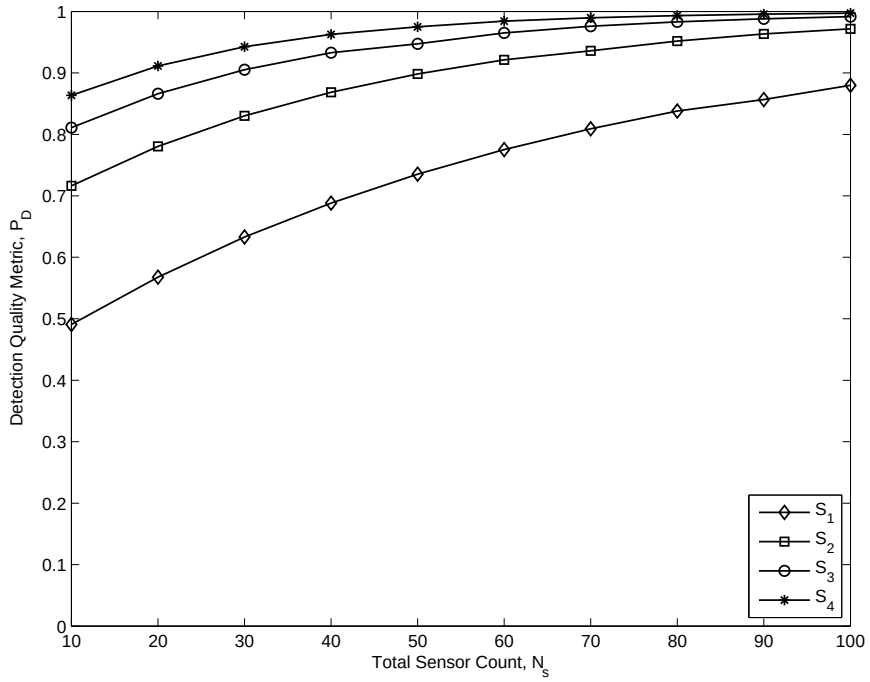

Figure 4.13. Network detection performance in CHA scenario segregated critical regions.

Table 4.2. List of symbols.

Symbol	**Factor**	**Level -1**	**Level 1**
A	Scenario Type	BAS	CHA
B	Critical Reg. Dist.	Adjacent	Segregated
C	Critical Reg. Count	2	4

Table 4.3. Detection probability values used in our analysis.

	BAS		**CHA**	
	2 Reg.	**4 Reg.**	**2 Reg.**	**4 Reg.**
Adjacent	0.913	0.947	0.813	0.851
Segregated	0.943	0.988	0.898	0.975

We define three variables x_A, x_B and x_C for each factor as follows:

$$x_A = \begin{cases} -1 & \text{if the scenario type is BAS} \\ 1 & \text{if the scenario type is CHA} \end{cases} \tag{4.10}$$

$$x_B = \begin{cases} -1 & \text{if the critical regions are adjacent} \\ 1 & \text{if the critical regions are segregated} \end{cases} \tag{4.11}$$

$$x_C = \begin{cases} -1 & \text{if the critical region count is 2} \\ 1 & \text{if the critical region count is 4} \end{cases} \tag{4.12}$$

The performance y in detection probability can now be regressed on x_A, x_B and x_C using a nonlinear regression model of the form

$$\begin{aligned} y_i =& q_0 + q_A x_{Ai} + q_B x_{Bi} + q_C x_{Ci} + q_{AB} x_{Ai} x_{Bi} + q_{AC} x_{Ai} x_{Ci} + q_{BC} x_{Bi} x_{Ci} + \\ & q_{ABC} x_{Ai} x_{Bi} x_{Ci} \end{aligned} \tag{4.13}$$

where i is the observation index. Substituting our eight observations in the model, we get eight equations which can be solved uniquely for the eight unknowns. The sign table method described in Table 4.4 enables a simple solution for these equations.

Table 4.4. The sign table used in the 2^k factor analysis.

I	A	B	C	AB	AC	BC	ABC	y
1	-1	-1	-1	1	1	1	-1	0.913
1	1	-1	-1	-1	-1	1	1	0.813
1	-1	1	-1	-1	1	-1	1	0.943
1	1	1	-1	1	-1	-1	-1	0.898
1	-1	-1	1	1	-1	-1	1	0.947
1	1	-1	1	-1	1	-1	-1	0.851
1	-1	1	1	-1	-1	1	-1	0.988
1	1	1	1	1	1	1	1	0.975
7.328	-0.255	0.280	0.193	0.140	0.036	0.049	0.028	*Total*
0.916	-0.032	0.035	0.024	0.017	0.005	0.006	0.004	*Total / 8*
q_0	q_A	q_B	q_C	q_{AB}	q_{AC}	q_{BC}	q_{ABC}	

The importance of a factor is equal to the proportion of the total variation in the experiment results that is explained by the factor. If a factor has a larger component on the variation of the result, it is considered more important. The sample variance of

y, denoted as s_y^2 is:

$$s_y^2 = \frac{\sum_{i=1}^{2^3} (yi - \bar{y})^2}{2^3 - 1} \tag{4.14}$$

where $\bar{y}$ is the mean of results from all eight observations. The numerator of the division that is given on the right-hand side of the equation is called the total variation of y or sum of squares total (SST). It consists of seven parts for a 2^3 factorial design:

$$\begin{aligned} SST =& \sum_{i=1}^{2^3} (yi - \bar{y})^2 \\ =& 2^3 q_A^2 + 2^3 q_B^2 + 2^3 q_C^2 + 2^3 q_{AB}^2 + 2^3 q_{AC}^2 + 2^3 q_{BC}^2 + 2^3 q_{ABC}^2 \\ =& SSA + SSB + SSC + SSAB + SSAC + SSBC + SSABC \end{aligned} \tag{4.15}$$

where each part represent the portion of the total variation explained by the effect of A, B, C, and their interaction with each other, respectively. Each portion of the factor is called the sum of squares due to that factor. Their ratio to SST, when expressed as a percentage, gives an easy way to gauge the importance of that factor. Thus, the importance of each factor on the results can be easily calculated. For example, the importance of the scenario type which is denoted as factor A in our analysis is SSA/SST. The fraction values for each factor and their interaction are calculated in a similar manner. The results are listed in Table 4.5.

Table 4.5. Fraction of variation explained by each factor.

Factor	**Variable**	**Fraction (in %)**
Scenario type	A	31.7
Region distribution	B	38.3
Region count	C	18.2
Interaction of A and B	AB	9.6
Interaction of A and C	AC	0.6
Interaction of B and C	BC	1.2
Interaction of A, B and C	ABC	0.4

The results show that region distribution has the greatest impact on the network DetQM. Its impact factor is about 38.3 %. It can be concluded that the placement of critical regions among the border area is very important since it shapes the traffic among the non-critical regions, too. Following the region distribution, comes the scenario type in the fraction of variation ordering. The essential difference between the given scenarios is the preference probability to the critical regions. Determining the preference probabilities accurately is critical to the performance of the network since it is a major component in the variation. These two factors make up about 70 % of the variation. In the third place comes the region count factor which has about 18.2 % fraction on the variation. In the total, the single component factors make up about 90 % of the fraction whereas the remaining 10 % is distributed among the interaction of the factors. As a conclusion, we can say that the distribution of critical regions and the preference probability of the critical regions are the key factors for the given scenarios.

4.3. Detection Quality Measure in Different Region Shapes

The DetQM depends on the limit angles of the integral that is calculated using the tools from the geometric probability. The relationship between the region shape is analyzed in order to see the relationship between DetQM and height width ratio. While keeping the total area constant, at $2 \cdot 10^6 m^2$, the h/w ratio is changed from 0.1 representing a narrow and long border scenario to 1.0 representing a square border scenario. Four different levels of required detection probability are defined and the number of sensors that are needed to achieve the required detection level is calculated. The calculations are done for two sensing models, binary and Elfes sensing models. The detection range for the binary sensing is set at $r = 20\ m$. The Elfes ranges are set at $r = 20\ m$ and $r_e = 10\ m$ and the detection parameters are $\lambda = 0.2$ and $\beta = 0.6$.

The required number of sensors for different h/w ratios are shown in Figure 4.15. The first notable property is the difference between the required number of sensors for different sensing models. The outer sensing range is chosen to be same for both sensing models. However, the exponential part of the Elfes model causes the sensor to provide a lower detection probability. Hence, the network requires more Elfes model sensor nodes to achieve the same detection probability level the binary sensor nodes can guarantee.

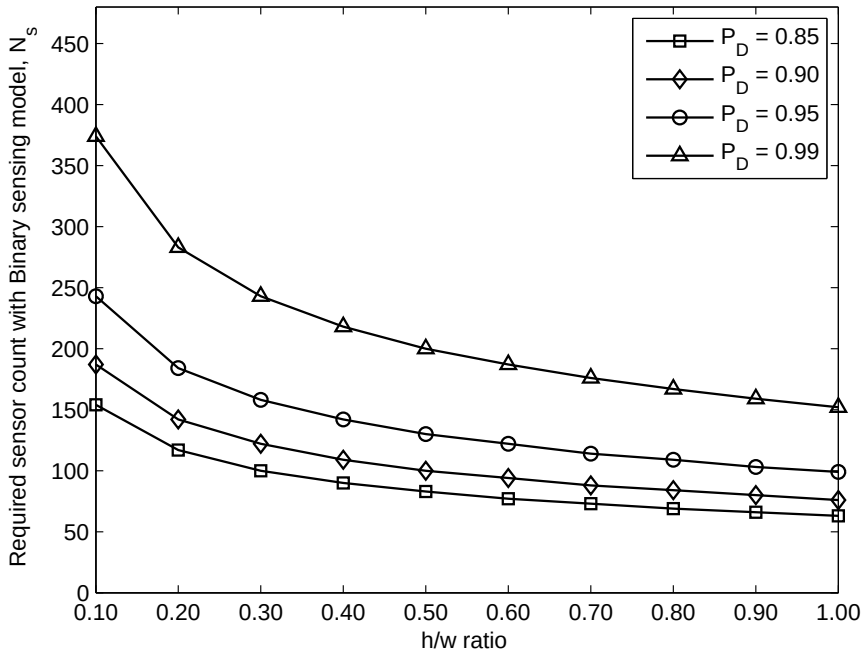

Figure 4.14. Required number of sensors for binary sensing model.

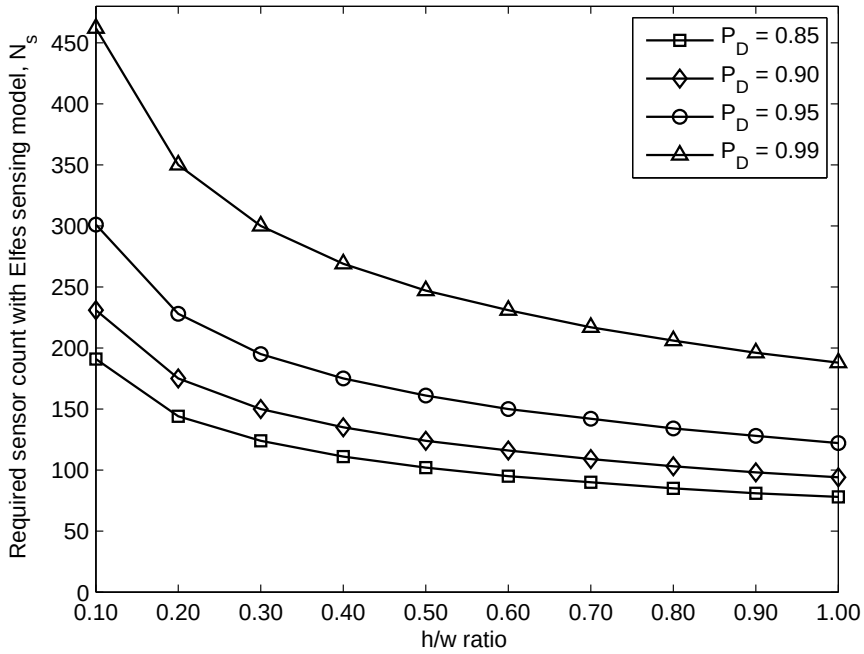

Figure 4.15. Required number of sensors for Elfes sensing model.

Another observable property is the relation between the required number of sensors for different h/w ratios. The required number of sensors that provide the same level of detection probability falls when the shape of the border area becomes more square like. At the $h/w = 0.1$ level, the border area has a shape of a long narrow strip. At the $h/w = 1.0$ level, the border area has a shape of a square, since both sides are equal

in length. The latter case requires much less number of sensors than the previous one for the same detection level.

It can be deduced that the shape of the region on the network performance is clear. For the same area size, the number of required sensors change significantly. One of the reasons of this dramatic change is the directions of the traveler paths and the limiting angles on the possible set of paths. The network planner should take the region dimensioning into account besides the terrain structure and try to segment the monitored zones into more square-like regions in order to achieve better detection ratio with the limited number of sensors.

5. CONCLUSIONS

The surveillance wireless sensor networks are mission critical networks that require a certain detection capability which is measured with detection quality of the network. On the other hand, the behavior of the intruders within the monitored border zone has important effects on the detection quality. In this thesis, we studied the detection quality problem in a border area under different intruder behaviors with different parameters sets. In doing so, the effects of various scenarios and sensor parameters are analyzed. The ultimate goal is to determine the required number of sensors to forecast the target detection probability, improve the network performance according to the field properties and to obtain an acceptable detection probability level.

The analysis of the border area according to its trespassing preference differences can be done using statistical and image processing tools. We propose a method by applying simple segmentation of data based on the number of detections made by each sensor. Using this method, the boundaries of regions with different intrusion frequencies and the respective trespassing probabilities can be easily calculated. The accuracy of the method is also shown with simulations.

The identification of regions within the border area consists of the initial step of a SWSN design. According to the properties and locations of these regions, the design of the SWSN should be modified to achieve the optimum detection quality with limited sensor resources. The detection quality of a wireless network depends on many general and scenario specific parameters such as, the number of sensor nodes, the sensing model and the range, the dimensions and preferences of regions existing within the border area.

In this thesis, we propose a closed form formulation for the detection quality measure applicable to any convex region with a preferred region. We apply it to the rectangular border scenario case and modify the generic formula to be applicable to the scenario. To test the validity of the theoretical model, we run simulations with different parameter sets and compare the results with the analytical ones. The simulation results match with analytical results with a high accuracy, thus proving its validity and applicability in the realistic scenarios. The single region scenario is

generalized for the cases where the border area consists of multiple regions with different widths and preference probabilities and represented using a closed form formulation. The properties of different regions and their distributions among the border area are inspected and their impact on the detection quality are inspected. The advantage of having a closed form formulation is the ability to forecast the performance of a such system before deployment and give the network operator means to improve the detection quality in the design phase. The distribution of the available sensors among different regions is an important problem. Using the proposed closed form, the optimum number of sensors per region can be easily calculated and so the optimum detection quality can be achieved.

As a future work of this thesis, the effect of the energy consumption in sensing and communication in different regions of the border area can be analyzed. If the temporal effects of such regions can be represented with analytical methods, the expected lifetime of a SWSN can be easily calculated and its weak points can be diagnosed in the design phase. Moreover, the effects of different routing strategies and medium access layer protocols on the detection quality and the network lifetime can be analyzed. Three dimensional field models with realistic terrains can also be incorporated into the work.

APPENDIX A: ANALYTICAL AND SIMULATION RESULT TABLES

All of the simulation results for the given parameter set are not presented within the figures. These simulation results and the corresponding analytical values are given in the following tables. These tables can also be used as lookup references for different border surveillance scenarios.

Table A.1. Analytical and simulated DetQM values for areas with different border region width and TFP preference ratio. The border region width is 20000 m and TFP width is 200 m.

TFP	**50**		**100**		**150**		**200**		**250**	
Pr.	**Sim.**	**An.**	**Sim.**	**An.**	**Sim.**	**An.**	**Sim.**	**An.**	**Sim.**	**An.**
0.0	0.1798	0.1576	0.3185	0.2904	0.4289	0.4023	0.5186	0.4965	0.5922	0.5759
0.1	0.1739	0.1536	0.3086	0.2835	0.4167	0.3934	0.5063	0.4863	0.5796	0.5648
0.2	0.1664	0.1497	0.2987	0.2767	0.4068	0.3845	0.4935	0.4760	0.5667	0.5538
0.3	0.1589	0.1457	0.2912	0.2698	0.3959	0.3756	0.4817	0.4658	0.5526	0.5427
0.4	0.1549	0.1417	0.2824	0.2629	0.3867	0.3667	0.4695	0.4555	0.5429	0.5317
0.5	0.1529	0.1377	0.2700	0.2560	0.3747	0.3577	0.4466	0.4453	0.5246	0.5206
0.6	0.1475	0.1337	0.2601	0.2491	0.3604	0.3488	0.4448	0.4350	0.5155	0.5096
0.7	0.1324	0.1297	0.2529	0.2422	0.3509	0.3399	0.4294	0.4248	0.5049	0.4985
0.8	0.1307	0.1257	0.2446	0.2353	0.3329	0.3310	0.4215	0.4145	0.4971	0.4875
0.9	0.1216	0.1217	0.2318	0.2285	0.3284	0.3221	0.4130	0.4043	0.4742	0.4764
1.0	0.1123	0.1177	0.2271	0.2216	0.3019	0.3132	0.4051	0.3940	0.4669	0.4654
TFP	**300**		**350**		**400**		**450**		**500**	
Pr.	**Sim.**	**An.**	**Sim.**	**An.**	**Sim.**	**An.**	**Sim.**	**An.**	**Sim.**	**An.**
0.0	0.6527	0.6427	0.7035	0.6991	0.7460	0.7465	0.7820	0.7865	0.8127	0.8201
0.1	0.6408	0.6313	0.6912	0.6875	0.7345	0.7351	0.7713	0.7754	0.8038	0.8095
0.2	0.6284	0.6199	0.6775	0.6760	0.7246	0.7238	0.7636	0.7644	0.7946	0.7989
0.3	0.6180	0.6084	0.6687	0.6645	0.7085	0.7124	0.7513	0.7533	0.7810	0.7883
0.4	0.6050	0.5970	0.6568	0.6530	0.7034	0.7010	0.7416	0.7423	0.7749	0.7777
0.5	0.5882	0.5855	0.6414	0.6414	0.6988	0.6897	0.7280	0.7313	0.7624	0.7672
0.6	0.5716	0.5741	0.6313	0.6299	0.6840	0.6783	0.7209	0.7202	0.7625	0.7566
0.7	0.5591	0.5626	0.6243	0.6184	0.6611	0.6669	0.7100	0.7092	0.7388	0.7460
0.8	0.5546	0.5512	0.6138	0.6069	0.6639	0.6556	0.6940	0.6981	0.7406	0.7354
0.9	0.5433	0.5398	0.6076	0.5954	0.6414	0.6442	0.6823	0.6871	0.7262	0.7248
1.0	0.5224	0.5283	0.5737	0.5838	0.6286	0.6328	0.6703	0.6760	0.7099	0.7142

Table A.2. Analytical and simulated DetQM values for areas with different border region width and TFP preference ratio. The border region width is 20000 m and TFP width is 200 m.

TFP	**600**		**700**		**800**		**900**		**1000**	
Pr.	**Sim.**	**An.**	**Sim.**	**An.**	**Sim.**	**An.**	**Sim.**	**An.**	**Sim.**	**An.**
0.0	0.8607	0.8724	0.8958	0.9094	0.9213	0.9357	0.9405	0.9544	0.9552	0.9676
0.1	0.8535	0.8629	0.8895	0.9012	0.9157	0.9287	0.9359	0.9485	0.9519	0.9627
0.2	0.8434	0.8534	0.8815	0.8929	0.9108	0.9216	0.9317	0.9425	0.9468	0.9578
0.3	0.8371	0.8439	0.8755	0.8846	0.9038	0.9146	0.9264	0.9366	0.9431	0.9528
0.4	0.8252	0.8344	0.8709	0.8764	0.9005	0.9075	0.9223	0.9307	0.9406	0.9479
0.5	0.8195	0.8249	0.8614	0.8681	0.8939	0.9005	0.9167	0.9247	0.9374	0.9430
0.6	0.8127	0.8155	0.8604	0.8599	0.8857	0.8934	0.9122	0.9188	0.9329	0.9380
0.7	0.8043	0.8060	0.8481	0.8516	0.8791	0.8863	0.9076	0.9129	0.9280	0.9331
0.8	0.7943	0.7965	0.8325	0.8433	0.8754	0.8793	0.9059	0.9069	0.9212	0.9282
0.9	0.7884	0.7870	0.8336	0.8351	0.8746	0.8722	0.8992	0.9010	0.9256	0.9232
1.0	0.7751	0.7775	0.8210	0.8268	0.8656	0.8652	0.8911	0.8951	0.9144	0.9183

Table A.3. Analytical and simulated DetQM values for areas with different border region width and TFP preference ratio. The TFP width is kept constant at 200 m and the number of sensors deployed is 200.

TFP	**2000** m		**4000** m		**6000** m		**8000** m		**10000** m	
Pr.	**Sim.**	**An.**	**Sim.**	**An.**	**Sim.**	**An.**	**Sim.**	**An.**	**Sim.**	**An.**
0.0	0.9787	0.9951	0.9323	0.9428	0.8562	0.8656	0.7835	0.7898	0.7200	0.7222
0.1	0.9803	0.9949	0.9307	0.9405	0.8529	0.8603	0.7770	0.7823	0.7124	0.7133
0.2	0.9819	0.9948	0.9293	0.9381	0.8473	0.8550	0.7699	0.7748	0.7015	0.7044
0.3	0.9829	0.9946	0.9289	0.9358	0.8414	0.8497	0.7621	0.7673	0.6976	0.6955
0.4	0.9852	0.9945	0.9300	0.9334	0.8406	0.8444	0.7529	0.7598	0.6843	0.6866
0.5	0.9865	0.9944	0.9252	0.9311	0.8409	0.8391	0.7550	0.7523	0.6746	0.6777
0.6	0.9886	0.9942	0.9251	0.9287	0.8312	0.8338	0.7440	0.7448	0.6656	0.6688
0.7	0.9895	0.9941	0.9273	0.9264	0.8274	0.8285	0.7471	0.7373	0.6695	0.6600
0.8	0.9906	0.9940	0.9241	0.9240	0.8243	0.8232	0.7292	0.7298	0.6551	0.6511
0.9	0.9924	0.9938	0.9278	0.9217	0.8185	0.8179	0.7095	0.7223	0.6407	0.6422
1.0	0.9955	0.9937	0.9226	0.9193	0.8172	0.8126	0.7169	0.7149	0.6252	0.6333
TFP	**12000** m		**14000** m		**16000** m		**18000** m		**20000** m	
Pr.	**Sim.**	**An.**	**Sim.**	**An.**	**Sim.**	**An.**	**Sim.**	**An.**	**Sim.**	**An.**
0.0	0.6665	0.6634	0.6210	0.6126	0.5819	0.5686	0.5484	0.5302	0.5186	0.4965
0.1	0.6575	0.6537	0.6102	0.6025	0.5708	0.5583	0.5359	0.5199	0.5068	0.4863
0.2	0.6457	0.6440	0.5988	0.5924	0.5590	0.5480	0.5240	0.5095	0.4937	0.4760
0.3	0.6369	0.6343	0.5915	0.5822	0.5476	0.5377	0.5166	0.4992	0.4837	0.4658
0.4	0.6234	0.6246	0.5792	0.5721	0.5334	0.5273	0.4995	0.4889	0.4679	0.4555
0.5	0.6193	0.6149	0.5666	0.5620	0.5214	0.5170	0.4826	0.4785	0.4622	0.4453
0.6	0.6081	0.6052	0.5584	0.5518	0.5101	0.5067	0.4768	0.4682	0.4454	0.4350
0.7	0.6049	0.5955	0.5501	0.5417	0.4989	0.4964	0.4587	0.4579	0.4414	0.4248
0.8	0.5875	0.5858	0.5412	0.5316	0.5003	0.4861	0.4376	0.4476	0.4158	0.4145
0.9	0.5776	0.5761	0.5275	0.5214	0.4742	0.4758	0.4332	0.4372	0.4184	0.4043
1.0	0.5758	0.5664	0.5134	0.5113	0.4713	0.4655	0.4204	0.4269	0.3993	0.3940

Table A.4. Analytical and simulated DetQM values for areas with different border region width and TFP preference ratio. The TFP width is kept constant at 200 m and the number of sensors deployed is 800.

TFP	**2000** m		**4000** m		**6000** m		**8000** m		**10000** m	
Pr.	**Sim.**	**An.**	**Sim.**	**An.**	**Sim.**	**An.**	**Sim.**	**An.**	**Sim.**	**An.**
0.0	0.9755	1.0000	0.9954	1.0000	0.9967	0.9997	0.9942	0.9980	0.9882	0.9940
0.1	0.9779	1.0000	0.9959	1.0000	0.9969	0.9996	0.9941	0.9976	0.9876	0.9928
0.2	0.9804	1.0000	0.9964	1.0000	0.9971	0.9995	0.9941	0.9971	0.9872	0.9916
0.3	0.9827	1.0000	0.9968	1.0000	0.9973	0.9994	0.9940	0.9967	0.9865	0.9904
0.4	0.9853	1.0000	0.9973	1.0000	0.9977	0.9993	0.9942	0.9962	0.9852	0.9892
0.5	0.9877	1.0000	0.9977	1.0000	0.9978	0.9992	0.9936	0.9957	0.9858	0.9880
0.6	0.9901	1.0000	0.9982	1.0000	0.9979	0.9991	0.9942	0.9953	0.9843	0.9868
0.7	0.9927	1.0000	0.9986	1.0000	0.9979	0.9990	0.9939	0.9948	0.9845	0.9856
0.8	0.9951	1.0000	0.9991	1.0000	0.9987	0.9989	0.9937	0.9943	0.9824	0.9843
0.9	0.9976	1.0000	0.9995	1.0000	0.9988	0.9989	0.9937	0.9939	0.9841	0.9831
1.0	1.0000	1.0000	0.9999	1.0000	0.9987	0.9988	0.9929	0.9934	0.9816	0.9819
TFP	**12000** m		**14000** m		**16000** m		**18000** m		**20000** m	
Pr.	**Sim.**	**An.**	**Sim.**	**An.**	**Sim.**	**An.**	**Sim.**	**An.**	**Sim.**	**An.**
0.0	0.9790	0.9872	0.9675	0.9775	0.9533	0.9654	0.9370	0.9513	0.9218	0.9357
0.1	0.9777	0.9849	0.9647	0.9740	0.9501	0.9607	0.9325	0.9454	0.9164	0.9287
0.2	0.9760	0.9827	0.9625	0.9706	0.9468	0.9560	0.9285	0.9395	0.9113	0.9216
0.3	0.9741	0.9804	0.9604	0.9671	0.9413	0.9513	0.9253	0.9335	0.9065	0.9146
0.4	0.9726	0.9782	0.9582	0.9637	0.9393	0.9466	0.9211	0.9276	0.8975	0.9075
0.5	0.9714	0.9759	0.9541	0.9602	0.9366	0.9419	0.9158	0.9217	0.8946	0.9005
0.6	0.9691	0.9737	0.9513	0.9568	0.9333	0.9372	0.9090	0.9158	0.8882	0.8934
0.7	0.9696	0.9714	0.9497	0.9533	0.9279	0.9325	0.9057	0.9099	0.8799	0.8863
0.8	0.9669	0.9692	0.9456	0.9499	0.9288	0.9278	0.9028	0.9040	0.8830	0.8793
0.9	0.9673	0.9669	0.9437	0.9464	0.9238	0.9231	0.8970	0.8980	0.8714	0.8722
1.0	0.9643	0.9647	0.9414	0.9430	0.9218	0.9184	0.8903	0.8921	0.8703	0.8652

Table A.5. Analytical and simulated DetQM values for areas with different border region width and TFP preference ratio. The TFP width ratio is 0.1 and the number of sensors deployed is 200.

TFP	**2000** m		**4000** m		**6000** m		**8000** m		**10000** m	
Pr.	**Sim.**	**An.**	**Sim.**	**An.**	**Sim.**	**An.**	**Sim.**	**An.**	**Sim.**	**An.**
0.0	0.9792	0.9951	0.9105	0.9410	0.8419	0.8614	0.7824	0.7835	0.7078	0.7142
0.1	0.9809	0.9949	0.9112	0.9389	0.8389	0.8568	0.7764	0.7771	0.7014	0.7068
0.2	0.9826	0.9948	0.9126	0.9368	0.8368	0.8521	0.7691	0.7706	0.6951	0.6993
0.3	0.9838	0.9946	0.9145	0.9347	0.8340	0.8474	0.7632	0.7642	0.6886	0.6919
0.4	0.9853	0.9945	0.9154	0.9326	0.8298	0.8427	0.7573	0.7577	0.6796	0.6845
0.5	0.9870	0.9944	0.9158	0.9304	0.8292	0.8380	0.7526	0.7512	0.6752	0.6770
0.6	0.9885	0.9942	0.9178	0.9283	0.8281	0.8334	0.7491	0.7448	0.6722	0.6696
0.7	0.9900	0.9941	0.9180	0.9262	0.8244	0.8287	0.7372	0.7383	0.6627	0.6621
0.8	0.9917	0.9940	0.9220	0.9241	0.8227	0.8240	0.7338	0.7319	0.6504	0.6547
0.9	0.9928	0.9938	0.9218	0.9219	0.8200	0.8193	0.7316	0.7254	0.6494	0.6473
1.0	0.9948	0.9937	0.9210	0.9198	0.8172	0.8146	0.7214	0.7190	0.6447	0.6398
TFP	**12000** m		**14000** m		**16000** m		**18000** m		**20000** m	
Pr.	**Sim.**	**An.**	**Sim.**	**An.**	**Sim.**	**An.**	**Sim.**	**An.**	**Sim.**	**An.**
0.0	0.6602	0.6541	0.6161	0.6023	0.5777	0.5574	0.5405	0.5184	0.5102	0.4843
0.1	0.6515	0.6462	0.6071	0.5943	0.5674	0.5496	0.5306	0.5108	0.4998	0.4770
0.2	0.6429	0.6384	0.5974	0.5864	0.5586	0.5418	0.5208	0.5032	0.4902	0.4697
0.3	0.6338	0.6305	0.5884	0.5784	0.5472	0.5339	0.5111	0.4957	0.4805	0.4625
0.4	0.6272	0.6226	0.5772	0.5705	0.5369	0.5261	0.4990	0.4881	0.4713	0.4552
0.5	0.6174	0.6148	0.5684	0.5625	0.5288	0.5183	0.4909	0.4805	0.4596	0.4479
0.6	0.6082	0.6069	0.5623	0.5545	0.5187	0.5104	0.4799	0.4729	0.4495	0.4407
0.7	0.6027	0.5990	0.5504	0.5466	0.5066	0.5026	0.4718	0.4653	0.4418	0.4334
0.8	0.5947	0.5912	0.5390	0.5386	0.4980	0.4948	0.4619	0.4578	0.4306	0.4261
0.9	0.5856	0.5833	0.5323	0.5307	0.4887	0.4870	0.4532	0.4502	0.4222	0.4189
1.0	0.5728	0.5754	0.5226	0.5227	0.4754	0.4791	0.4424	0.4426	0.4098	0.4116

Table A.6. Analytical and simulated DetQM values for areas with different border region width and TFP preference ratio. The TFP width ratio is 0.1 and the number of sensors deployed is 800.

TFP	**2000** m		**4000** m		**6000** m		**8000** m		**10000** m	
Pr.	**Sim.**	**An.**	**Sim.**	**An.**	**Sim.**	**An.**	**Sim.**	**An.**	**Sim.**	**An.**
0.0	0.9620	1.0000	0.9856	1.0000	0.9837	0.9996	0.9828	0.9978	0.9666	0.9933
0.1	0.9659	1.0000	0.9870	1.0000	0.9852	0.9996	0.9839	0.9974	0.9683	0.9923
0.2	0.9697	1.0000	0.9885	1.0000	0.9866	0.9995	0.9851	0.9970	0.9701	0.9913
0.3	0.9736	1.0000	0.9899	1.0000	0.9883	0.9994	0.9862	0.9966	0.9719	0.9903
0.4	0.9772	1.0000	0.9913	1.0000	0.9897	0.9993	0.9872	0.9962	0.9735	0.9893
0.5	0.9810	1.0000	0.9928	1.0000	0.9913	0.9992	0.9885	0.9958	0.9750	0.9882
0.6	0.9848	1.0000	0.9942	1.0000	0.9928	0.9991	0.9895	0.9954	0.9769	0.9872
0.7	0.9887	1.0000	0.9957	1.0000	0.9944	0.9991	0.9905	0.9950	0.9782	0.9862
0.8	0.9924	1.0000	0.9971	1.0000	0.9958	0.9990	0.9916	0.9946	0.9802	0.9852
0.9	0.9962	1.0000	0.9985	1.0000	0.9974	0.9989	0.9924	0.9942	0.9813	0.9842
1.0	1.0000	1.0000	1.0000	1.0000	0.9989	0.9988	0.9938	0.9938	0.9828	0.9832
TFP	**12000** m		**14000** m		**16000** m		**18000** m		**20000** m	
Pr.	**Sim.**	**An.**	**Sim.**	**An.**	**Sim.**	**An.**	**Sim.**	**An.**	**Sim.**	**An.**
0.0	0.9765	0.9857	0.9497	0.9750	0.9237	0.9616	0.9165	0.9462	0.9001	0.9293
0.1	0.9757	0.9839	0.9496	0.9723	0.9241	0.9581	0.9151	0.9419	0.8976	0.9243
0.2	0.9747	0.9820	0.9493	0.9696	0.9240	0.9546	0.9134	0.9377	0.8952	0.9194
0.3	0.9739	0.9802	0.9487	0.9669	0.9244	0.9511	0.9124	0.9334	0.8937	0.9145
0.4	0.9728	0.9784	0.9493	0.9642	0.9247	0.9475	0.9107	0.9291	0.8912	0.9096
0.5	0.9721	0.9766	0.9492	0.9615	0.9239	0.9440	0.9093	0.9248	0.8895	0.9047
0.6	0.9712	0.9748	0.9487	0.9589	0.9247	0.9405	0.9084	0.9206	0.8865	0.8998
0.7	0.9694	0.9730	0.9485	0.9562	0.9246	0.9370	0.9063	0.9163	0.8855	0.8949
0.8	0.9695	0.9711	0.9487	0.9535	0.9233	0.9334	0.9052	0.9120	0.8816	0.8899
0.9	0.9688	0.9693	0.9483	0.9508	0.9254	0.9299	0.9029	0.9077	0.8813	0.8850
1.0	0.9677	0.9675	0.9479	0.9481	0.9253	0.9264	0.9028	0.9035	0.8773	0.8801

Table A.7. DetQM for uniform and optimized sensor allocations for different values of p_{t_1}.

Total	**Uniform**			**Optimized ($p_{t_1} = 0.1$)**			**Optimized ($p_{t_1} = 0.2$)**		
N_t	N_{t_1}	N_{t_2}	P_D	N_{t_1}	N_{t_2}	P_D	N_{t_1}	N_{t_2}	P_D
10	5	5	0.195	0	10	0.316	0	10	0.281
20	10	10	0.351	0	20	0.521	0	20	0.463
30	15	15	0.478	0	30	0.654	0	30	0.582
40	20	20	0.579	0	40	0.741	4	36	0.663
50	25	25	0.661	0	50	0.797	9	41	0.729
60	30	30	0.727	5	55	0.836	14	46	0.782
70	35	35	0.780	10	60	0.868	19	51	0.824
80	40	40	0.823	15	65	0.894	24	56	0.858
90	45	45	0.857	20	70	0.914	29	61	0.886
100	50	50	0.885	25	75	0.931	34	66	0.908
Total	**Uniform**			**Optimized ($p_{t_1} = 0.3$)**			**Optimized ($p_{t_1} = 0.4$)**		
N_t	N_{t_1}	N_{t_2}	P_D	N_{t_1}	N_{t_2}	P_D	N_{t_1}	N_{t_2}	P_D
10	5	5	0.195	0	10	0.246	0	10	0.211
20	10	10	0.351	0	20	0.405	5	15	0.364
30	15	15	0.478	5	25	0.521	10	20	0.488
40	20	20	0.579	10	30	0.614	15	25	0.588
50	25	25	0.661	15	35	0.689	20	30	0.668
60	30	30	0.727	20	40	0.750	25	35	0.733
70	35	35	0.780	25	45	0.799	30	40	0.785
80	40	40	0.823	30	50	0.838	35	45	0.827
90	45	45	0.857	35	55	0.869	40	50	0.860
100	50	50	0.885	40	60	0.895	45	55	0.887

Table A.8. DetQM for uniform and optimized sensor allocations for different values of width w.

Width	**Uniform**			**Optimized ($p_{t_1} = 0.1$)**			**Optimized ($p_{t_1} = 0.2$)**		
w	N_{t_1}	N_{t_2}	P_D	N_{t_1}	N_{t_2}	P_D	N_{t_1}	N_{t_2}	P_D
2000	50	50	0.716	25	75	0.931	34	66	0.908
4000	50	50	0.491	2	98	0.811	20	80	0.748
6000	50	50	0.372	0	100	0.721	7	93	0.643
8000	50	50	0.300	0	100	0.643	0	100	0.571
10000	50	50	0.251	0	100	0.578	0	100	0.514
12000	50	50	0.216	0	100	0.524	0	100	0.466
14000	50	50	0.189	0	100	0.479	0	100	0.426
16000	50	50	0.169	0	100	0.441	0	100	0.392
18000	50	50	0.152	0	100	0.409	0	100	0.363
20000	50	50	0.139	0	100	0.381	0	100	0.338
Width	**Uniform**			**Optimized ($p_{t_1} = 0.3$)**			**Optimized ($p_{t_1} = 0.4$)**		
w	N_{t_1}	N_{t_2}	P_D	N_{t_1}	N_{t_2}	P_D	N_{t_1}	N_{t_2}	P_D
2000	50	50	0.716	40	60	0.895	45	55	0.887
4000	50	50	0.491	32	68	0.711	41	59	0.691
6000	50	50	0.372	24	76	0.591	37	63	0.563
8000	50	50	0.300	16	84	0.510	34	66	0.476
10000	50	50	0.251	9	91	0.452	30	70	0.414
12000	50	50	0.216	1	99	0.408	27	73	0.367
14000	50	50	0.189	0	100	0.373	23	77	0.330
16000	50	50	0.169	0	100	0.343	20	80	0.300
18000	50	50	0.152	0	100	0.318	17	83	0.276
20000	50	50	0.139	0	100	0.296	13	87	0.256

REFERENCES

1. Pister, K., *29 Palms Fixed/Mobile Experiment*, 2001, `http://robotics.eecs.berkeley.edu/~pister/29Palms0103/`, accessed at June 2011.

2. American Border Patrol, *American Border Patrol - Photo of the Day*, 2010, `http://www.americanpatrol.com/ABP/PHOTO-OF-THE-DAY/2010/ARCHIVE/100204.html`, accessed at May 2011.

3. *BlueServo Virtual BorderWatch*, 2010, `http://www.blueservo.net`, accessed at May 2011.

4. Wang, Y., L. Huang, J. Wu, and H. Xu, "Wireless Sensor Networks for Intensive Irrigated Agriculture", *Consumer Communications and Networking Conference, 2007. CCNC 2007. 4th IEEE*, pp. 197–201, 2007.

5. Wark, T., P. Corke, P. Sikka, L. Klingbeil, Y. Guo, C. Crossman, P. Valencia, D. Swain, and G. Bishop-Hurley, "Transforming Agriculture Through Pervasive Wireless Sensor Networks", *IEEE Pervasive Computing*, Vol. 6, pp. 50–57, 2007.

6. Liu, H., Z. Meng, and S. Cui, "A Wireless Sensor Network Prototype for Environmental Monitoring in Greenhouses", *Wireless Communications, Networking and Mobile Computing, 2007. WiCom 2007. International Conference on*, pp. 2344–2347, 2007.

7. Pierce, F. and T. Elliott, "Regional and On-Farm Wireless Sensor Networks for Agricultural Systems in Eastern Washington", *Computers and Electronics in Agriculture*, Vol. 61, No. 1, pp. 32–43, 2008.

8. Hou, J. and Y. Gao, "Greenhouse Wireless Sensor Network Monitoring System Design Based on Solar Energy", *Proceedings of International Conference on Challenges in Environmental Science and Computer Engineering*, Vol. 2, pp. 475–479, IEEE Computer Society, Los Alamitos, CA, USA, 2010.

9. Orwat, C., A. Graefe, and T. Faulwasser, "Towards Pervasive Computing in Health Care - A Literature Review", *BMC Medical Informatics and Decision Making*, Vol. 8, No. 1, p. 26, 2008.

10. Sneha, S. and U. Varshney, "Enabling Ubiquitous Patient Monitoring: Model, Decision Protocols, Opportunities and Challenges", *Decision Support Systems*, Vol. 46, No. 3, pp. 606–619, 2009.

11. Alemdar, H. and C. Ersoy, "Wireless Sensor Networks for Healthcare: A Survey", *Computer Networks*, Vol. 54, No. 15, pp. 2688–2710, 2010.

12. Barrenetxea, G., F. Ingelrest, G. Schaefer, and M. Vetterli, "Wireless Sensor Networks for Environmental Monitoring: The SensorScope Experience", *Communications, 2008 IEEE International Zurich Seminar on*, pp. 98–101, 2008.

13. Akyildiz, I. F., W. Su, Y. Sankarasubramaniam, and E. Cayirci, "Wireless Sensor Networks: A Survey", *Computer Networks*, Vol. 38, No. 4, pp. 393–422, 2002.

14. Chong, C.-Y. and S. Kumar, "Sensor Networks: Evolution, Opportunities, and Challenges", *Proceedings of the IEEE*, Vol. 91, No. 8, pp. 1247–1256, 2003.

15. Baronti, P., P. Pillai, V. W. Chook, S. Chessa, A. Gotta, and Y. F. Hu, "Wireless Sensor Networks: A Survey on The State of The Art and The 802.15.4 and Zigbee Standards", *Computer Communications*, Vol. 30, No. 7, pp. 1655–1695, 2007.

16. Akyildiz, I. F., T. Melodia, and K. R. Chowdhury, "A survey on wireless multimedia sensor networks", *Computer Networks*, Vol. 51, No. 4, pp. 921–960, 2007.

17. Yick, J., B. Mukherjee, and D. Ghosal, "Wireless Sensor Network Survey", *Computer Networks*, Vol. 52, No. 12, pp. 2292–2330, 2008.

18. Warneke, B., M. Last, B. Liebowitz, and K. S. J. Pister, "Smart Dust: Communicating with a Cubic-Millimeter Computer", *Computer*, Vol. 34, pp. 44–51,

2001.

19. Arora, A., P. Dutta, S. Bapat, V. Kulathumani, H. Zhang, V. Naik, V. Mittal, H. Cao, M. Demirbas, M. Gouda, Y. Choi, T. Herman, S. Kulkarni, U. Arumugam, M. Nesterenko, A. Vora, and M. Miyashita, "A Line In The Sand: A Wireless Sensor Network For Target Detection, Classification, and Tracking", *Computer Networks*, Vol. 46, pp. 605–634, 2004.

20. Dudek, D., C. Haas, A. Kuntz, M. Zitterbart, D. Krüger, P. Rothenpieler, D. Pfisterer, and S. Fischer, "A Wireless Sensor Network for Border Surveillance", *Proceedings of the 7th ACM Conference on Embedded Networked Sensor Systems*, SenSys '09, pp. 303–304, ACM, New York, NY, USA, 2009.

21. O'Rourke, J., *Art Gallery Theorems and Algorithms*, Oxford University Press, Oxford, UK, 1987.

22. Cardei, M. and J. Wu, *Handbook of Sensor Networks*, chapter Coverage in Wireless Sensor Networks, CRC Press, Boca Raton, FL, USA, 2004.

23. Yan, T., T. He, and J. A. Stankovic, "Differentiated Surveillance for Sensor Networks", *Proceedings of the 1st international conference on Embedded networked sensor systems*, SenSys '03, pp. 51–62, ACM, New York, NY, USA, 2003.

24. Zhang, H. and J. Hou, "Maintaining Sensing Coverage and Connectivity in Large Sensor Networks", *Ad Hoc & Sensor Wireless Networks*, Vol. 1, No. 1-2, 2005.

25. Misra, S., M. P. Kumar, and M. S. Obaidat, "Connectivity Preserving Localized Coverage Algorithm for Area Monitoring Using Wireless Sensor Networks", *Computer Communications*, Vol. In Press, Corrected Proof, 2010.

26. Zhao, Q. and M. Gurusamy, "Connected K-Target Coverage Problem In Wireless Sensor Networks With Different Observation Scenarios", *Computer Networks*, Vol. 52, No. 11, pp. 2205–2220, 2008.

27. Wettergren, T. A. and R. Costa, "Optimal Placement of Distributed Sensors Against Moving Targets", *ACM Trans. Sen. Netw.*, Vol. 5, pp. 26:1–26:25, 2009.

28. Fang, Z. and J. Wang, "Convex Combination Approximation for the Min-Cost WSN Point Coverage Problem", Li, Y., D. Huynh, S. Das, and D.-Z. Du (editors), *Wireless Algorithms, Systems, and Applications*, Vol. 5258 of *Lecture Notes in Computer Science*, pp. 188–199, Springer Berlin Heidelberg, 2008.

29. Liu, B., O. Dousse, J. Wang, and A. Saipulla, "Strong Barrier Coverage Of Wireless Sensor Networks", *MobiHoc '08: Proceedings of the 9th ACM international symposium on Mobile ad hoc networking and computing*, pp. 411–420, ACM, New York, NY, USA, 2008.

30. Chen, A., S. Kumar, and T. H. Lai, "Local Barrier Coverage in Wireless Sensor Networks", *IEEE Transactions on Mobile Computing*, Vol. 9, pp. 491–504, 2010.

31. Saipulla, A., C. Westphal, B. Liu, and J. Wang, "Barrier Coverage of Line-Based Deployed Wireless Sensor Networks", *IEEE INFOCOM 2009 - The 28th Conference on Computer Communications*, pp. 127–135, IEEE, 2009.

32. Su, L., Q. Yang, Q. Li, and X. Xu, "Coverage Algorithm and Protocol in Heterogeneous Sensor Networks", Lu, X. and W. Zhao (editors), *Networking and Mobile Computing*, Vol. 3619 of *Lecture Notes in Computer Science*, pp. 53–63, Springer Berlin / Heidelberg, 2005.

33. *SEGA-Node TIMS Radar*, 2006, `http://www.sperient.com/sega/`, accessed at July 2011.

34. *Osiris Photo-Electric Sensors*, 2010, `http://www.schneider-electric.ca`, accessed at May 2011.

35. Cardei, M., J. Wu, and M. Lu, "Improving Network Lifetime Using Sensors With Adjustable Sensing Ranges", *International Journal of Sensor Networks*, Vol. 1, pp.

41–49, 2006.

36. Zhou, Z., S. R. Das, and H. Gupta, "Variable Radii Connected Sensor Cover In Sensor Networks", *ACM Trans. Sen. Netw.*, Vol. 5, pp. 8:1–8:36, 2009.

37. Meguerdichian, S., F. Koushanfar, G. Qu, and M. Potkonjak, "Exposure in Wireless Ad-Hoc Sensor Networks", *MobiCom '01: Proceedings of the 7th annual international conference on Mobile computing and networking*, pp. 139–150, ACM, New York, NY, USA, 2001.

38. Onur, E., C. Ersoy, and H. Deli, "How Many Sensors For An Acceptable Breach Detection Probability?", *Computer Communications*, Vol. 29, No. 2, pp. 173–182, 2006.

39. Lazos, L., R. Poovendran, and J. A. Ritcey, "Analytic Evaluation of Target Detection in Heterogeneous Wireless Sensor Networks", *ACM Trans. Sen. Netw.*, Vol. 5, No. 2, pp. 1–38, 2009.

40. Donmez, M. Y., R. Kosar, and C. Ersoy, "An Analytical Approach to The Deployment Quality of Surveillance Wireless Sensor Networks Considering The Effect of Jammers and Coverage Holes", *Computer Networks*, Vol. 54, No. 18, pp. 3449–3466, 2010.

41. Abu Sajana, R., R. Subramanian, P. Kumar, S. Krishnan, B. Amrutur, J. Sebastian, M. Hegde, and S. Anand, "A Low-Complexity Algorithm for Intrusion Detection in a PIR-based Wireless Sensor Network", *Intelligent Sensors, Sensor Networks and Information Processing (ISSNIP), 2009 5th International Conference on*, pp. 337–342, 2009.

42. Li, Y. Y. and L. Parker, "Intruder Detection Using a Wireless Sensor Network with an Intelligent Mobile Robot Response", *Southeastcon, 2008. IEEE*, pp. 37–42, 2008.

43. Ahmed, N., M. Rutten, T. Bessell, S. Kanhere, N. Gordon, and S. Jha, "Detection and Tracking Using Particle-Filter-Based Wireless Sensor Networks", *Mobile Computing, IEEE Transactions on*, Vol. 9, No. 9, pp. 1332–1345, 2010.

44. Clouqueur, T., V. Phipatanasuphorn, P. Ramanathan, and K. K. Saluja, "Sensor Deployment Strategy for Detection of Targets Traversing a Region", *Mobile Networks and Applications*, Vol. 8, pp. 453–461, 2003.

45. Onur, E., C. Ersoy, and H. Delic, "Analysis of Target Detection Probability In Randomly Deployed Sensor Networks", *Communications Letters, IEEE*, Vol. 11, No. 10, pp. 778–780, 2007.

46. Ram, S., D. Majunath, S. Iyer, and D. Yogeshwaran, "On the Path Coverage Properties of Random Sensor Networks", *Mobile Computing, IEEE Transactions on*, Vol. 6, No. 5, pp. 494–506, 2007.

47. Camp, T., J. Boleng, and V. Davies, "A Survey of Mobility Models for Ad Hoc Network Research", *Wireless Communications and Mobile Computing*, Vol. 2, No. 5, pp. 483–502, 2002.

48. Zheng, Q., X. Hong, and S. Ray, "Recent Advances In Mobility Modeling For Mobile Ad Hoc Network Research", *Proceedings of the 42nd annual Southeast regional conference*, ACM-SE 42, pp. 70–75, ACM, New York, NY, USA, 2004.

49. Bai, F. and A. Helmy, *A Survey of Mobility Models in Wireless Adhoc Networks*, Vol. 2, chapter 1, pp. 1–30, Springer, New York, NY, USA, 2006.

50. Pazand, B. and C. McDonald, "A Critique of Mobility Models for Wireless Network Simulation", *Computer and Information Science, 2007. ICIS 2007. 6th IEEE/ACIS International Conference on*, pp. 141–146, 2007.

51. Ahmed, S., G. C. Karmakar, and J. Kamruzzaman, "An Environment-Aware Mobility Model For Wireless Ad Hoc Network", *Computer Networks*, Vol. 54, No. 9,

pp. 1470–1489, 2010.

52. Turbiville, G. J., "US-Mexican Border Security: Civil-Military Cooperation", *Military Review*, Vol. 79, pp. 29–39, 1999.

53. Moses, R. L., O. L. Moses, D. Krishnamurthy, and R. Patterson, "A Self-Localization Method for Wireless Sensor Networks", *EURASIP Journal on Applied Signal Processing*, Vol. 4, pp. 348–358, 2002.

54. Sichitiu, M. and V. Ramadurai, "Localization of Wireless Sensor Networks with a Mobile Beacon", *Mobile Ad-hoc and Sensor Systems, 2004 IEEE International Conference on*, pp. 174–183, 2004.

55. Teng, G., K. Zheng, and W. Dong, "Adapting Mobile Beacon-Assisted Localization in Wireless Sensor Networks", *Sensors*, Vol. 9, No. 4, pp. 2760–2779, 2009.

56. Shang, Y., W. Rumi, Y. Zhang, and M. Fromherz, "Localization from Connectivity in Sensor Networks", *Parallel and Distributed Systems, IEEE Transactions on*, Vol. 15, No. 11, pp. 961–974, 2004.

57. Stoleru, R., T. He, J. A. Stankovic, and D. Luebke, "A High-Accuracy, Low-Cost Localization System For Wireless Sensor Networks", *SenSys '05: Proceedings of the 3rd international conference on Embedded networked sensor systems*, pp. 13–26, ACM, New York, NY, USA, 2005.

58. Moore, D., J. Leonard, D. Rus, and S. Teller, "Robust Distributed Network Localization with Noisy Range Measurements", *Proceedings of the 2nd international conference on Embedded networked sensor systems*, SenSys '04, pp. 50–61, ACM, New York, NY, USA, 2004.

59. Kuang, X. and H. Shao, "Maximum Likelihood Localization Algorithm Using Wireless Sensor Networks", *Proceedings of the First International Conference on Innovative Computing, Information and Control*, ICICIC '06, pp. 263–266, IEEE

Computer Society, Washington DC, USA, 2006.

60. Stoleru, R., P. Vicaire, T. He, and J. A. Stankovic, "Stardust: A Flexible Architecture For Passive Localization In Wireless Sensor Networks", *Proceedings of the 4th international conference on Embedded networked sensor systems*, SenSys '06, pp. 57–70, ACM, New York, NY, USA, 2006.

61. Goldenberg, D. K., P. Bihler, M. Cao, J. Fang, B. D. O. Anderson, A. S. Morse, and Y. R. Yang, "Localization in Sparse Networks Using Sweeps", *Proceedings of the 12th annual international conference on Mobile computing and networking*, MobiCom '06, pp. 110–121, ACM, New York, NY, USA, 2006.

62. Peng, C., G. Shen, Y. Zhang, Y. Li, and K. Tan, "BeepBeep: A High Accuracy Acoustic Ranging System Using COTS Mobile Devices", *Proceedings of the 5th international conference on Embedded networked sensor systems*, SenSys '07, pp. 1–14, ACM, New York, NY, USA, 2007.

63. Lucarelli, D., A. Saksena, R. Farrell, and I.-J. Wang, "Distributed Inference for Network Localization Using Radio Interferometric Ranging", *Proceedings of the 5th European conference on Wireless sensor networks*, EWSN'08, pp. 52–73, Springer-Verlag, Berlin, Heidelberg, 2008.

64. Mao, G., B. Fidan, and B. D. O. Anderson, "Wireless Sensor Network Localization Techniques", *Computer Networks*, Vol. 51, pp. 2529–2553, 2007.

65. Amundson, I. and X. D. Koutsoukos, "A Survey On Localization For Mobile Wireless Sensor Networks", *Proceedings of the 2nd international conference on Mobile entity localization and tracking in GPS-less environments*, MELT'09, pp. 235–254, Springer-Verlag, Berlin, Heidelberg, 2009.

66. Cao, Q., T. Yan, J. Stankovic, and T. Abdelzaher, "Analysis of Target Detection Performance for Wireless Sensor Networks", Prasanna, V. K., S. Iyengar, P. G. Spirakis, and M. Welsh (editors), *Distributed Computing in Sensor Systems*, Vol. 3560

of *Lecture Notes in Computer Science*, pp. 276–292, Springer Berlin / Heidelberg, 2005.

67. Dougherty, E. R. and R. A. Lotufo, *Hands-on Morphological Image Processing*, SPIE Publications, Bellingham, WA, USA, 2003.

68. *Mathworks Matlab*, 2010, `http://www.mathworks.com/matlabcentral/`, accessed at January 2012.

69. Hall, P., *Introduction to the Theory of Coverage Processes*, John Wiley & Sons Inc, Hoboken, NJ, USA, 1988.

70. Law, Y. W., L. van Hoesel, J. Doumen, P. Hartel, and P. Havinga, "Energy-Efficient Link-Layer Jamming Attacks Against Wireless Sensor Network Mac Protocols", *SASN '05: Proceedings of the 3rd ACM workshop on Security of ad hoc and sensor networks*, pp. 76–88, ACM, New York, NY, USA, 2005.

71. Mcewan, T. E., "Differential Pulse Radar Motion Sensor", 1999.

72. Dutta, P. K., A. K. Arora, and S. B. Bibyk, "Towards Radar-Enabled Sensor Networks", *IPSN '06: Proceedings of the 5th international conference on Information processing in sensor networks*, pp. 467–474, ACM, New York, NY, USA, 2006.

73. Azevedo, S. and T. McEwan, "Micropower Impulse Radar", *Potentials, IEEE*, Vol. 16, No. 2, pp. 15–20, 1997.

74. Solomon, H., *Geometric Probability*, Philadelphia, PA: Society for Industrial and Applied Mathematics, Philadephia, PA, USA, 1978.

75. Katoh, N., T. Ibaraki, and H. Mine, "Notes on the Problem of the Allocation of Resources to Activities in Discrete Quantities", *The Journal of the Operational Research Society*, Vol. 31, No. 7, pp. 595–598, 1980.

76. Ibaraki, T. and N. Katoh, *Resource Allocation Problems: Algorithmic Approaches*

(Foundations of Computing), The MIT Press, Cambridge, MA, USA, 1988.

77. Elfes, A., "Occupancy Grids: A Stochastic Spatial Representation for Active Robot Perception", Iyengar, S. S. and A. Elfes (editors), *Autonomous Mobile Robots: Perception, Mapping, and Navigation (Vol. 1)*, pp. 60–70, IEEE Computer Society Press, Los Alamitos, CA, 1991.

78. Arfken, G. B., *Mathematical Methods for Physicists*, chapter The Incomplete Gamma Function and Related Functions, pp. 565–572, Orlando, FL: Academic Press, 1985.

79. McKeeman, W. M., "Algorithm 145: Adaptive Numerical Integration by Simpson's Rule", *Commun. ACM*, Vol. 5, p. 604, 1962.

80. Cardei, M., J. Wu, M. Lu, and M. Pervaiz, "Maximum network lifetime in wireless sensor networks with adjustable sensing ranges", *Wireless And Mobile Computing, Networking And Communications, 2005. (WiMob'2005), IEEE International Conference on*, Vol. 3, pp. 438–445, 2005.

81. Huynh, A., J. Zhang, Q.-Z. Ye, and S. Gong, "Wireless Monitoring System For Cultural Heritage", *Sensors & Transdusers Journal*, Vol. Vol. 118, pp. 1–12, 2010.

82. Bencini, L., G. Collodi, D. D. Palma, G. Manes, and A. Manes, "An Embedded Wireless Sensor Network System for Cultural Heritage Monitoring", *Sensor Technologies and Applications, International Conference on*, Vol. 0, pp. 185–190, 2010.

83. Nolan, J. S., *The Pyramids of Egypt*, 2003, `http://www.multimedia-publishing.com/the_pyramids.htm`, accessed at July 2011.

84. Jain, R., *The Art of Computer Systems Performance Analysis*, Wiley-Interscience, Hoboken, NJ, USA, 1991.